LIÈGE université
Gembloux
Agro-Bio Tech

Plant immunity triggered by the *Bacillus* lipopeptide surfactin and structural variants

Ning DING

Année civile : 2026

COMMUNAUTÉ FRANÇAISE DE BELGIQUE
UNIVERSITÉ DE LIÈGE – GEMBLOUX AGRO-BIO TECH

Plant immunity triggered by the *Bacillus* lipopeptide surfactin and structural variants

Ning DING

Dissertation originale présentée en vue de l'obtention du grade de docteur en sciences agronomiques et ingénierie biologique

Promoteurs : Dr. Marc ONGENA, Dr. Hansong DONG
Année civile : 2026

Abstract

Cyclic lipopeptides (CLPs) are secondary metabolites produced by plant beneficial rhizobacteria retaining diverse ecological functions and playing key roles in defence against phytopathogens. These amphiphilic compounds, consisting of a hydrophilic cyclic peptide linked to a hydrophobic fatty acid chain, exhibit strong membrane-active properties that underpin most of their biological activities. This includes the potential to prime host immunity and trigger the so-called induced systemic resistance (ISR) against pathogen infection. Nevertheless, how the CLP structure may modulate its activity regarding plant immune activation, remains poorly understood.

This study aimed to provide new insights into such structure-activity relationship for *Bacillus* CLPs of the Surfactin family, which are among the best characterized for ISR triggering in various plants and against a broad spectrum of pathogens. To this end, we compared the immune activation potential of canonical surfactin (Srf), produced by *B. velezensis*, with that of pumilacidin (Pumi) and lichenysin (Liche), which are natural Srf variants from the closely related species *B. pumilus* and *B. licheniformis*. Additionally, we exploited the inherent flexibility of the CLP biosynthetic machinery by supplementing culture media with branched-chain amino acids (BCAAs) as biosynthetic precursors to generate novel Srf peptide variants, thereby probing the structural determinants governing plant immunity activation. The immunogenic activity of these CLPs was comprehensively assessed, encompassing early immune signaling events such as reactive oxygen species (ROS) burst, calcium (Ca^{2+}) influx, and nitric oxide (NO) production, in *Arabidopsis thaliana* roots and root protoplasts. Macroscopically, the CLPs were also compared for their potential to trigger ISR against *Botrytis cinerea*.

Our data reveal that minor structural modifications within the Srf peptide moiety significantly influence plant immune activation. Notably, the nature of the amino acid at positions 4 and/or 7 proves critical for optimal activity: Val/(i)Leu substitutions like in Pumi render the molecule inactive, whereas Liche with Glu/Gln exchange retains full activity despite the loss of one net negative charge. This latter observation is particularly noteworthy as it represents the first characterization of the immunogenic potential of Liche from the beneficial epiphytic species *B. licheniformis*. The attenuated activity of Pumi is further interpreted in the context of the *B. pumilus* endophytic lifestyle, suggesting an ecological relevance for reduced CLP potency. Furthermore, BCAA-directed CLP variant profiles are strain-dependent, with novel structural variants arising from amino acid substitutions at positions 3 or 6, albeit produced in limited amounts, and retaining immune activation potential comparable to that of their canonical counterparts. Finally, employing three complementary methodological approaches, we investigated the mechanisms underlying CLP-triggered ISR, revealing a possible role for the phytoalexins camalexin and coumarin as plant defence compounds.

Collectively, these findings provide valuable insights into CLP structure-activity relationships while underscoring the need for further research to fully elucidate their precise mechanisms of immune activation. This work highlights the potential of discovering, engineering, or synthesizing highly efficacious CLPs, and emphasizes the importance of investigating understudied yet potent compounds, such as Liche, for plant protection applications.

Résumé

Les lipopeptides cycliques (CLPs) sont des métabolites secondaires produits par des rhizobactéries bénéfiques pour les plantes remplissant diverses fonctions écologiques et jouant un rôle clé dans la défense contre les phytopathogènes. Ces composés amphiphiles, constitués d'un peptide cyclique hydrophile lié à une chaîne d'acides gras hydrophobe, présentent de fortes propriétés d'interaction membranaire qui sous-tendent la plupart de leurs activités biologiques. Cela inclut la capacité à stimuler l'immunité de l'hôte et à déclencher ce que l'on appelle la résistance systémique induite (ISR) contre les infections par les pathogènes. Néanmoins, la manière dont la structure des CLP peut moduler leur activité concernant l'activation de l'immunité végétale, reste mal comprise.

Cette étude visait à apporter de nouvelles perspectives sur ces relations structure-activité pour les CLPs de la famille de la surfactine produits par *Bacillus*, qui comptent parmi les mieux caractérisées pour la stimulation de l'ISR chez diverses plantes et contre un large spectre d'agents pathogènes. À cette fin, nous avons comparé le potentiel d'activation immunitaire de la surfactine canonique (Srf), produite par *B. velezensis*, avec celui de la pumilacidine (Pumi) et de la lichenysine (Liche), qui sont des variants naturels de la Srf produites par les espèces apparentées *B. pumilus* et *B. licheniformis*. De plus, nous avons exploité la flexibilité inhérente du mécanisme de biosynthèse des CLPs en enrichissant les milieux de culture en acides aminés à chaîne ramifiée (BCAAs) comme précurseurs biosynthétiques afin de générer de nouveaux variants peptidiques. Cela a permis d'étudier les déterminants structurels régissant l'activation de l'immunité végétale. Cette activité immunogène a été évaluée de manière exhaustive par rapport aux événements précoces de signalisation immunitaire, incluant la production d'espèces réactives de l'oxygène (ROS), l'influx de calcium (Ca^{2+}) et la production d'oxyde nitrique (NO), dans les racines et les protoplastes de racines *d'Arabidopsis thaliana*. Au niveau macroscopique, les CLPs ont également été comparés quant à leur capacité à déclencher une réponse immunitaire systémique (ISR) contre *Botrytis cinerea*.

Nos données révèlent que même des modifications structurelles mineures au sein du peptide influencent significativement l'activation immunitaire des plantes. Notamment, la nature des acides aminés aux positions 4 et/ou 7 s'avère critique pour une activité optimale : des substitutions Val/(i)Leu, comme dans Pumi, rendent la molécule inactive, tandis que Liche, avec un changement Glu/Gln, conserve une activité totale malgré la perte d'une charge négative nette. Cette dernière observation est particulièrement remarquable, car elle constitue la première caractérisation du potentiel immunogène de la Liche issue de l'espèce épiphyte bénéfique *B. licheniformis*. L'activité atténuée de Pumi est mise en relation avec le mode de vie endophyte de *B. pumilus*, ce qui indique la pertinence écologique d'un potentiel immunogène réduit de ce CLP. De plus, les variants de CLPs générés via l'ajout de BCAAs dépendent de la souche, avec de nouveaux variants structurels résultant de

substitutions d'acides aminés aux positions 3 ou 6. Bien que produits en quantités limitées, ils conservent un potentiel d'activation de la réponse immunitaire comparable à celui de leurs homologues canoniques. Enfin, en utilisant trois approches méthodologiques complémentaires, nous avons étudié les mécanismes sous-jacents à l'ISR déclenchée par la surfactine, révélant un rôle possible des phytoalexines de type camalexine et coumarine en tant que composés de défense des plantes.

Dans l'ensemble, ces résultats fournissent des informations précieuses sur les relations structure-activité des CLPs tout en soulignant la nécessité de poursuivre les recherches afin d'élucider pleinement leurs mécanismes précis d'activation immunitaire. Ce travail met en évidence le potentiel de découverte, d'ingénierie ou de synthèse de CLP hautement efficaces, et souligne l'importance d'étudier des composés peu étudiés mais puissants, tels que la lichenysine, pour des applications en protection des plantes.

Acknowledgments

My four years and a bit as a PhD candidate at TERRA, Gembloux Agro-Bio Tech, were transformative, filled with growth, friendship, and invaluable lessons. This journey has been one of the brightest chapters of my life.

First, I would like to express my deepest gratitude to my supervisors. Prof. Ongena, thank you for your unwavering patience and guidance. You taught me the value of perseverance and I learned to be more professional. Thank you! Prof. Dong, your expertise and encouragement kept me moving forward, and have me to be more positive. Without your support, I would not have been able to get this far, thank you!

Thanks to the support system of the Microbial Processes and Interactions (MiPI) Lab and the University of Liège, I was able to learn more, avoid unnecessary problems, and overcome some difficulties. Thanks to Dr. Christian Dubos for kindly donating *Arabidopsis* mutants *bglu42* and *f6'h1-1*. My sincere thanks also go to the China Scholarship Council, thanks for making this journey possible. Thanks to Shandong Agricultural University where I studied for seven years, to prepare for this experience.

Thank you to my thesis committee for the guidance throughout my PhD program; thank you to my jury members, for the insightful feedback that shaped my research and growth.

To the best colleagues ever: Jelena, Guillaume(s), Romain; Aurélien, Anthony, Cathy, Seb; Stéphanie, Marco, Sam, Andrew. Thank you for your tremendous supports, whether it was helping with experiments, data analysis, or simply brightening my days. Adrien, Farah, François, Willy, Vincent, Henry, Alizée, Gaëlle, Alexis, Cristina, Sigrid, Steven, Thomas, Kawtar, Viginie, Sonia, Jérôme, Nesrien, Ikram, Ange, Sofia, Juan, Andreea, Mariem, Arpita, Sandrino, Claire, Marjorie, Benoit, Zixin, Huan and other lovely labmates, your camaraderie made every challenge easier. Marina and Magritte, your constant assistance meant a lot to me.

Thank you all for the meaningful conversations that were an endless source of inspiration for me: Yundong, Xia, Ran, Jiahui, Jin, Huiyuan, Kaiyi, Yongfeng, Shuang, Lu, Aiping, Shuo, Yu, Yangyang, Shifeng, Hongru, Xiaoxian, Fangzhou, Lin, Tuyen, Aida, Xiaoyan, Yansen, Hongqing, Shadow, Said, Xiang, Yuqian, Lingshan, Liangliang. Stéphanie, your warmth stays with me; Elif, your kindness motivates me; Sydney and Cristian, your positivity energy is contagious; Amélie, your resilience cheers me up; Mauri, your brilliance shines bright; Steve, thanks for helping me rebuild my confidence from another perspective; Lijun, your friendship across distances is cherished; Baozhen, though missed your wedding, I know your happiness is boundless.

Finally, gratitude is extended to my parents for their unwavering support, unconditional love, and forgiveness for the years spent apart.

I still remember arriving in Belgium with a suitcase and a big backpack. That was a long journey through Hong Kong, Bangkok, and Dubai. A kind stranger at Brussels-Nord guided me to transfer between platforms, and Valy welcomed me into her home. Pierre and Henry, they helped me settle in gradually. This family made my first year warm and memorable.

With a heart full of gratitude, I step forward, and carry these great memories into the next chapter. Have a very good day and see you next time. ;)

Table of contents

List of figures

List of tables

List of acronyms

CLPs (cyclic lipopeptides)
Srf (surfactin)
Pumi (pumilacidin)
Liche (lichenysin)
BCAAs (branched-chain amino acids)
ISR (induced systemic resistance)
PBB (plant beneficial bacteria)
VOCs (volatile organic compounds)
PRRs (pattern-recognition receptors)
RKs (receptor kinases)
RPs (receptor-like proteins)
PAMPs (pathogen- associated molecular patterns)
MAMPs (microbe-associated molecular patterns)
DAMPs (damage-associated molecular patterns)
GSH (glutathione)
R genes (resistance genes)
ETI (effector triggered immunity)
ERFs (ethylene response factors)
ROS (reactive oxygen species)
RNS (reactive nitrogen species)
NR (nitrate reductase)
XOR (xanthine oxidoreductase)
ET (ethylene)
SA (salicylic acid)
JA (jasmonic acid)
ABA (abscisic acid)
GAs (gibberellins)
CKs (cytokinins)
CaMs (calmodulins)
CMLs (calmodulin-like proteins)
HR (hypersensitive response)
PCD (programmed cell death)
SAR (systemic acquired resistance)
FA (fatty acid)
AA (amino acid)
BGCs (biosynthetic gene clusters)
NRPSs (non-ribosomal peptide synthetases)
A (adenylation)
T (thiolation)

PCP (peptidyl carrier protein)
C (condensation)
Cs (starter condensation)
E (epimerization)
TE (thioesterase)
PKS (polyketide synthase)
AL (acyl ligase)
CMCs (critical micelle concentrations)
HPLC (high-performance liquid chromatography)
TFA (trifluoroacetic acid)
ACN (acetonitrile)
Q-TOF (quadrupole-time of flight)
LC (liquid chromatography)
MS (mass spectrometry)
UPLC (ultra performance liquid chromatography)
ESI (electrospray ionization)
NMR (nuclear magnetic resonance)
GC (gas chromatography)
$[ROS]_{intra}$ (intracellular reactive oxygen species)
dpi (days post infection)
RT-qPCR (reverse transcription quantitative polymerase chain reaction)

Chapter 1

General introduction

Part of the context presented in this chapter has been published in: Ding, N.; Dong, H.; Ongena, M. Bacterial Cyclic Lipopeptides as Triggers of Plant Immunity and Systemic Resistance Against Pathogens. *Plants* 2025, *14*, 2644. https://doi.org/10.3390/plants14172644.

1. Sustainable strategies in agriculture

Agriculture constitutes the principal foundation for global food security, essential for sustaining a growing human population (Kansman et al., 2023). However, agricultural productivity is continually threatened by pests and pathogens. This problem is intensified by climatic variability, agricultural intensification that reduces ecosystem biodiversity, and the limited genetic resistance found in many crop germplasm, all of which contribute to significant annual yield losses. While chemical pesticides provide an economically viable and rapid intervention, representing a conventional mainstay of crop protection, their protracted and intensive use presents significant risks to environmental integrity and public health (Etesami, 2024). In response, integrated and sustainable pest and disease management strategies have been developed.

Advanced monitoring systems utilize technological innovations, including satellite remote sensing, radar, unmanned aerial vehicles and so on to facilitate timely pest detection, forecasting, and precision management (Gao et al., 2020). Agricultural control practices are to disrupt pest life cycles using techniques such as adjusting sowing dates, inter-row weeding, crop rotation, and winter irrigation (Gómez et al., 2025; J. Liu et al., 2023). While physical control methods employ tools such as light traps with specific spectral lures, targeted chemical strategies involve the application of species-specific insect pheromones (Kansman et al., 2023). Biocontrol utilizes the predatory, parasitic, or antagonistic capacities of natural enemies within the ecosystem (Etesami, 2024). Furthermore, advances in biotechnology facilitate the development of genetically modified crops with enhanced heritable resistance to specific pests and diseases (Zafar et al., 2020).

1.1. Biocontrol and biopesticides

Biocontrol is mediated through several well-characterized mechanisms, notably the consumptive and non-consumptive effects of predators, the direct antagonism via microbially derived bioactive substances, the indirect method, such as the elicitation of plant innate immunity, and the deployment of semiochemical signals (Stenberg et al., 2021). To be clear, plant-growth promotion and the vectoring of biocontrol agents are not classified as mechanisms of biocontrol (Stenberg et al., 2021).

Entomopathogenic nematodes have been effectively deployed as biological insecticides in integrated pest management programs and demonstrate direct efficacy against various orchard insect pests (Hamrouni et al., 2025). Additionally, research has established that numerous bacterial genera, notably *Bacillus* and *Pseudomonas*, exhibit broad-spectrum antimicrobial activity against a wide range of pathogenic bacteria and fungi affecting plants; among fungal biological control agents, genera

such as *Trichoderma*, *Aspergillus*, *Penicillium* and certain yeasts are predominantly utilized for the suppression of both bacterial and fungal phytopathogens; select bacteriophages and mycoviruses have also been demonstrated to be effective as highly specific biocontrol agents against certain plant pathogens (Boro et al., 2022; Lahlali et al., 2022). The primary biocontrol mechanisms vary among microbial genera. For instance, *Trichoderma* spp. encompass mycoparasitism, competition for nutrients, and antibiosis, while *Bacillus* spp. predominantly utilize a diverse arsenal that includes the synthesis of lipopeptides and lytic enzymes, siderophore production, as well as the elicitation of induced systemic resistance (ISR) in host plants (Villavicencio-Vásquez et al., 2025).

Biopesticides are broadly classified into three types: biochemical pesticides, which are natural substances, like plant extracts or pheromones; plant-incorporated protectants, which are substances produced by plants after the incorporation of specific genetic material; microbial pesticides, based on bacteria, fungi, viruses, protozoa, or algae (Hamrouni et al., 2025). Globally, research is consistently directed toward creating new formulations characterized by ease of use, heightened efficacy against phytopathogens, applicability to diverse crops, and improved safety profiles for ecosystems and humans (Hamrouni et al., 2025). Formulation techniques aimed at ensuring stability during storage and distribution need further attention (Hamrouni et al., 2025). The timeline (Figure 1-1) represents the historical process of known biopesticides; in 2021, the global biocontrol market was valued at approximately USD 4.32 billion (Etesami et al., 2023; Hamrouni et al., 2025).

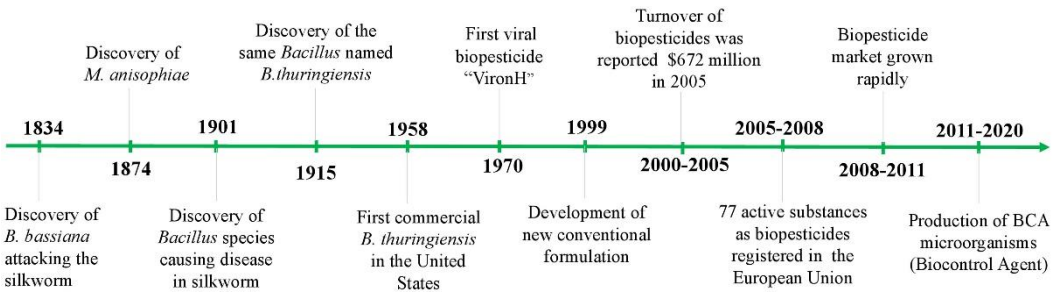

Figure 1-1 A historical timeline of key developments in biopesticides (Hamrouni et al., 2025).

It is worth mentioning that due to the complex interplay among the antagonist, pathogen, host plant, and the ambient environmental conditions, most biocontrol agents are not as effective as expected in field applications, after showing great efficacy in controlling/suppressing pathogens under laboratory conditions (Lahlali et al., 2022). This presents a significant challenge in the exploration and development of reliable biocontrol strategies.

1.1.1. Plant beneficial bacteria as biocontrol agents

As sessile organisms, plants are particularly vulnerable to environmental threats and have evolutionarily adapted by recruiting plant beneficial bacteria (PBB) from soil microbiomes. The application of PBB agents is considered as a safe and an eco-friendly way to increase both crops productivity and disease resistance (Dihazi et al., 2012). PBB such as *Bacillus*, *Pseudomonas*, *Acetobacter*, *Azospirillum*, *Paenibacillus*, *Serratia*, *Burkholderia*, *Herbaspirillum*, *Rhodococcus*, *Actinobacteria*, *and Lactobacillus* (Backer et al., 2018) boost plant growth by increasing nutrient absorption, activating the plant's defence mechanisms against pathogens, or suppressing pathogen populations (Khan et al., 2022). These microbial partners function as biocontrol agents, and enhance host resilience via two principal mechanisms, including direct antagonism through the inhibition or elimination of phytopathogens, as well as induction of systemic immune responses that prime the plant for enhanced defence (Aci et al., 2022; Vieira et al., 2024). The latter leads to enhanced resistance against subsequent infections, a phenomenon known as ISR.

The main genera of PBB are *Bacillus* and *Pseudomonas* (Hashem et al., 2019). *Bacillus*, such as *B. subtilis*, *B. velezensis*, *B. amyloliquefaciens*, *B. pumilus*, *B. pasteurii*, *B. mycoides*, *B. sphaericus*, *B. azotofixans* show great growth promoting activities (Saxena et al., 2020; Vessey, 2003). Additionally, *Bacillus* species serve as key biocontrol agents against various phytopathogens due to their production of antibiotics and resistant endospores (Shafi et al., 2017). Certain *Bacillus* species' antimicrobial metabolites can manage plant diseases as an alternative to harmful chemical pesticides, reducing health risks and environmental pollution (Fira et al., 2018). *Bacillus* spp. produce a range of small-sized compounds (also referred as bioactive secondary metabolites, BSMs), including non-ribosomally synthesized compounds (e.g., oligopeptides, cyclic lipopeptides (CLPs), and polyketides), as well as post-translationally modified molecules such as lanthipeptides and bacteriocins (Figure 1-2).

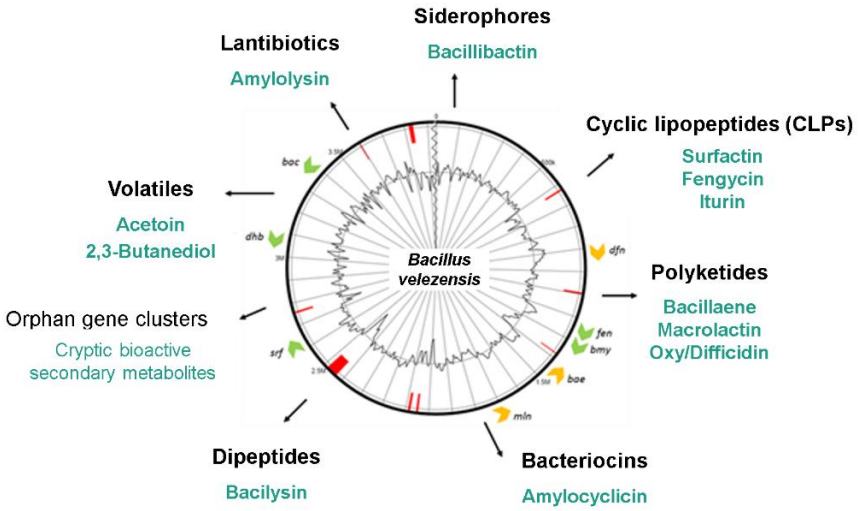

Figure 1-2 Bioactive molecules produced by *Bacillus velezensis.*

This figure represents *Bacillus velezensis* BSMs including polyketides, bacteriocins, dipeptides, volatile metabolites, lantibiotics, siderophores and cyclic lipopeptides (CLPs).

BSMs from *Pseudomonas* spp. also contribute to biocontrol by mediating complex interactions among plants, pathogens, and antagonists. Key BSMs involved in these interactions include phenazines, phloroglucinols, pyoluteorins, pyrrolnitrins, CLPs, hydrogen cyanide, and volatile organic compounds (VOCs) such as nunamycin and nunapeptin (Dimkić et al., 2022).

2. Plant immunity

2.1. Canonical plant responses to biotic challenges

Plants respond to diverse challenges by reprogramming their physiological processes (Molina et al., 2024). Plant cell walls act as safeguards against stresses that may influence wall composition or structure, and therefore cell wall integrity (Delmer et al., 2024). Pathogens must overcome the cell wall by degrading modifying enzymes (Zheng et al., 2021). When cell wall integrity changes, the signaling process would be activated according to different sensors or receptors that trigger specific adaptive responses to the new situation (Wolf, 2022).

In addition to the cell wall monitoring system, plasma membrane-anchored pattern-recognition receptors (PRRs), mainly receptor kinases (RKs) and receptor-like proteins (RLPs), help plants to detect pathogen-derived ligands, which are known as

pathogen- or microbe-associated molecular patterns (PAMPs or MAMPs), such as lipopolysaccharide, elongation factor EF-Tu, and flagellin from bacteria, chitin from fungi, and Pep13 from oomycete *Phytophthora megasperma* (Bender & Zipfel, 2023; Jones et al., 2024; Xu & Yang, 2025). Additionally, some receptors can also perceive plant self-derived damage-associated molecular patterns (DAMPs) such as ATP, oligosaccharides, NAD(P), glutathione (GSH), specialized peptides, oligogalacturonides from plant cells, released or synthesized upon plant tissue damage or infection by pathogens (De Lorenzo & Cervone, 2022; Jones et al., 2024; Xu & Yang, 2025). MAMP, PAMP or DAMP recognition by PRRs activate pattern triggered immunity (PTI) and disease resistance responses. This is often at the cost of reduced growth due to growth–defense trade-offs (Boller et al., 2009). The plant immune system also recognizes microbial effectors (Avr proteins) through intracellular receptors that are encoded by plant resistance (R) genes, or activating effector triggered immunity (ETI) (De Falco & Zipfel, 2021). PTI and ETI are shown to cooperate functionally in disease resistance, and ETI largely potentiates PTI (Ngou et al., 2021; Yuan, Jiang, et al., 2021; Yuan, Ngou, et al., 2021).

During plant-pathogen interactions, a series of signals are initiated to trigger plant defence responses. Pattern perception by PRRs activates complex signaling events within the plant which occurs across a timeframe of minutes to hours: the initial signals are triggered almost immediately after detection, hormone synthesis, phytoalexin synthesis and shifts in gene expression follow within a few hours, and these lead to later changes in growth and long-lasting resistance (Yu et al., 2017). These complex and diverse signaling pathways interact, forming intricate signal transduction networks. WRKYs and ethylene response factors (ERFs) are large families of plant-specific transcription factors that play a central role in regulating plant immune responses to a wide range of pathogens (Li et al., 2016). Although the specific calcium ion (Ca^{2+}) channels responsible for mediating the MAMP-induced increase in cytosolic calcium concentration ($[Ca^{2+}]_{cyt}$) remain unidentified, the biphasic elevation of cytosolic Ca^{2+} induced by MAMPs can be attributed to distinct sources: the initial peak is predominantly driven by an influx of extracellular Ca^{2+}, whereas the subsequent peak necessitates the release of Ca^{2+} from internal stores (Yu et al., 2017). Reactive oxygen species (ROS) comprise partially reduced oxygen derivatives, including superoxide ($O_2^{\bullet-}$), hydrogen peroxide (H_2O_2), as well as hydroxyl radicals ($^{\bullet}OH$) (X. Yu et al., 2017). The elevation of $[Ca^{2+}]_{cyt}$ appears to be a prerequisite for ROS generation triggered by MAMPs, while ROS burst plays a critical role in generating the secondary peak or sustained plateau of $[Ca^{2+}]_{cyt}$ (Ranf et al., 2011).

Reactive nitrogen species (RNS) comprise both nitrogen-centered radicals, such as nitric oxide (NO) and nitrogen dioxide (NO_2), as well as non-radical nitrogen-containing compounds, including nitrate (NO_3^-), nitrous acid (HNO_2), peroxynitrite ($ONOO^-$), nitroxyl anion (NO^-), nitrosonium cation (NO^+), dinitrogen tetroxide (N_2O_4), and dinitrogen trioxide (N_2O_3); among RNS, NO is the well studied one

(Gogoi et al., 2024). While enzyme nitrate reductase (NR) is the main contributor of NO production in plants (Hancock & Neill, 2019), studies employing NR-deficient *Arabidopsis* lines (*nia1*, *nia2*, and *nia1/nia2*) show that NO production dependent on NR is vital for multiple plant processes (Astier et al., 2018). Other enzymes such as xanthine oxidoreductase (XOR), have also been proposed to participate in NO production (Hancock & Neill, 2019). Although the precise enzymatic sources responsible for MAMP-induced NO biosynthesis in plants remain unidentified (Yu et al., 2017), this NO also appears to be closely linked to Ca^{2+} signaling, as evidenced by the inhibition of this response by Ca^{2+} channel blockers (Ma et al., 2008). When plants are exposed to light, ROS and RNS are predominantly generated in chloroplasts and peroxisomes, whereas under dark conditions, they are generated in mitochondria (Gogoi et al., 2024). NO and ROS could induce stomatal closure within an hour by MAMPs, along with the phytohormones ethylene (ET) and various oxylipins (Arnaud & Hwang, 2015; Melotto et al., 2006).

The model plant *Arabidopsis thaliana* exhibits a canonical defence hormone framework that salicylic acid (SA) primarily mediates resistance to biotrophic and hemibiotrophic pathogens, while jasmonic acid (JA) and ET are central to defence against necrotrophs (Kim et al., 2022). The signaling of other hormones, including abscisic acid (ABA), gibberellins (GAs), auxin, and cytokinins (CKs), modulates this framework principally through crosstalk with SA and JA pathways, introducing contextual ambivalence into the immune response (Kim et al., 2022).

Although immune responses are activated in both PTI and ETI, they are distinguished by distinct temporal dynamics and quantitative outputs (Kim et al., 2022). Upon recognition of pathogen-derived elicitors, the resistant host activates its signal transduction pathways, including the MAPK cascade and Ca^{2+} signaling, as well as R genes. The influx of Ca^{2+} into the cytoplasm activates calmodulins (CaMs) and calmodulin-like proteins (CMLs), induces downstream NO synthesis, and subsequently triggers primary immune responses, including the hypersensitive response (HR). Additionally, NO may regulate an HR/ programmed cell death (PCD) through a synergistic effect with ROS. Besides being a signal to activate systemic acquired resistance (SAR), ROS can directly act as antibacterial effectors and enhance the structural resistance of the host (Ding et al., 2022).

Current understanding of phytoalexins largely stems from two research approaches: intensive studies within a few plant families, notably Leguminosae (Fabaceae) and Solanaceae, and investigations of single or limited species across diverse families such as Amaryllidaceae, Euphorbiaceae, Orchidaceae, Chenopodiaceae, Compositae, and others (Jeet et al., 2014). Coumarins and camalexins are commonly documented phytoalexins. Coumarins are secondary metabolites derived from the phenylpropanoid pathway (Matern, 1991), found predominantly in higher plants though they have also been identified in certain microorganisms and animal species (Stringlis et al., 2019). Their accumulation is a defensive response to infection by

phytopathogens such as viruses, bacteria, fungi, and oomycetes (Stringlis et al., 2019). Natural coumarins, exhibit considerable structural diversity, being classified into four major categories based on their chemical architecture: simple coumarins, such as esculetin, scopoletin, umbelliferone; furanocoumarins, such as psoralen, bergapten, angelicin; pyranocoumarins, such as xanthyletin, seselin, as well as pyrone-ring substituted derivatives including biscoumarins such as dicoumarol, and benzocoumarins, such as urolithins (Annunziata et al., 2020). Camalexin, an indole phytoalexin biosynthesized from tryptophan in *Arabidopsis* and related *Brassicaceae* species, is strongly induced by various pathogens, including bacteria, fungi, viruses, and oomycetes; MAMPs-induced camalexin is frequently less pronounced than that triggered by direct pathogen infection (Ahuja et al., 2012; Millet et al., 2010).

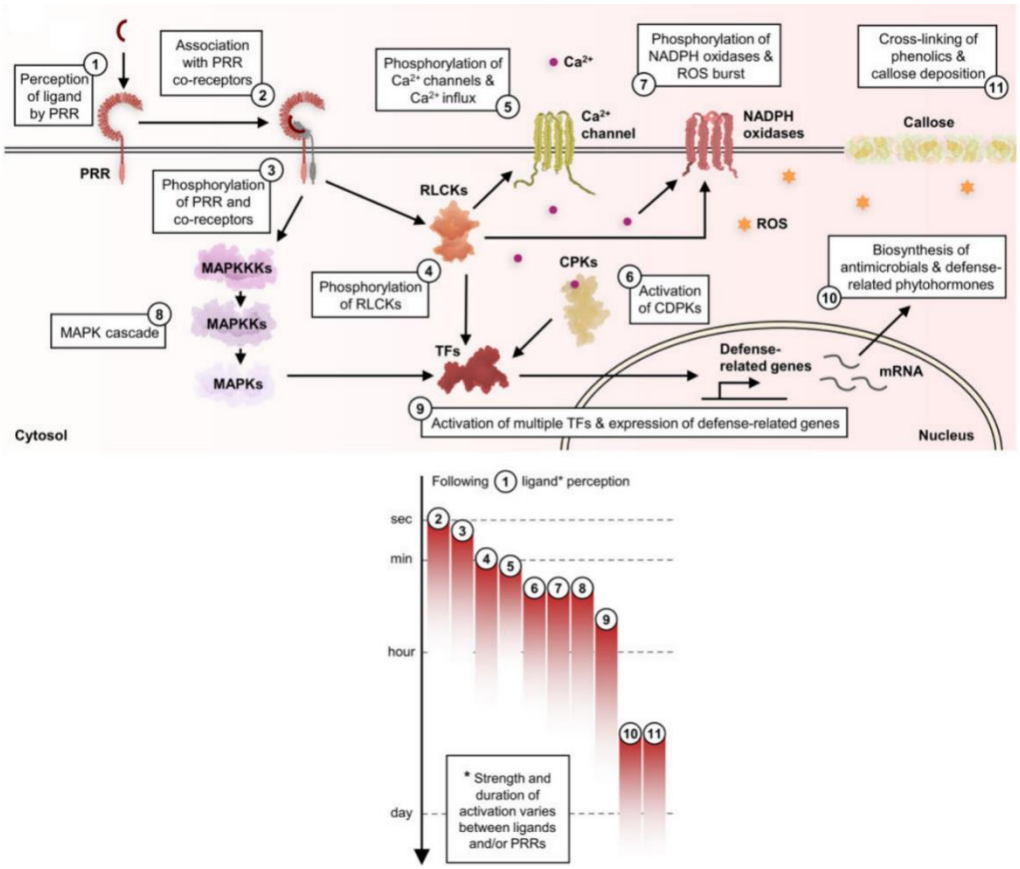

Figure 1-3 Plant immune signaling (Ngou et al., 2022).

Plant immune signaling begins when pattern recognition receptors detect ligands. This leads to signal productions such as Ca^{2+}, ROS, and then kinase activation, gene expression changes, phytohormones and phytoalexins biosynthesis, callose deposition across a timeframe of minutes to hours (Ngou et al., 2022).

Plant systemic immunity, activated through localized plant-microbe interactions, is categorized as either SAR or ISR, distinguished by both the infection site and the nature of the inducing microorganism (Vlot et al., 2021). SAR is predominantly initiated via ETI and confers broad-spectrum protection against diverse biotrophic pathogens, and its induction via PTI was also documented (Spoel & Dong, 2012). While SAR typically originates from foliar interactions with pathogenic microbes, ISR is initiated through root colonization by beneficial microorganisms (Vlot et al., 2021). Although SA serves as the primary signaling molecule in SAR, additional systemic signals have been identified that specifically activate distal immunity without affecting local defence responses (Vlot et al., 2021). Foliar infections that trigger SAR in *Arabidopsis* can modulate root/rhizosphere microbiome assembly, particularly enriching for PBBs, which subsequently activate ISR, establishing a layered defence strategy (Vlot et al., 2021). A demonstrated example includes the leaf pathogen *Hyaloperonospora arabidopsidis* inducing root recruitment of PBB strains *Xanthomonas*, *Stenotrophomonas*, and *Microbacterium* and thus collectively priming *Arabidopsis* for enhanced pathogen defence (Berendsen et al., 2018).

2.1.1. Plant ISR trigged by PBB

ISR is phenotypically similar to SAR but different in some aspects. For instance, ISR results in a systemic, non-specific and broad-spectrum action that shares phenotypic similarity to the SAR with the same efficiency; however, ISR does not induce HR and visible symptoms like how SAR does (Salwan et al., 2022). ISR and SAR share common signaling receptor non-expresser of NPR1, which finally provides a broad spectrum of resistance against plant pathogens (Cao et al., 1997; Pieterse et al., 1998). ISR is mainly dependent on phytohormones JA and ET (Panpatte et al., 2020). For instance, ISR elicited by *Bacillus cereus* AR156 in *Arabidopsis* operates through the NPR1-dependent co-activation of SA- and JA/ET-mediated signaling pathways (Niu et al., 2011). Additionally, colonization of *Arabidopsis thaliana* roots by *Pseudomonas fluorescens* WCS417r induces JA/ET-dependent ISR effective against diverse pathogens, with with the R2R3-MYB transcription factor MYB72 acting upstream of ET in this ISR pathway; MYC2 also acts as ISR transcriptional regulators in early recognition during *Pseudomonas fluorescens* WCS417r mediated immune response (Pozo et al., 2008; Van der Ent et al., 2008; Pieterse et al., 2025). Progress in elucidating the mechanistic basis and practical application of ISR induced by plant-beneficial rhizobacteria is summarized in Figure 1-4.

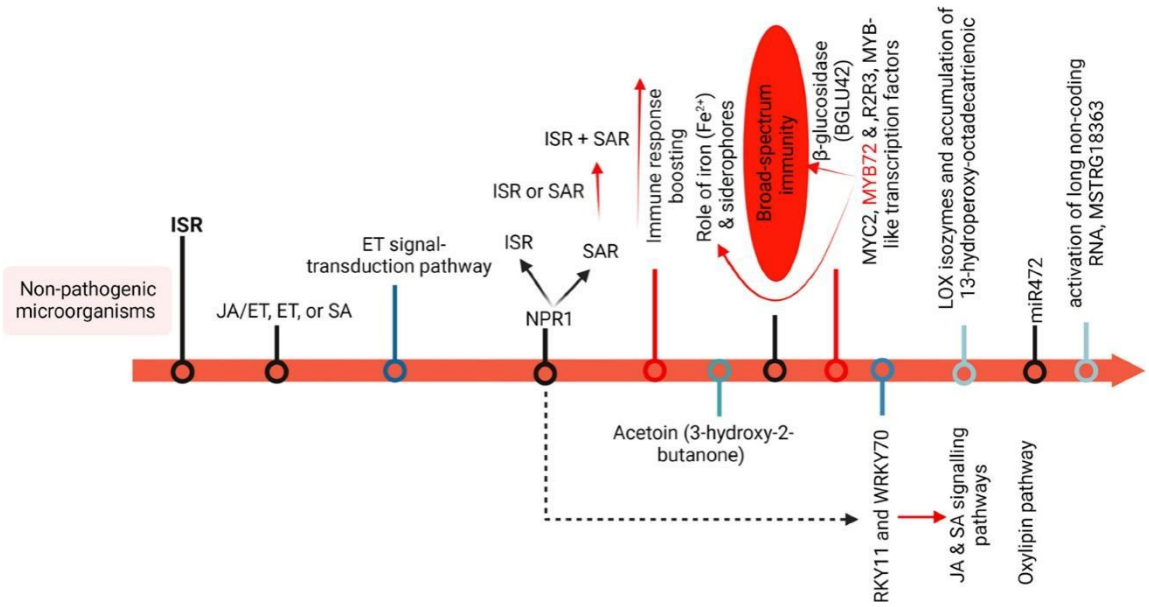

Figure 1-4 Key discoveries in the understanding and application of ISR elicited by plant-beneficial rhizobacteria (Salwan et al., 2023).

Several beneficial rhizosphere microorganisms both promote plant growth and elicit ISR, indicating immunomodulatory strategies that balance defense cost-efficiency with the maintenance of mutualistic symbiosis (Pieterse et al., 2025). *Bacillus*, *Pseudomonas* and *Azospirillum* represent the primary PBBs known to trigger ISR (Kloepper et al., 2004; Van Wees et al., 2008). For instance, *Bacillus*-triggered ISR provides effective protection against a wide range of pathogens, including systemic viruses, leaf-spotting bacteria and fungi, crown rot, stem blight, root-knot nematodes, late blight, blue mold, and damping-off (Etesami et al., 2023). Certain symbiotic rhizobacteria have demonstrated ISR activity when applied as coinoculants with other PBB strains (Elbadry et al., 2006). ISR induced by a specific PBB strain can confer broad-spectrum resistance within a plant, yet the activity of the strain is frequently host-specific (Charpe et al., 2025).

PBB-mediated ISR is generally considered to operate independently of the discrete ligand-receptor recognition events that characterize PTI and ETI, suggesting that PBB-ISR engages plant immune networks through mechanistic principles that extend beyond, and are not fully explained by the classical PTI/ETI paradigm (Pieterse et al., 2025). Root-synthesized coumarins have been identified as key systemic mediators of *Pseudomonas*-mediated ISR along the rhizosphere-to-shoot signaling axis, functioning additionally as integrative molecular signals that coordinate iron homeostasis and plant growth promotion (Stassen et al., 2021; Verbon et al., 2017).

Bacillus cereus AR156 has been reported to elicit ISR-mediated resistance against *Botrytis cinerea*, *Pseudomonas syringae* pv. tomato DC3000, and *Phytophthora capsici* in *Arabidopsis*, with camalexin biosynthesis priming identified as a key mechanistic basis of this broad-spectrum protective response (Li et al., 2024).

Among all the elicitors from PBB metabolites that trigger ISR in plants, such as acyl-homoserine lactones, CLPs, rhamnolipids, N-alkylated benzylamine derivatives, siderophores, VOCs, and other antibiotics (polyketides, phenazine) (Pršić & Ongena, 2020), CLPs produced by *Bacillus* and *Pseudomonas* were well documented. Within this particular nutritional environment, the bacterium also adjusts the composition of produced Srf homologs, preferentially generating variants that exhibit heightened efficacy in inducing plant immune responses (Hoff et al., 2021).

3. CLP structures, biosynthesis, ecological and biocontrol functions

3.1. Chemical diversity of CLPs

PBB represent a phylogenetically diverse group of rhizosphere-associated microorganisms that promote crop productivity. Many PBB can produce CLPs but CLPs from *Bacillus* and *Pseudomonas* spp. are the best described (Table 1-1 and Figure 1-5).

Table 1-1 Simplified primary chemical structures of CLPs reported to trigger ISR in plants. *a*Thr refers to *allo*-threonine. The underlined AA residues refer to the AAs in the cyclic peptide ring. The red color marked D-AAs, and the rest are L-AAs. So far, AAs of sessilin A to be L or D form are not clear.

CLPs	FA	AA																
		1	2	3	4	5	6	7	8	9	10	11	12	13	14	15	16	17	18
Surfactins	C_{12}-C_{17}	Glu	Leu	Leu	Val	Asp	Leu	Leu	/	/	/	/	/	/	/	/	/	/	/
Fengycins	C_{14}-C_{18}	Glu	Orn	Tyr	*a*Thr	Glu	Ala	Pro	Gln	Tyr	Ile	/	/	/	/	/	/	/	/
Iturins	C_{14}-C_{17}	Asn	Tyr	Asn	Gln	Pro	Asn	Ser	/	/	/								
Bacillomycins	C_{14}-C_{17}	Asn	Tyr	Asn	Pro	Glu	Ser	Thr	/	/	/								
Massetolide A	C_{10}	Leu	Glu	*a*Thr	*a*Ile	Leu	Ser	Leu	Ser	Ile	/	/	/	/	/	/	/	/	/
WLIP	C_{10}	Leu	Glu	*a*Thr	Val	Leu	Ser	Leu	Ser	Ile	/	/	/	/	/	/	/	/	/
Sessilin A	C_8	Dhb	Pro	Ser	Leu	Val	Gln	Leu	Val	Val	Gln	Leu	Val	Dhb	Thr	Ile	Hse	Dab	Lys
Orfamide A	C_{14}	Leu	Glu	*a*Thr	Ile	Leu	Ser	Leu	Leu	Ser	Val	/	/	/	/	/	/	/	/

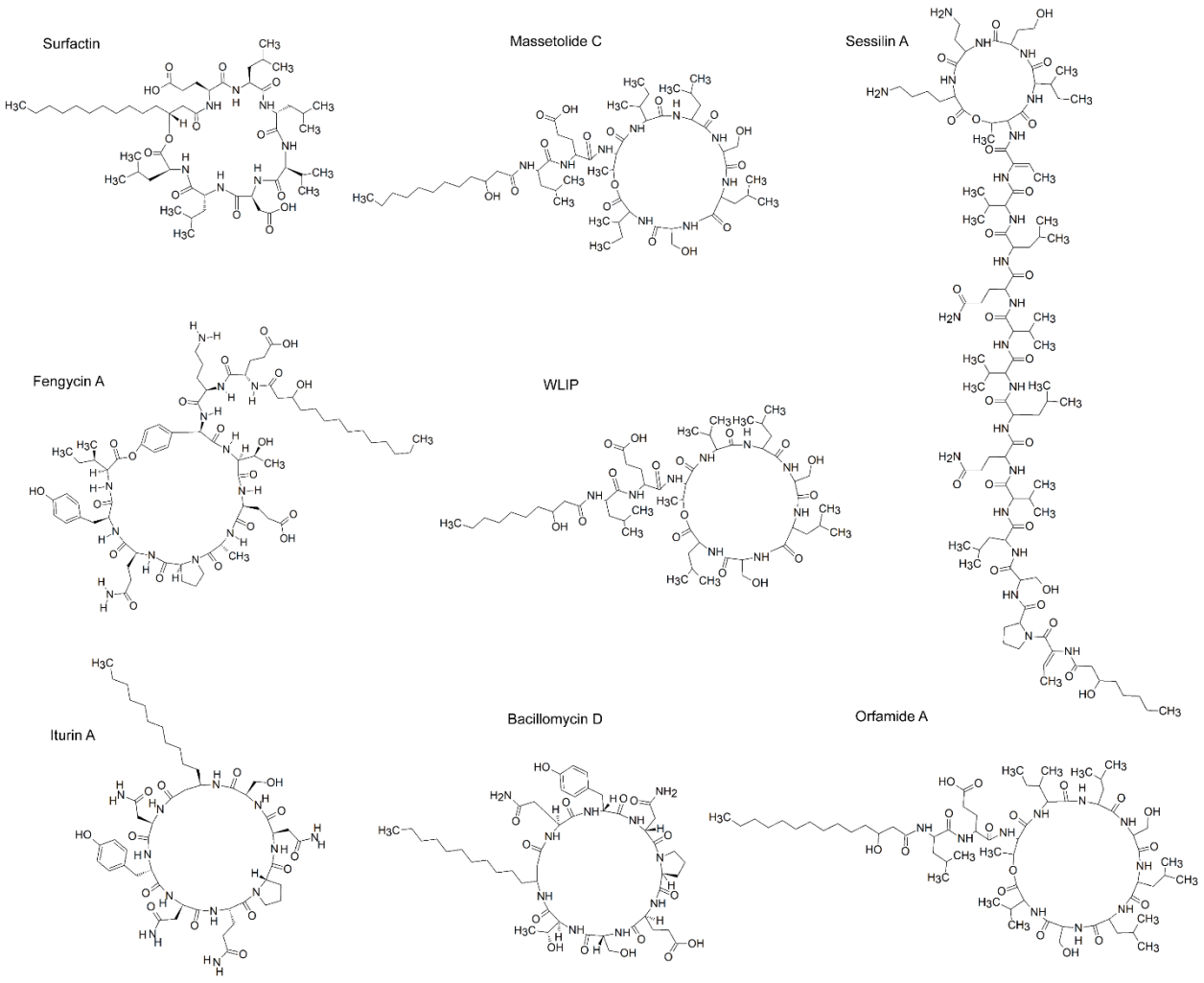

Figure 1-5 Chemical structures of main CLPs with ISR-inducing activity.

The figure represents the mentioned CLPs (surfactin, fengycin A, iturin A, massetolide C, WLIP, bacillomycin D, sessilin A, and orfamide A) drawn with ChemSketch 12.01.

3.1.1. *Bacillus* CLPs

Bacillus-derived CLPs are classified into three principal families: Surfactins (including surfactin, pumilacidin, lichenysin, bamilocyn, and halobacilin), Fengycins (fengycin/plipastatin and maltacin), and Iturins (iturin, mycosubtilin, bacillomycin, mojavensin, mixirins, and bacillopeptins) (Dobrzyński et al., 2023; Miljaković et al., 2020; Théatre et al., 2022). Additional structurally distinct CLPs include kurstakin,

locillomycin, antiadhesin, circulocin, and licheniformin (Théatre et al., 2022). The structures of main *Bacillus* CLPs are presented in Figure 1-6. These compounds exhibit variations in both their FA moieties (ranging from β-hydroxy to β-amino forms, with either ester or amide linkages) and their cyclic peptide structures (comprising 5-10 amino acid residues in various L/D configurations) (Théatre et al., 2022). The β-hydroxy-type CLPs, including surfactin, fengycin, kurstakin, antiadhesin, bamylocin A, circulocin, and locillomycin, predominantly feature ester bonds, while β-amino-type compounds like iturin, licheniformin contain characteristic amide linkages. Notably, some CLPs such as circulocins incorporate unusual guanylated FA chains (Théatre et al., 2022). Functionally, each CLP family displays distinct antimicrobial profiles. Surfactins exhibit some limited activity against both bacteria and fungi, while iturins and fengycins demonstrate particularly potent antifungal properties (Miljaković et al., 2020; Rabbee et al., 2023).

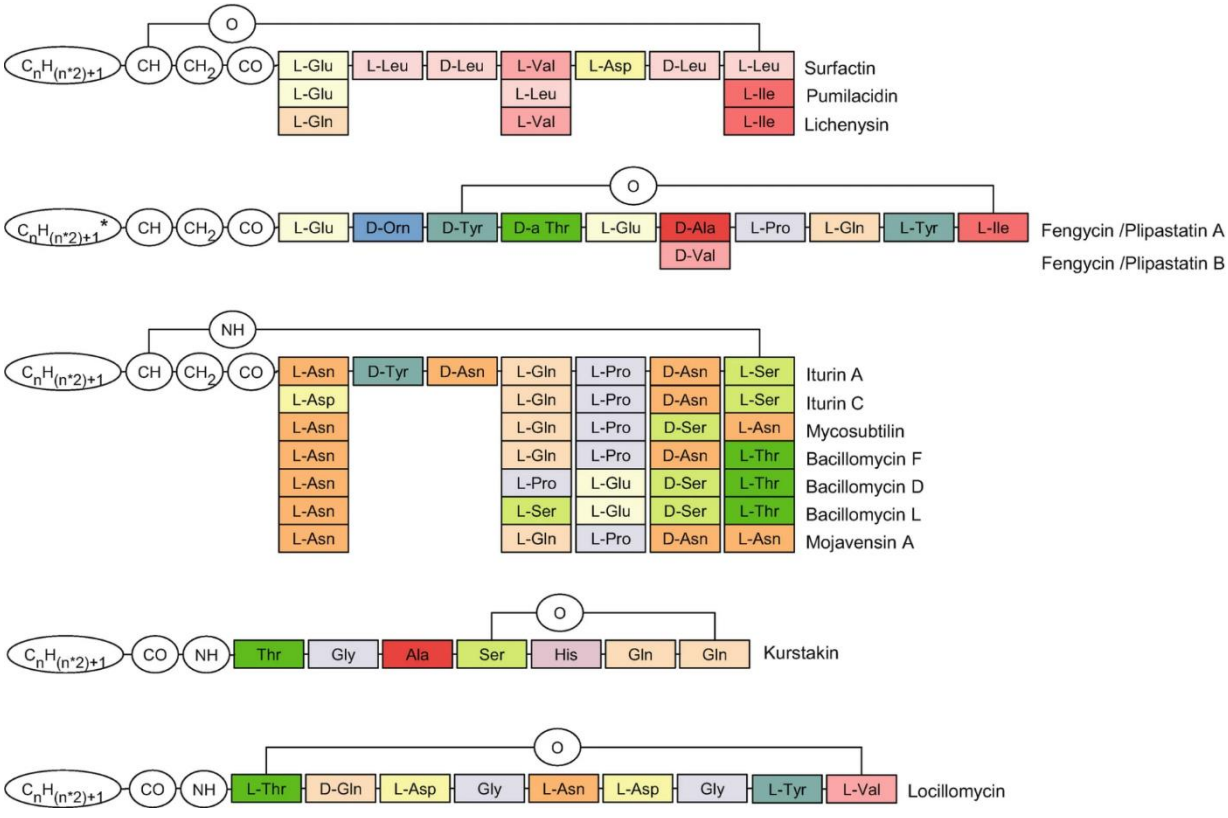

Figure 1-6 Structures of main lipopeptide families from *Bacillus* (Théatre et al., 2022).

3.1.2. *Pseudomonas* CLPs

CLPs produced by *Pseudomonas* species can be categorized based on whether they are derived from beneficial strains (PBB, biocontrol agents) or pathogenic strains (phytopathogens). This division highlights the dual roles of *Pseudomonas* CLPs, either as biocontrol tools in sustainable agriculture or as virulence determinants in plant diseases, depending on the ecological nature of the producing strain (Oni et al., 2022).

Beneficial *Pseudomonas* strains, such as *P. fluorescens*, *P. putida*, and *P. protegens*, produce CLPs that contribute to biocontrol, biofilm formation, and plant growth promotion (Raaijmakers et al., 2006). These include the viscosin group (e.g., viscosin, viscosinamide, massetolide, WLIP, pseudodesmin, pseudophomin), the amphisin group (e.g., lokisin/anikasin, milkisin/stechlisin/tensin, arthrofactin, pholipeptin, amphisin, oakridgin, nepenthesin), and the bananamide group (e.g., bananamide A-G, MDN-0066, prosekin) (Raaijmakers et al., 2006). Additional CLPs from beneficial strains include orfamide, putisolvin, gacamide, xantholysin, entolysin, and cocoyamide, which exhibit antimicrobial and surfactant properties that support their role in microbial competition and root colonization (Cesa-Luna et al., 2023; Oni et al., 2022; Raaijmakers et al., 2006).

In contrast, pathogenic *Pseudomonas* strains, such as *P. syringae*, *P. tolaasii*, and *P. corrugata*, produce CLPs that function as virulence factors that promote host cell lysis through pore formation, disrupting host cell membranes and promoting disease (Cesa-Luna et al., 2023). Pathogenic *Pseudomonas* CLPs primarily belong to the Mycin (e.g., syringotoxin) and Peptin (e.g., fuscopeptin) families (Cesa-Luna et al., 2023). The syringomycin group (e.g., syringomycin, syringostatin, pseudomycin A, cormycin A, syringafactin, cichofactin, virginiafactin, thanamycin) is particularly notable for its phytotoxic effects (Raaijmakers et al., 2006). Similarly, the tolaasin group (e.g., tolaasin, sessilin, corpeptin, FP-B) induces necrosis in plants and mushrooms, while the poaeamide group (e.g., PPZPM, poaeamide A) is associated with pathogenic *P. poae* (Raaijmakers et al., 2006).

3.1.3. CLPs from other bacterial genera

Besides *Bacillus* and *Pseudomonas* species, numerous soil-dwelling bacteria that contribute to plant health and ecological adaptation also produce CLPs. Among these, *Paenibacillus*-derived CLPs exhibit remarkable structural and functional diversity. Fusaricidin, a non-cationic lipopeptide structurally analogous to surfactins, fengycins, and iturins, features a hexapeptide ring with both ester and amide linkages, along with a guanidinylated β-hydroxy fatty acid (FA) moiety (Grady et al., 2016; Olishevska et al., 2019). Structural variations among fusaricidins arise from amino acid (AA) substitutions at three positions within the peptide ring, conferring activity against

fungi and gram-positive bacteria (Grady et al., 2016). *Paenibacillus* also produces cationic CLPs including: the polymyxin family (polymyxin A, B, C, D, E/colistin, M/mattacin, P, S, T), which vary in AA composition at specific residue positions; octapeptins (e.g., battacin) that exhibit broad-spectrum antimicrobial activity with reduced toxicity; the 13-AA-residue paenibacterin that disrupts both outer and cytoplasmic membranes; and other structurally distinct cationic CLPs such as polypeptins (such as pelgipeptin), paenibacterin, and gavaserin (Cochrane & Vederas, 2016; Grady et al., 2016; Huang & Yousef, 2014). Notably, octapeptins demonstrate efficacy against both gram-negative and gram-positive bacteria through mechanisms distinct from classical polymyxins (Cochrane & Vederas, 2016; Grady et al., 2016; Huang & Yousef, 2014).

Serratia species synthesize structurally distinct CLPs, primarily from the serrawettin family (serratamolide A to G, serrawettin W2 to W3). Serratamolide A (serrawettin W1) features a symmetric dilactone structure with two β-hydroxy FAs linked to two AAs (L-Ser_1-L-Ser_2), displaying antitumor, antimicrobial, and plant-protective properties (Clements et al., 2019; Heath et al., 1961; Thies et al., 2014). Structural variations among serrawettin homologs (serratamolide B–G) arise FA chain lengths (C_8–C_{14}) and unsaturation patterns (Clements et al., 2019). In contrast, serrawettin W2 contains a pentapeptide core (D-Leu_1-L-Ser_2-L-Thr_3-D-Phe_4-L-Ile_5) (Clements et al., 2019). The stephensiolide family (A-K), originally identified from mosquito-associated *Serratia* sp., combines antibiotic activity with roles in bacterial motility. Genomic analyses suggest these compounds may facilitate ecological niche colonization (Ganley et al., 2018).

Actinomycetia-class bacteria represent a significant source of structurally diverse CLPs with notable bioactivities. *Kitasatospora cystarginea* produces cystargamides, characterized by a hexapeptide ring linked to an unusual 2,3-epoxy FA (C_{10}) chain. Notably, cystargamide B has emerged as a promising lead compound for dengue fever treatment (Kitani et al., 2018). *Actinoplanes* species synthesize ramoplanin, a lipoglycodepsipeptide antibiotic featuring a 16-AA cyclic peptide conjugated to C_8-C_{10} FA, demonstrating potent activity against gram-positive bacteria (Kügler et al., 2015). *Streptomyces* species exhibit remarkable biosynthetic capacity, producing numerous CLPs including the clinically approved antibiotic daptomycin (Cubicin®), containing a 13-AA cyclic structure, some calcium-dependent antibiotics (CDA, A54145) and other structurally distinct compounds (amphomycin, laspartomycin, arylomycins) (Aftab & Sajid, 2017; Kügler et al., 2015; S. Zhang et al., 2023).

3.2. Biosynthesis of CLPs

CLP biosynthesis is a tightly regulated, multistep process which involves three key stages: precursor activation, sequential peptide chain elongation with concurrent

FA incorporation, and final export of the mature metabolite (Dini et al., 2024; Qi et al., 2023). The modules of a non-ribosomal peptide, each responsible for incorporating a specific AA, are generally arranged in an order that is colinear with the resulting peptide sequence (Théatre et al., 2021). These multi-modular enzyme complexes are encoded by well-characterized giant biosynthetic gene clusters (BGCs) (De Roo et al., 2022; Götze & Stallforth, 2020), which have been identified and characterized in *Bacillus* and *Pseudomonas* species (Roongsawang et al., 2011). Non-ribosomal peptide synthetases (NRPSs) function as sophisticated molecular assembly lines, incorporating AA residues and facilitating various cyclization reactions (Götze & Stallforth, 2020) due to functional domains: adenylation (A), thiolation/peptidyl carrier protein (T/PCP), condensation (C), starter condensation (Cs), epimerization (E), thioesterase (TE) (Kopp & Marahiel, 2007; Pilz et al., 2023; Strieker et al., 2010).

Here, Srf, the widely characterized model CLP is used to explain CLPs synthesis. Firstly, the hydrophobic FA and hydrophilic AA moieties of Srf are synthesized independently: FA chains, including both straight and branched forms, are derived from acetyl-CoA and malonyl-CoA via elongation and modification (Qin et al., 2025), while AA biosynthesis pathways supply the requisite peptide building blocks (Qiao et al., 2024; Wu et al., 2019). Then, Srf is assembled by the NRPS complex via a thiotemplate mechanism. In *Bacillus* spp., this process is orchestrated by a 27 kb gene cluster encoding three NRPS subunits: *SrfAA* (402 kDa), *SrfAB* (401 kDa), and *SrfAC* (144 kDa) (Qin et al., 2025). This enzymatic assembly forms a linear arrangement of seven catalytic modules, with each module sequentially incorporating a specific AA into the growing peptide chain (Kashif et al., 2022; Yasmin et al., 2022). *SrfAA* and *SrfAB* each incorporate three AAs (Leu-Glu-Val and Asp-Val-Leu, respectively), while *SrfAC* adds the final Leu residue (Yasmin et al., 2022). Distinguished from the classic A-T structure by a C-A-T architecture, the initiation NRPS module contains an N-terminal Cs domain, which is responsible for attaching a CoA-activated β-hydroxy FA (largely sourced from primary metabolism) to the initial AA (Théatre et al., 2021). Each NRPS module minimally comprises three core domains: an A domain that selects and activates specific AA substrates, T/PCP binds activated residues via thioester linkage, and C domain catalyzes peptide bond formation between adjacent PCP-bound residues (Kopp & Marahiel, 2007; Ongena & Jacques, 2008). Optional E domains convert selected L-AAs to their D-configuration, which enhances structural diversity. The terminal module contains a TE domain that release the Srf via hydrolysis or macrocyclization, ultimately generating cyclic (including branched cyclic) lipopeptide, linking Leu_7 to the FA hydroxyl group (Kopp & Marahiel, 2007). Last, newly synthesized Srf is secreted via dedicated efflux systems, preventing cytotoxic accumulation and facilitating ecological functions (Rahman et al., 2021).

For most strains, CLPs are biosynthesized exclusively through NRPS-mediated thiotemplate mechanisms (Raaijmakers et al., 2010). However, *Bacillus* species employ distinct pathways for different CLP families: the Surfactin and Fengycin families, containing β-hydroxy FAs, are produced by dedicated NRPS systems; the

iturin family, characterized by β-amino FAs, is synthesized via a polyketide synthase-non-ribosomal peptide synthetase (PKS-NRPS) hybrid pathway (Yang et al., 2020). The locillomycin biosynthetic machinery also employs a PKS-NRPS hybrid complex that substitutes the canonical Cs domain with an integrated PKS acyl ligase (AL) domain for FA incorporation (Duban et al., 2022). In Bacilli, three efflux pumps (YcxA, KrsE, and YerP) mediate Srf export, and overexpressing each corresponding gene individually increased its release rate (Théatre et al., 2021).

3.2.1 Branched-chain amino acids related CLP biosynthesis

Figure 1-7 presents the branched-chain amino acids (BCAAs, L-valine (L-Val), L-leucine (L-Leu), L-isoleucine (L-Ile)) serve as primary metabolic precursors for branched-chain FA biosynthesis (Xia & Wen, 2023). This occurs through three distinct metabolic phases in Srf biosynthesis: biosynthesis of the BCAAs themselves, generation of branched-chain FA and CoA-activated 3-hydroxy FA precursors, as well as NRPS-mediated assembly of the lipopeptide scaffold. Lately, the influence of each BCAA as precursor in the growth medium of *Bacillus velezensis* YA215 on the FA structure of surfactin (Yu et al., 2024) or *Bacillus subtilis* ATCC 6633 on the FA structure of mycosubtilin was investigated (Guez et al., 2022).

Core enzymes of central carbon metabolism, including glycolysis, the pentose phosphate pathway, and the citric acid cycle, critically influence AA and FA metabolism. These pathways collectively supply essential precursors and metabolic energy to drive enhanced Srf biosynthesis through both direct and indirect mechanisms (Xia & Wen, 2023). Exogenously supplied AAs can modify both the AA sequence of the peptide ring and the structure of the hydroxy FA in the resulting CLPs (Liu et al., 2012). While it is known that supplementation with BCAAs can direct the production of CLP variants with AA substitutions at positions 2, 4, or 7 (Grangemard et al., 1999), research specifically shows that increasing L-Val in the culture medium leads to a dose-dependent rise in the production of the $SrfVal_7$ variant (Peypoux & Michel, 1992). Supplementation with L-Ile or L-Val can boost the production of the $SrfVal_7$ variant (Peypoux & Michel, 1992). Of the BCAAs tested (L-Val, L-Leu, and L-Ile), the addition of L-Val led to the greatest relative yield of Srf (Yu et al., 2024). Additionally, genetic engineering of the branched fatty acid metabolic pathway (such as influencing the BCAA degradation) in *Bacillus subtilis* was used to enhance the production of C_{14}Srf (Dhali et al., 2017).

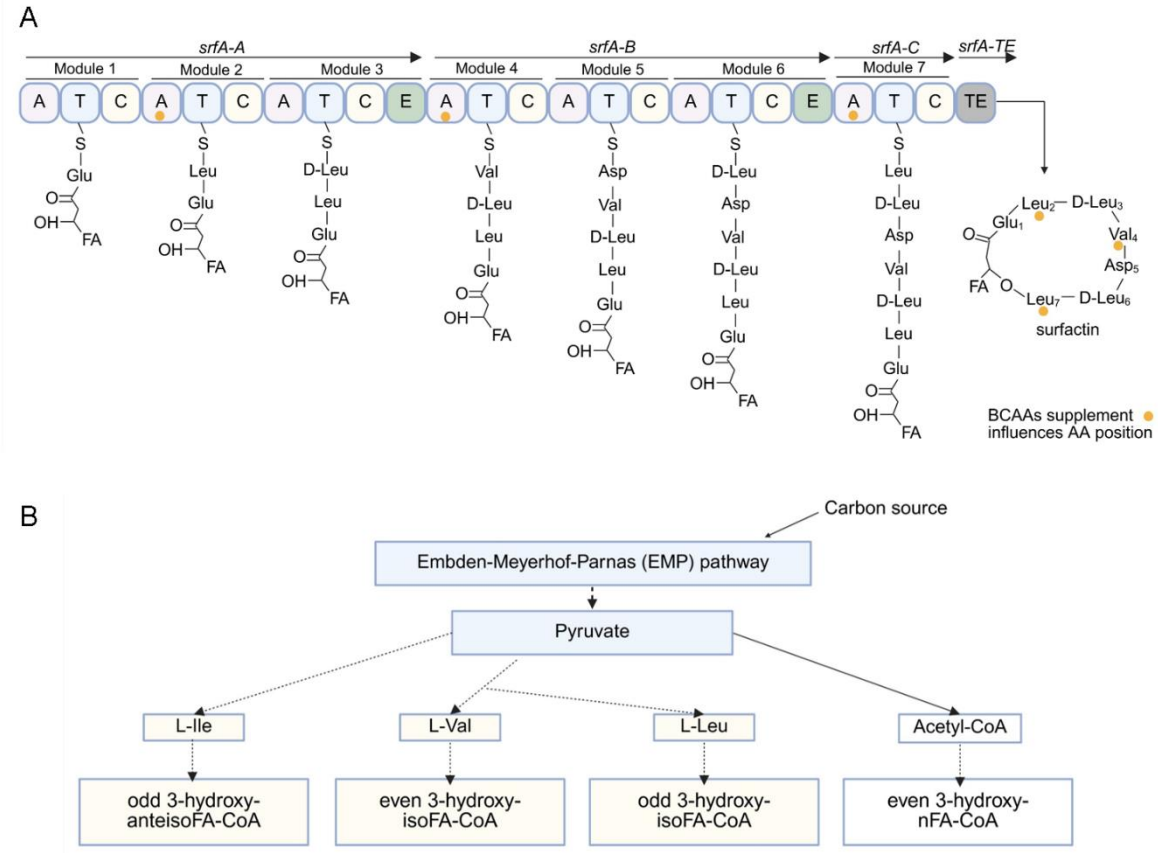

Figure 1-7 The biosynthesis pathways of branched-chain amino acids participating in Srf biosynthesis.

A. Supplementation with BCAAs direct the production of Srf variants with AA substitutions; **B**. The biosynthesis pathways of branched-chain amino acids participating in Srf FA biosynthesis.

3.3. Ecological functions of CLPs

3.3.1. Swarming motility

The amphiphilic nature of CLPs, from their hydrophobic FA chains and hydrophilic peptide moieties, enables CLPs to function as potent biosurfactants, reducing surface tension at interfaces, thereby diminishing friction between the producing bacteria and solid surfaces; this reduction in friction facilitates a form of surface translocation known as sliding motility (Jautzus et al., 2022; van Gestel et al., 2015). Furthermore, specific CLPs such as Srf have been demonstrated to promote flagellar-dependent

swarming motility by upregulating the synthesis of flagella (Ghelardi et al., 2012). Collectively, these mechanisms of enhanced motility are critical for bacterial colonization of the rhizosphere, as they allow CLP-producing bacteria to the root surface, access new niches, and initiate an escape response from antagonistic signals produced by competing microbes (Andrić et al., 2021; Guan et al., 2024; Romanowski et al., 2023; Zhou et al., 2024).

3.3.2. Biofilm development

Biofilm formation is a developmental process wherein microbial cells adhere to each other and become encased within a self-produced extracellular polymeric matrix (Arnaouteli et al., 2021). This structure provides a protective barrier for the microbial community against environmental toxins and impedes infiltration by competing organisms (Arnaouteli et al., 2016; Molina-Santiago et al., 2019). The role of Srf in biofilm formation and subsequent root colonization is strain-specific among *Bacillus* species (Boubsi et al., 2023; Thérien et al., 2020). Other CLPs are also key regulators of biofilm dynamics: massetolide A, xantholysin, and sessilin promote biofilm formation, while orfamide, viscosin, arthrofactin, and putisolvin facilitate biofilm dispersal (Bonnichsen et al., 2015; Kuiper et al., 2004; Zhou et al., 2024).

3.3.3. Antimicrobial function

As antimicrobial agents, CLPs have a direct inhibitory effect on phytopathogens (Markelova & Chumak, 2025). Changes in both FA and AA alter the structure of CLP, thereby modulating its antimicrobial function. Among the mycosubtilin isoforms, anteiso-C_{17} exhibited stronger antifungal activity against *B. cinerea* compared to iso-C_{17}, whereas the straight-chain n-C_{16} demonstrated higher efficacy than its branched-chain counterpart, iso-C_{16} (Béchet et al., 2013). Extending the fatty acyl chain length of paenipeptins from C_7 to C_8 or replacing valine with isoleucine at position 2 in the peptide core resulted in enhanced antimicrobial activity and increased hemolytic effects as the overall hydrophobicity of the lipopeptides increased (Huang et al., 2017).

3.4. Biocontrol function and agricultural use of CLPs

CLPs are versatile biocontrol agents that fight plant pathogens in three key ways: they help the original strain outcompete pathogens for space and resources, directly kill fungi with antimicrobial compounds, and boost the plant's overall immune system (Sani et al., 2024), which positions them as promising biopesticides. Additionally, their amphiphilic properties give CLPs remarkably low critical micelle concentrations (CMCs), enabling them to function as effective additives that enhance the surfactant properties of pesticide sprays (Sani et al., 2024), which makes them great helpers for

current pesticide products. However, due to the high associated production costs and the low yields characteristic of known microbial production strains, the commercial production of high-purity CLPs (e.g., ≥98%) remains too expensive to invest, with current market prices estimated in the range of thousands of euros per gram (www.sigmaaldrich.com). Therefore, the industrial-scale production and commercial deployment of CLPs remain to be fully realized.

4. CLPs as ISR inducers

As promising biocontrol agents, CLPs also play key roles as elicitors of ISR in plants. Studies have generally been carried out with a loss of function in CLP-deficient mutant strains compared to the wild type, and/or bioassays showing systemic resistance induced by treatment with CLP compounds that have been isolated from bacterial crude extracts, and are sufficiently pure as determined by high-performance liquid chromatography (HPLC). Common experimental designs include pretreating roots with CLPs or bacterial strains, then challenging leaves with a pathogen (using either seedlings or detached leaves); treating leaves locally with CLPs or bacteria, then inoculating distal leaves with a pathogen; or treating roots in soil, then applying a stem pathogen.

4.1. CLPs as inducers of plant-species-dependent ISR

Bacillus-derived CLPs, particularly those from the Surfactin, Fengycin, and Iturin families demonstrate varying capacities to activate the ISR, depending on both the host plant and the challenging pathogen. Surfactin is the most well studied for triggering ISR in many plants, especially dicotyledons, such as in bean, tomato, grapevine, *Arabidopsis*, and tobacco against *Botrytis cinerea*; in melon against *Podosphaera fusca*; in strawberry against *Colletotrichum gloeosporioides*; in peanut against *Sclerotium rolfsii* and *Athelia rolfsii*; in *Arabidopsis* against *Pseudomonas syringae* (Altrão et al., 2022; Cawoy et al., 2014; Debois et al., 2015; Farace et al., 2015; García-Gutiérrez et al., 2013; Hoff et al., 2021; Korangi Alleluya et al., 2023; Ongena et al., 2007; Rodríguez et al., 2018; Stoll et al., 2021; G. Wu et al., 2018; Yamamoto et al., 2015). Notably, comparative studies reveal functional specialization among CLP families. In melon plants, fengycin and iturin mutants fail to induce ISR against *Podosphaera fusca*, unlike surfactin (García-Gutiérrez et al., 2013). A parallel response is observed in grapevine plants, where plipastatin (a Fengycin-family CLP) does not trigger ISR against *Botrytis cinerea*, contrasting with surfactin's activity (Farace et al., 2015).

Fengycin has also been demonstrated to induce ISR in multiple plant systems. For instance, it provides protection in tomato against *Botrytis cinerea*, in *Arabidopsis* against *Pseudomonas syringae*, and in Chinese cabbage against *Plasmodiophora*

brassicae (He et al., 2023; Ongena et al., 2007; Wu et al., 2018; Zhou et al., 2021). Similarly, the Iturin family CLPs (iturin and bacillomycin) exhibit ISR-eliciting activity across diverse hosts: iturin mediates protection in strawberry against *Colletotrichum gloeosporioides*, chili pepper against *Phytophthora capsici*, and *Arabidopsis* against *P. syringae* (Altrão et al., 2022; Park et al., 2016; Yamamoto et al., 2015). While bacillomycin induces ISR in *Arabidopsis* against both *P. syringae* and *B. cinerea* (Wu et al., 2018). Mycosubtilin has also been reported to trigger plant's immune responses (Farace et al., 2015; Mejri et al., 2018; Raouani et al., 2022; Platel et al., 2023) but whether it translates in systemic resistance against infection remains to be demonstrated. Intriguingly, rice-*Pyricularia oryzae* interactions require the synergistic application of fengycin and iturin (with or without surfactin) for ISR induction, regardless of soil conditions (acid sulfate or healthy potting soil) (Lam et al., 2021).

CLPs induce ISR with host specificity. For instance, 5 µM of surfactin effectively triggers ISR in bean plants against *B. cinerea* and in peanut plants against *Sclerotium rolfsii* (Ongena et al., 2007; Rodríguez et al., 2018). However, this concentration fails to induce resistance in tomato plants against *B. cinerea* (Stoll et al., 2021). Fengycin demonstrates complementary activity patterns, showing no ISR induction in bean plants regardless of the application method (using either fengycin-overproducing strains or 5 µM of the purified compound), but it effectively priming resistance in tomato plants when applied via fengycin-deficient bacterial strains (Ongena et al., 2007). These observations align with previous findings showing that surfactin, but not fengycin or iturin, can induce ISR against *Podosphaera fusca* in melon plants (García-Gutiérrez et al., 2013). Together, these results underscore the intricate relationship between CLP structure and host-pathogen combinations in determining ISR efficacy.

Current research demonstrates that *Pseudomonas*-synthesized CLPs can elicit ISR in a highly pathosystem-dependent manner. For instance, massetolide A primes tomato defences against *Phytophthora infestans* infection (Tran et al., 2007), while sessilin and orfamide, either individually or in combination, induce protective responses in bean plants challenged with *Rhizoctonia solani* (Ma et al., 2016). Striking specificity is observed in rice systems, where orfamide confers resistance to *Cochliobolus miyabeanus* but not to *Magnaporthe oryzae*, and the structurally distinct CLP WLIP shows opposing selectivity against *M. oryzae* (Ma et al., 2017; Omoboye et al., 2019). These findings collectively underscore that CLP-mediated ISR activation depends critically on precise molecular recognition events between specific CLP structures and particular plant-pathogen combinations. Table 1-2 shows CLPs from *Bacillus* and *Pseudomonas* species that elicit ISR across diverse plant-pathogen systems.

Table 1-2 CLPs reported to trigger ISR in plants.

CLP name	Plant	Pathogen	Method	Reference
Surfactin	Bean	*Botrytis cinerea*	Pure compound; mutants	(Ongena et al., 2007)
Surfactin	Tomato	*Botrytis cinerea*	Mutants	(Ongena et al., 2007)
Surfactin	Melon	*Podosphaera fusca*	Mutant; mutant and commercial C_{15} surfactin; commercial C_{15} surfactin	(García-Gutiérrez et al., 2013)
Surfactin	Tomato	*Botrytis cinerea*	Strains producing different amount of surfactin	(Cawoy et al., 2014)
Surfactin	Strawberry	*Colletotrichum gloeosporioides*	Pure compound	(Yamamoto et al., 2015)
Surfactin	Grapevine	*Botrytis cinerea*	Pure compound	(Farace et al., 2015)
Surfactin	*Arabidopsis*	*Botrytis cinerea*	Pure compound	(Debois et al., 2015)
Surfactin	*Arabidopsis*	*Botrytis cinerea*	Mutant	(Wu et al., 2018)
Surfactin	*Arabidopsis*	*Pseudomonas syringae*	Mutant	(Wu et al., 2018)
Surfactin	Peanut	*Sclerotium rolfsii*	Pure compound	(Rodríguez et al., 2018)
Surfactin	Tobacco	*Botrytis cinerea*	Pure compound	(Hoff et al., 2021)
Surfactin	Tomato	*Botrytis cinerea*	Commercial compound	(Stoll et al., 2021)
Surfactin	*Arabidopsis*	*Pseudomonas syringae*	Commercial compound	(Altrão et al., 2022)
Surfactin	*Arabidopsis jar1-1*	*Pseudomonas syringae*	Commercial compound	(Altrão et al., 2022)
Surfactin	Peanut	*Athelia rolfsii*	Pure compound	(Korangi Alleluya et al., 2023)
Fengycin	Tomato	*Botrytis cinerea*	Mutant	(Ongena et al., 2007)
Fengycin	*Arabidopsis*	*Pseudomonas syringae*	Mutant	(Wu et al., 2018)
Fengycin H	Tomato	*Botrytis cinerea*	Pure compound	(Zhou et al., 2021)
Fengycin	Chinese cabbage	*Plasmodiophora brassicae*	Mutant	(He et al., 2023)
Iturin A	Strawberry	*Colletotrichum gloeosporioides*	Commercial compound	(Yamamoto et al., 2015)
Iturin A	Chili pepper	*Phytophthora capsici*	Pure compound	(Park et al., 2016)
Bacillomycin D	*Arabidopsis*	*Pseudomonas syringae*	Mutant	(Wu et al., 2018)
Bacillomycin D	*Arabidopsis*	*Botrytis cinerea*	Mutant	(Wu et al., 2018)
Iturin A	*Arabidopsis*	*Pseudomonas syringae*	Pure compound	(Altrão et al., 2022)
Iturin A	*Arabidopsis jar1-1*	*Pseudomonas syringae*	Pure compound	(Altrão et al., 2022)
Surfactin and fengycin	Bean	*Botrytis cinerea*	Mutant	(Ongena et al., 2007)
Fengycin and iturin	Rice	*Pyricularia oryzae*	Mutants	(Lam et al., 2021)
Surfactin, fengycin and iturin	Rice	*Pyricularia oryzae*	Mutants	(Lam et al., 2021)
Massetolide A	Tomato	*Phytophthora infestans*	Mutant; pure compound	(Tran et al., 2007)
Sessilin	Bean	*Rhizoctonia solani*	Mutants; pure compound	(Ma et al., 2016)
Orfamide	Bean	*Rhizoctonia solani*	Mutants; pure compound	(Ma et al., 2016)
Orfamide	Rice	*Cochliobolus miyabeanus*	Pure compound; mutant	(Ma et al., 2017)
WLIP	Rice	*Magnaporthe oryzae*	Mutants	(Omoboye et al., 2019)
Sessilin and orfamide	Bean	*Rhizoctonia solani*	Mutants	(Ma et al., 2016)

4.2. Differential activation of ISR by CLPs across concentration gradients

The capacity of CLPs to induce systemic resistance exhibits striking concentration dependence and structural specificity. In *Arabidopsis thaliana*, Srf demonstrates pathogen-specific activation thresholds that 1 µM suffices for protection against *Botrytis cinerea* but fails against *Pseudomonas syringae*, while intermediate concentrations (2-16 µM) are effective against the bacterial pathogen *Pseudomonas syringae*, but not higher concentration at 32 µM (Altrão et al., 2022; Debois et al., 2015). Most studies report optimal ISR induction at 10 µM Srf across diverse pathosystems, including in melon plants against *Podosphaera fusca*, in *Arabidopsis*, tobacco, grapevine plants against *B. cinerea* and in peanut plants against *Sclerotium rolfsii* and *Athelia rolfsii* (Debois et al., 2015; Farace et al., 2015; García-Gutiérrez et al., 2013; Hoff et al., 2021; Korangi Alleluya et al., 2023; Rodríguez et al., 2018). There is thus a clear concentration-response relationship. While 5 µM Srf is ineffective in tomato plants, 25 µM provides protection against *B. cinerea* (Stoll et al., 2021). Similar dose-responses occur with other CLPs, such as orfamide, which requires more than 25 µM for ISR in rice plants against *Cochliobolus miyabeanus* (Ma et al., 2017). Iturin exhibits a narrow effective range (0.5-2 µM) in *Arabidopsis* against *Pseudomonas syringae*, unlike at a lower concentration of 0.25 µM and a higher concentration of 4 µM (Altrão et al., 2022). Higher iturin concentrations (10 µM) are needed to trigger ISR in strawberry infected with *Colletotrichum gloeosporioides* (Yamamoto et al., 2015). These findings highlight our limited understanding of how CLP structural features govern ISR activation. Concentration-dependent effects and pathogen-specific induction patterns imply the existence of sophisticated perception mechanism that requires further molecular characterization.

4.3. Synergistic relationship of CLPs application triggering ISR in plants

Growing evidence indicates that CLPs from diverse bacterial species can act synergistically to enhance their biological functions. While single CLP-mediated ISR has been well-documented, recent studies highlight the critical role of CLP combinations in modulating plant immune responses. For instance, Iturin family CLPs and surfactin cooperate to promote robust biofilm formation (Luo et al., 2015), while mixtures of fengycin and surfactin induce a stronger ISR in bean plants against *B. cinerea* than either CLP alone does (Ongena et al., 2007). Similarly, sessilin and orfamide exhibit synergistic activity against *Rhizoctonia solani* in bean plants, when in combination (Ma et al., 2016).

ISR induction in rice plants against *Pyricularia oryzae* strictly requires the combined application of fengycin and iturin, irrespective of soil conditions (Lam et

al., 2021). Notably, surfactin that fails to trigger ISR alone, potentiates the effect of fengycin-iturin mixtures, revealing complex higher-order interactions among CLPs (Lam et al., 2021). These observations challenge the traditional view of CLP activity as a single component and suggest that natural CLP mixtures may function cooperatively to elicit immune responses that individual compounds cannot achieve alone.

Such synergistic effects underscore the ecological relevance of CLP diversity in rhizosphere communities and highlight the need to reconsider biocontrol strategies using rationally designed CLP combinations. However, the molecular mechanisms underlying these interactions remain poorly understood, emphasizing a key gap in our knowledge of how microbial metabolites collectively shape plant immunity.

4.4. Molecular mechanisms of CLP recognition in plants

Plants detect the presence of microbes through plasma membrane-localized PRRs that perceive conserved MAMPs, which initiates PTI. In contrast to this direct defence response, PBB typically induce a more subtle priming ISR to enhance readiness for future pathogen challenges without incurring immediate metabolic costs. While PTI triggers rapid, energy-intensive defence responses, ISR-mediated priming provides targeted protection that activates is fully activated only upon subsequent pathogen recognition. This distinction is exemplified by surfactin's mode of action in *Arabidopsis thaliana*. Unlike classical MAMPs (e.g., flagellin), surfactin does not elicit ROS bursts or strongly upregulate defence-related genes during initial perception (Debois et al., 2015). Instead, it establishes a primed state that enables amplified defence responses upon actual pathogen encounter.

The biological activity of CLPs stems from their specific interactions with eukaryotic membrane components. As amphiphilic molecules, CLPs spontaneously integrate into plasma membranes, whose complex structures composed of glycerolipids, sphingolipids, and sterols, through thermodynamically favorable hydrophobic interactions (Aranda et al., 2023; Balleza et al., 2019). These interactions exhibit remarkable structural specificity that governs their immune-modulating effects. Mycosubtilin demonstrates selective affinity for ergosterol in fungal membranes (Nasir & Besson, 2012), while surfactin preferentially incorporates into phospholipid bilayers, inducing subtle membrane perturbations rather than outright disruption. This delicate structural modulation appears sufficient to initiate downstream signaling cascades culminating in ISR (Deleu et al., 2005; Gilliard et al., 2022; Hoff et al., 2021; Ongena et al., 2007; Pršić & Ongena, 2020). Fengycins, by contrast, exert their effects through more generalized alterations to membrane architecture and permeability (Deleu et al., 2005; Ongena et al., 2007). Structure-activity studies reveal critical determinants of CLP functionality. The bioactivity of

iturin derivatives depends on both the integrity of their cyclic peptide structure and their FA chain composition, as demonstrated in *Arabidopsis thaliana* (Kawagoe et al., 2015). Similarly, among surfactin homologs, those with longer FA chains (C_{14}-C_{15}) show superior immune-stimulating capacity in tobacco cells compared to shorter-chain variants (C_{12}-C_{13}) or structurally modified derivatives (linearized or methylated peptides) (Henry et al., 2011). These in vitro observations highlight the exquisite structure-function relationships governing CLP activity, though their physiological relevance requires further validation in planta.

The biological activity of CLPs is fundamentally governed by their unique structural architecture. Cyclization of the peptide backbone confers enhanced molecular stability (Hamley, 2015), and is essential for optimal bioactivity, as demonstrated by the consistently reduced efficacy of linear analogs. This structural requirement reflects the critical importance of three-dimensional conformation for target engagement, where the precise spatial arrangement of functional groups determines interaction specificity. CLP-membrane interactions exhibit remarkable structural selectivity based on several key physicochemical parameters. The amphipathic character of these molecules, dictated by FA chain length (typically C_{12}-C_{15}), branching patterns, and peptide ring composition (including AA stereochemistry), collectively determines their membrane insertion dynamics and subsequent biological effects (Balleza et al., 2019). These structure-activity relationships explain why subtle modifications, such as methylation or linearization of the peptide chain, can significantly alter immune-stimulating capacity (Henry et al., 2011). However, further investigation is required to better understand the impact of CLP chemical structure on their ISR functionality. For instance, additional structural analogues with variations in the peptide sequence should be tested. Interestingly, fluorinated iturin analogues display enhanced antimicrobial activity, and such derivatives could be tested for ISR (Gimenez et al., 2021; Phelan et al., 2019).

Recent mechanistic studies have revealed unconventional perception pathways for certain CLPs. Surfactin exhibits dose-dependent activity in the micromolar range and can modulate membrane fluidity without receptor binding. This suggests a lipid-driven signaling mechanism (Henry et al., 2011). This is further supported by its newly identified role in regulating miR846-mediated jasmonate signaling (Xie et al., 2018), representing a novel interface between membrane biophysics and transcriptional reprogramming. The molecular sensors responsible for CLP detection in plants were not fully characterized for a long time, and the downstream signaling networks connecting membrane perturbations to systemic responses remain poorly mapped (Deleu et al., 2005; Ongena et al., 2007). Sphingolipids are ubiquitous components of biological membranes, where they serve dual roles in maintaining membrane structural integrity and functioning as signaling molecules (Yang et al., 2025). Classical PRR-mediated immunity operates through the formation of higher-order receptor complexes with conserved co-receptors, which subsequently activate the receptor-like cytoplasmic kinases BIK1 and PBL1 as key convergent regulators of

plant immune signalling (Gilliard et al., 2026). In contrast, surfactin has been reported to activate the *Arabidopsis thaliana* immune system via direct interaction with membrane sphingolipids, thereby inducing ISR against *Botrytis cinerea* (Gilliard et al., 2026). However, translating in vitro structure-activity relationships to whole-plant systems requires rigorous validation, especially concerning concentration thresholds and tissue-specific effects.

Objectives and research strategy

Previous research has primarily examined the biocontrol properties of CLPs, focusing on their antimicrobial functions. Investigations into CLP-ISR have largely centered on three families: Surfactin, Fengycin, and Iturin. However, our understanding of the relationship between CLP structure and function, as well as the mechanisms underlying CLP-mediated plant immunity, remains limited.

To address this gap, this study explores the structural determinants of CLPs in triggering plant immune responses using two approaches. First, we employed canonical CLPs (Srf, Liche, Pumi) and secondly employed variants generated via branched-chain amino acid (BCAA) precursor-directed biosynthesis (Srf, Liche, and Pumi variants). Second, we assessed their capacity to elicit early immune events, including ROS, NO, and Ca^{2+} in *Arabidopsis thaliana* roots and protoplasts of root cells.

Additionally, ISR assays against *Botrytis cinerea* under laboratory conditions provided a complementary perspective. Building on insights from prior work, this study adopts a three-pronged experimental approach to elucidate the mechanisms of CLP-induced plant immunity. This approach covers aspects from the detection of the phytoalexin coumarin and camalexin, phytohormones, to the expressions of genes related to plant immunity after CLP treatment. The flowchart is shown below (Figure 1-8).

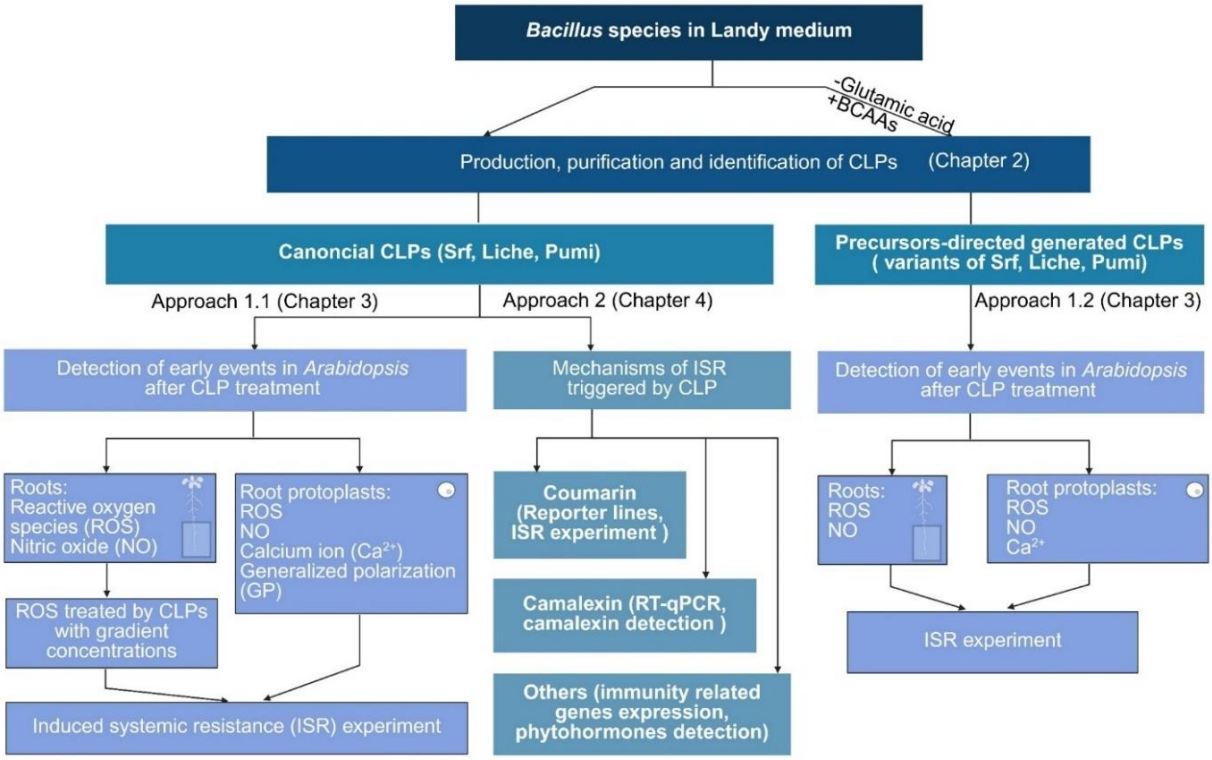

Figure 1-8 Flowchart of this study.

Chapter 2

Structural characterization of surfactin variants

1. Introduction

Fungal pathogens pose a significant threat to agricultural productivity by causing diverse plant diseases, thereby limiting crop yields (Ceulemans et al., 2021). Priming of seeds, leaves, or roots with live PBB, phytochemicals, or microbial components enables plants to mount faster and more robust defences against subsequent biotic stresses (Westman et al., 2019). Among the bioactive metabolites secreted by PBB *Bacillus* spp., CLPs are amphiphilic secondary metabolites with potent antimicrobial activity, making them key players in biocontrol (Groll et al., 1998; Grossman, 1995). Notably, CLPs elicit ISR in plants, conferring broad-spectrum protection against pathogens (Omoboye et al., 2019; Ongena & Jacques, 2008; Pieterse et al., 1998), thereby offering significant promise for agricultural applications.

CLPs vary in FA chain length as well as peptide composition, thus the Surfactin family consists of three types of CLPs: Srf, Liche and Pumi (Mülner et al., 2020). In nature, Srf is produced as a mixture of homologs, whose peptide typically consists of the following sequence: (L-)Glu_1-(L-)Leu_2-(D-)Leu_3-(L-)Val_4-(L-)Asp_5-(D-)Leu_6-(L-)Leu_7, which relates to a lactone ring by $C_{12\text{-}17}$ "horse-saddle" topology (β-hydroxy) FA (Heerklotz & Seelig, 2001, 2007; Jin et al., 2016; Peypoux et al., 1999; Qin et al., 2023). SrfVal_7 is a minor companion to Srf (Leu_7) (Peypoux & Michel, 1992). Liche, interestingly, has Gln and Ile in cyclic peptide positions 1 and 7 respectively, Val_7 was also reported (Qi et al., 2023). The FAs of Liche vary in length from C_{12} to C_{17} (Ali et al., 2022). Compared to canonical Srf, Pumi has a Val in the peptide ring at position 4, and an Ile or a Val in position 7, in place of a Leu (Théatre et al., 2022). The number of carbon atoms in the chain of Pumi varies from C_{13} to C_{17} (de Oliveira et al., 2020; Naruse et al., 1990). Srf, as described in Chapter 1, plays a great role in eliciting ISR in multiple plants. However, on the same topic, little was reported for Srf variants: Liche and Pumi.

Minor variations in AA composition or FA chain length, dictated by microbial biosynthesis under different environmental conditions, can encode distinct "messages" for the plant immune system. Previous work in our laboratory has demonstrated the loss eliciting activity from the linear, methylated, and linear/methylated derivatives C_{14}Srf (Henry et al., 2011). As it was explained in Chapter 1, CLPs are produced via NRPSs that enable precursor-directed modification of the peptide's AA composition and facilitating various cyclization reactions (Götze & Stallforth, 2020; Grangemard et al., 1997; Kowall et al., 1998). The A domains have relaxed substrate specificity, which allows them to activate a broader range of AA residues (Henry et al., 2011), and such flexibility allows the generation of CLP variants by growing the corresponding strains in the Landy medium supplemented with BCAAs: L-Leu, L-Val, L-Ile. Most reports focus on the yield of precursor-directed CLP production, and few focused on the detailed structures of CLP variants.

The objective of Chapter 2 is to prepare and characterize the needed CLPs for their further detection to comparatively analyze their immune-priming capabilities and evaluate the potential CLPs as foliar biofungicides through root application in *Arabidopsis* in (Chapter 3) as well as the three approaches for CLP-ISR mechanisms (Chapter 4).

2. Materials and methods

2.1. CLPs production and purification

Srf came from stock of this lab, was produced in the same way mentioned above. Srf (> 95% purity of a mix of homologs) was purified from spent supernatant of *Bacillus velezensis* liquid culture as previously described (Razafindralambo et al., 2009). To produce precursor-directed CLPs, L-Val, L-Leu, or L-Ile (Sigma-Aldrich) was applied at 5 g/L, respectively. In this study, canonical CLPs are Srf, Pumi, Liche. The precursor-directed generated CLPs, each of them is a CLP mixture from each medium, were called as Srf variants: Srf (Val), Srf (Ile); Pumi variants: Pumi (Val), Pumi (Leu). Srf, Liche, Pumi and their variants were obtained from liquid cultures of *B. velezensis* GA1, *B. pumilus* Philipo 41, respectively in Landy medium (Landy et al., 1948) at 30 °C for 72 h, using solution composed of 1 g/L yeast extract, 0.5 g/L $MgSO_4$, 1 g/L K_2HPO_4, 0.5 g/L KCl, 21 g/L MOPS (pH=7.0), 0.016 g/L L-tryptophan, 0.0016 g/L $CuSO_4$, 0.0024 g/L $MnSO_4$, 0.0008 g/L $FeSO_4$, 20 g/L glucose, 5 g/L glutamic acid; Liche variants including Liche (Val), Liche (Ile) were obtained from Landy medium of *B. licheniformis* BBG-143 with modification to replace 20 g/L glucose with 10 g/L xylose and 5 g/L sucrose; replace 5 g/L glutamic acid with 5 g/L glutamine. Each strain only produces one of mentioned CLPs.

Cultures were centrifuged at 15180 g for one hour to collect the supernatant. CLPs were then extracted from the cell-free supernatant using acid precipitation. The supernatant was acidified to pH at 2 with HCl, and incubated at 4 °C overnight for precipitation. CLP precipitates were collected by centrifugation (29753g for one hour) and resuspended in water and the pH adjusted to 8. CLPs were further processed by liquid-liquid extraction with solvent (50:50) composed of butanol (30%) and ethyl acetate (70%), recovered from the organic phase, and concentrated under vacuum. CLPs were purified by semi-preparative HPLC (Agilent Serie 1100 with VWD 214 nm), by using a C18 reversed phase column (Luna® Omega 5 µm, 250 x 10 mm) with acetonitrile (ACN) and water containing 0.1% trifluoroacetic acid (TFA) as the mobile phrase at a flow rate of 4 mL/min, with gradient elution of 0 min, 85% ACN; 35 min, 85% ACN, 5 min, 100% ACN; until 5 min, 85% ACN for Pumi; 0 min, 90% ACN; 20 min, 90% ACN, 5 min, 100% ACN; until 5 min, 90% ACN for Liche. The collected CLP-containing fractions were checked for purity by Shimadzu nexera series (UPLC) with DAD 190-800 nm, by using a waters acquity premier BEH C18 column 1.7 µm 2.1

mm x 50 mm) with the same solvent system at a flow rate of 0.6 mL/min, with gradient elution of 0 min 30% ACN, 2.43 min 95% ACN, 5.10 min 95% ACN, until 5.2 min 30% ACN, finished at 7 min 30% ACN. The purified material was freeze dried (lyophilisator Martin Christ alpha 3-4 LSC BASIC) before storage.

2.2. CLPs identification and quantification

The CLP structures were determined by MassHunter Workstation software (version B.09.00) after data collection from an Agilent Technologies 1290 Infinity, with a C18 reversed phase (waters acquity premier BEH C18 1.7 µm 2.1 mm x 50 mm) used at a flow rate of 0.6 mL/min and a temperature of 40 °C. The injection volume was 5 µL, and a gradient of acidified water containing 0.1% trifluoroacetic acid (TFA) (solvent A) and of acetonitrile (ACN) containing 0.1% TFA (solvent B) was used as mobile phase with a constant flow rate of 0.6 mL/min, with the min pressure at 0 bar, and the max pressure at 1 k bar, starting at 10% B for 1 min and rising to 100% B in 10 min, and keep 100% B for 3.5 min, then go back to the initial ratio for 3.5 min.

That was coupled with a mass detector (Agilent Technologies 6530 Accurate-Mass Q-TOF LC/MS) at positive mode with the parameters set up as follows: drying gas temperature of 300 °C, drying gas of 8 L/min, nebulizer of 35 psi, sheath gas temperature of 350 °C, flow rate of sheath gas of 11 L/min, capillary voltage of 3.5 kV, nozzle voltage (expt) of 1 kV, fragmentor voltage of 175 V, skimmer voltage of 65 V, and octopole radiofrequency of 750 V. For MS/MS analysis, the MS1 acquisition was configured with the following specifications: a mass range of 300-1500 m/z, a scan rate of 3 spectra/s, and the MS2 acquisition was configured with the following specifications: a mass range of 50-1500 m/z, a scan rate of 5 spectra/s, and a medium isolation width (approximately 4 AMU) using the native Decision Engine. Collision energies were fixed at compound-specific values: 20, 40 and 75 V. The precursor selection method was set to choose the top three ions for surfactin analysis, employing a minimum absolute intensity threshold of 10000 counts. Precursor were sorted by charge state followed by abundance (with a preference for a charge state of 1), using a common isotope model. An active exclusion protocol was implemented, excluding precursor after 3 spectra and releasing them after 0.5 minutes.

All CLPs employed in this study were freshly reconstituted from powdered stock prior to each experimental procedure. The concentration of CLPs, expressed relative to the concentration of Srf, was quantified using MassHunter Workstation software (version B.09.00) following chromatographic separation. Analysis was performed on an Agilent Technologies 1290 Infinity system equipped with a reversed-phase C18 column (Waters Acquity Premier BEH C18, 1.7 µm, 2.1 mm × 50 mm) maintained at 40 °C. The mobile phase consisted of acidified water with 0.1% TFA (solvent A) and acetonitrile with 0.1% TFA (solvent B), delivered at a constant flow rate of 0.6 mL/min. The injection volume was 5 µL, and a gradient elution was applied starting

at 10% B, increasing to 100% B over 11 minutes, holding at 100% B for 3.5 minutes, and then returning to initial conditions. System pressure was maintained between 0 and 1 kbar. The liquid chromatography system was coupled to a mass detector (Agilent Technologies 6530 Accurate-Mass Q-TOF LC/MS) operated in positive ionization mode. The mass spectrometric parameters were configured as follows: drying gas temperature, 300 °C; drying gas flow, 8 L/min; nebulizer pressure, 35 psi; sheath gas temperature, 350 °C; sheath gas flow, 11 L/min; capillary voltage, 3.5 kV; nozzle voltage, 1 kV; fragmentor voltage, 175 V; skimmer voltage, 65 V; and octopole RF voltage, 750 V. High-resolution mass spectra were acquired across a mass-to-charge (m/z) range of 100-1700.

3. Results

3.1. Structure and hydrophobicity of canonical CLPs

Three types of canonical CLPs were purified from culture broth by preparative HPLC (90% purity) and were tested as a mixture of homologs naturally co-produced by each strain. The CLPs exhibit minor variations in the length of their FA tail and/or the AA composition represented in Figure 2-1.

The identity of each CLP homolog was established through UPLC-ESI-QTOF MS/MS analysis, with spectra interpreted via MassHunter Qualitative Analysis 10.0 software. Total ion chromatograms were first inspected to identify precursor ions within the expected retention time. The corresponding product ion spectra for these CLP homologs were then extracted at a 35 V collision energy for detailed structural analysis. Following collision-induced dissociation, Srf homologs characteristically undergo lactone ring opening, producing linearized peptides that fragment along the backbone. This yields diagnostic N-terminal, FA-containing b-ion series and complementary C-terminal y-ion series. The AA sequence was determined by interpreting the sequential mass losses from the precursor ion evident in both the b- and y-ion ladders. All residue assignments were verified by matching the experimentally observed fragment masses to the theoretical masses derived from the elemental compositions of the constituent AAs and the β-hydroxy FA.

The structural elucidation of the C_{14} surfactin Leu_7 homolog (Figure 2-1G) served as a representative example, accomplished via MS/MS. Analysis was performed on the precursor ion at *m/z* 1022, identified as the protonated molecular ion $[M+H]^+$ for this variant, which incorporates a C_{14} β-hydroxy FA-Glu_1-Leu_2-Leu_3-Val_4-Asp_5-Leu_6-Leu_7. An N-terminal b-ion ladder established the sequence as Leu_7-Leu_6-Asp_5-Val_4-Leu_3-Leu_2-Glu_1. Sequence assignments were corroborated by mass losses corresponding to Leu/Ile (113.08 Da), Asp (115.03 Da), Val (99.06 Da), and Glu (129.04 Da). Complementary y-ion fragments further supported the sequence by

identifying fragments containing the C-terminal peptide region, including C_{14} β-hydroxy FA linked to Glu_1, followed by Leu_2, Leu_3, Val_4, and Asp_5. The C_{14} β-hydroxy FA moiety (~226.19 Da) was confirmed by acyl chain-containing fragments. Similarly, homologs with Val_7 were identified in Liche mixture and Pumi mixture. Although Leu and Ile share an identical mass and are therefore challenging to distinguish by UPLC-ESI-QTOF MS/MS alone, their differing hydrophobicity can be leveraged for identification. Based on their relative chromatographic affinities (Balleux et al., 2024), where Ile exhibits greater hydrophobicity than Leu, we confirmed the presence of Ile_7 in Liche and Pumi mixture, in contrast to the Leu_7 residue found in Srf mixture.

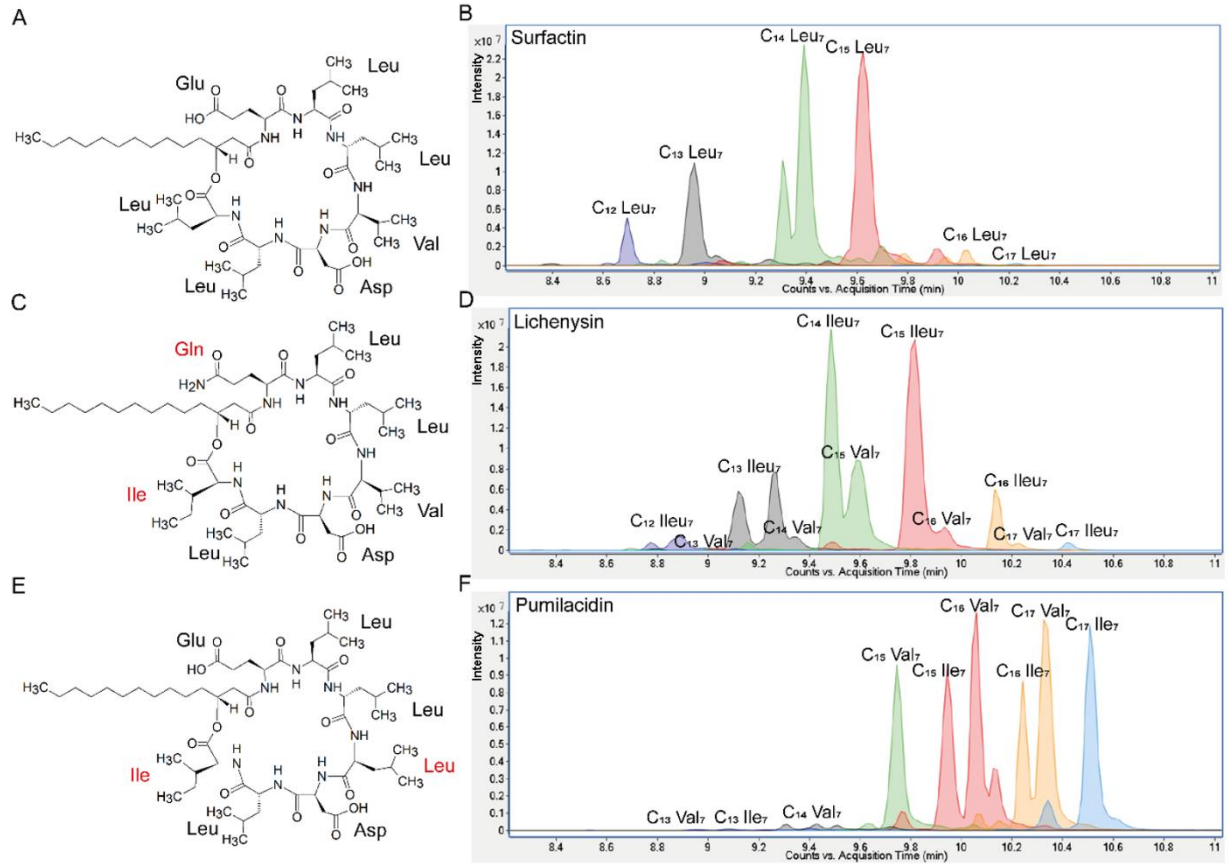

G

C_{14}Srf Leu_7 from canonical Srf mixture

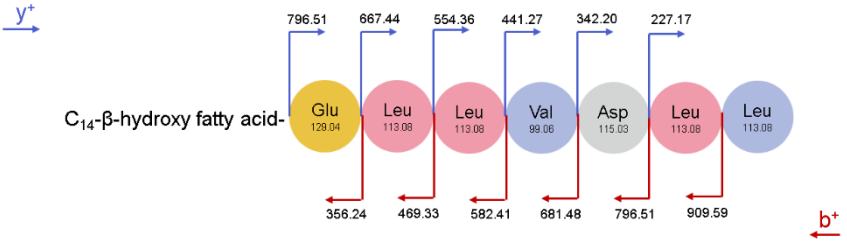

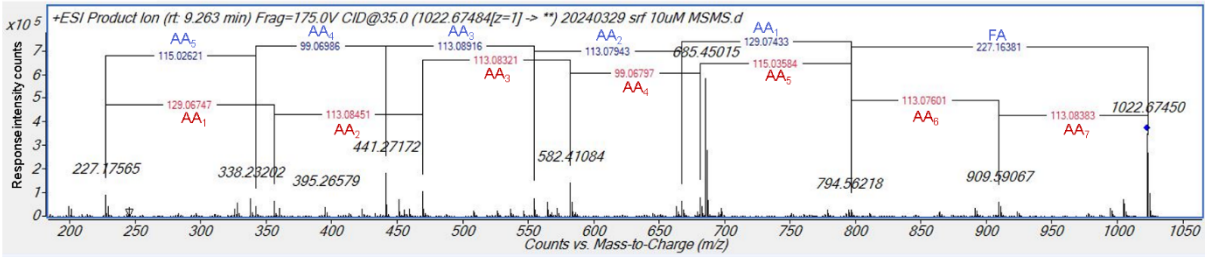

Figure 2-1 The chemical structures of canonical CLPs used in this study.

A, C, E. C_{14} Srf, C_{14} Liche, C_{14} Pumi, respectively. The red color highlights the differences between Liche, Pumi, and Srf in the cyclic peptide; **B, D, F**. UPLC-ESI-QTOF MS chromatograms showing the diversity and retention times of the various Srf, Liche and Pumi homologs that differ in FA chain length and branching. The blue, black, green, red, orange, blue colors marked Srf variants with similar FA and AA structure. **G.** The structure of C_{14} Srf Leu_7 is detected via UPLC-ESI-QTOF MS/MS spectra. The red and blue arrows show the b^+ and y^+, respectively. FA and AAs are marked red or blue in the MS/MS spectra accordingly.

The relative hydrophobicity of the selected CLPs was then estimated. Initial assessment employed Bigelow's method, which calculates a global hydrophobicity index (ϕ) from the side chains of the AAs. constituting the peptide moiety (Bigelow, 1967). Analysis revealed that AA substitutions in the peptide moiety account for the differential hydrophobicity observed among Srf, Liche, and Pumi, and, with Pumi exhibiting the most pronounced effect. This increase in Pumi's hydrophobicity was attributable to two specific residue changes: Val_4 to Leu_4 (1.7 to 2.4 kcal/res) and Leu_7 to Ile_7 (2.4 to 2.95 kcal/res). UPLC-MS retention times, indicative of interaction strength with the C18 matrix, wherein Srf homologs eluted first, followed by Liche and then Pumi (Figure 2-1B, D, F), also directly reflects the relative hydrophobicity of the CLPs.

Even though the structural differences between Srf, Liche, and Pumi are minor, they can affect their physicochemical properties such as their potential to reduce surface tension or to self-assemble in micelles when the CMC is reached in aqueous medium. For instance, the change of Val_4 to Leu_4 that is present in Pumi compared to Srf, has been reported to impact both properties (Théatre et al., 2022).

3.2. Structure of BCAA precursor-directed generated CLPs

Since supplementation with BCAAs can direct the production of CLP variants with AA substitutions at positions 2, 4, or 7 (Grangemard et al., 1999), our initial goal was to collect a wider array of CLP variants by BCAA supplementation. This would allow us to further investigate the structure-function relationship of the canonical CLPs: Srf, Pumi, and Liche, with minimal AA differences. To generate and compare Ile-substituted variants, L-Ile was added to the Srf producer strain to create $SrfIle_7$, whose function was compared to natural $PumiIle_7$ and $LicheIle_7$. In a complementary approach, L-Leu was provided to the Pumi and Liche producer strains to generate Leu-substituted variants for comparative functional analysis. As mentioned in the M&M, each purified mixture from BCAA-supplemented Landy medium is named as CLP (Val), CLP (Leu) or CLP (Ile) based on the CLP and AA added to the medium. The structures of CLP variants produced by strains cultivated in modified Landy

medium were analyzed using Q-TOF LC/MSMS, with the resulting data presented in chromatograms.

BCAA supplementation induced a strain-dependent production of CLP variants. This included not only changes in the yield of canonical CLP homologs but also the generation of novel CLP types. Following the same structural characterization workflow used for canonical CLPs, the homologs of these CLP variants were first identified via UPLC-MS/MS. Their identity was further verified by comparing their chromatographic retention times with those of known canonical homologs, a method based on differences in hydrophobicity. The data for Srf, Liche, and Pumi variants are presented in Figure 2-2, Figure 2-3, and Figure 2-4, respectively. Detailed information is available in Appendix Figures A1-1 to A1-3 and Tables A1-1 to A1-3.

It is worth noting that the Srf variant mixture is primarily composed of novel homologs, a profile that distinguishes it from those of the Pumi variants and Liche variants (Figure 2-2 EF, Figure 2-3 EF, Figure 2-4 EF). Furthermore, Srf variants exhibit greater diversity in both FA chain lengths and AA substitutions compared to Liche variants, while the Pumi producer appears to follow a distinct biosynthetic logic (Figure 2-2 EF, Figure 2-3 EF, Figure 2-4 EF).

We adopted the "Lxx" notation for the ambiguous sequence position of Leu or Ile, because the mass spectrometry platform could not differentiate between these isobaric residues (Kecskeméti et al., 2018). From the Srf (Ile) mixture, we identified many $SrfLxx_7$ and $SrfLxx_4Lxx_7$ homologs. In contrast, only the $C_{15}LicheLxx_4Lxx_7$ homolog was found in the Liche (Leu) mixture, with no $PumiLeu_7$ variant being detected. For clarity, peaks with different retention times but assigned with the same CLP name in this study are also likely due to the different FA derivatives. To preclude potential misinterpretation arising from the influence of FA modifications on hydrophobicity and confirm the exact AA at certain positions, the variants mentioned require further characterization using nuclear magnetic resonance (NMR) spectroscopy and gas chromatography-mass spectrometry (GC-MS). Subsequently, each CLP variant mixture was analyzed in detail through comparison with its corresponding canonical CLP mixture.

In the Srf (Val) mixture (Figure 2-2B), compared to canonical Srf (Figure 2-2A), the amount of all the original Srf homologs decreased ($C_{12}Leu_7$ was not detected, C_{13}-C_{16} decreased) as seen in Figure 2-2E compared with Figure 2-2D. Additionally, the form with Val at position 7 was detected, from $C_{13}Val_7$ to $C_{16}Val_7$. We also noticed the replacement of Leu_2 by Val_2, leading to the production of new molecules: $C_{14}Val_2Val_7$ and $C_{15}Val_2Val_7$. Likewise, the replacement of Leu_6 by Val_6, compared with canonical Srf sample, leads to the detection of new molecules: $C_{14}Val_6Leu_7$ and $C_{15}Val_6Leu_7$.

In the Srf (Ile) mixture (Figure 2-2C), we detected the replacement of Val_4 by Lxx_4 (Leu_4 or Ile_4), leading to the new molecules: $C_{15}Lxx_4Lxx_7$ and $C_{16}Lxx_4Lxx_7$. In theory, the unknown new CLP with the same retention time as existing molecule, has a high possibility to be the existing molecule. For example, two peaks of $C_{15}Lxx_4Lxx_7$ share the same retention with $C_{15}Leu_4Leu_7$ from canonical Pumi, making it a hypothesis to find C_{15}Pumi in Srf (Ile) mixture. However, this should be further examined in the future. While extra homologs of Lxx_7 (C_{12}-C_{15} and C_{17}) were detected, we found the decreased tendency of Leu_7 (C_{12}-C_{15} decreased, C_{16}-C_{17} disappeared) in Srf (Ile) mixture.

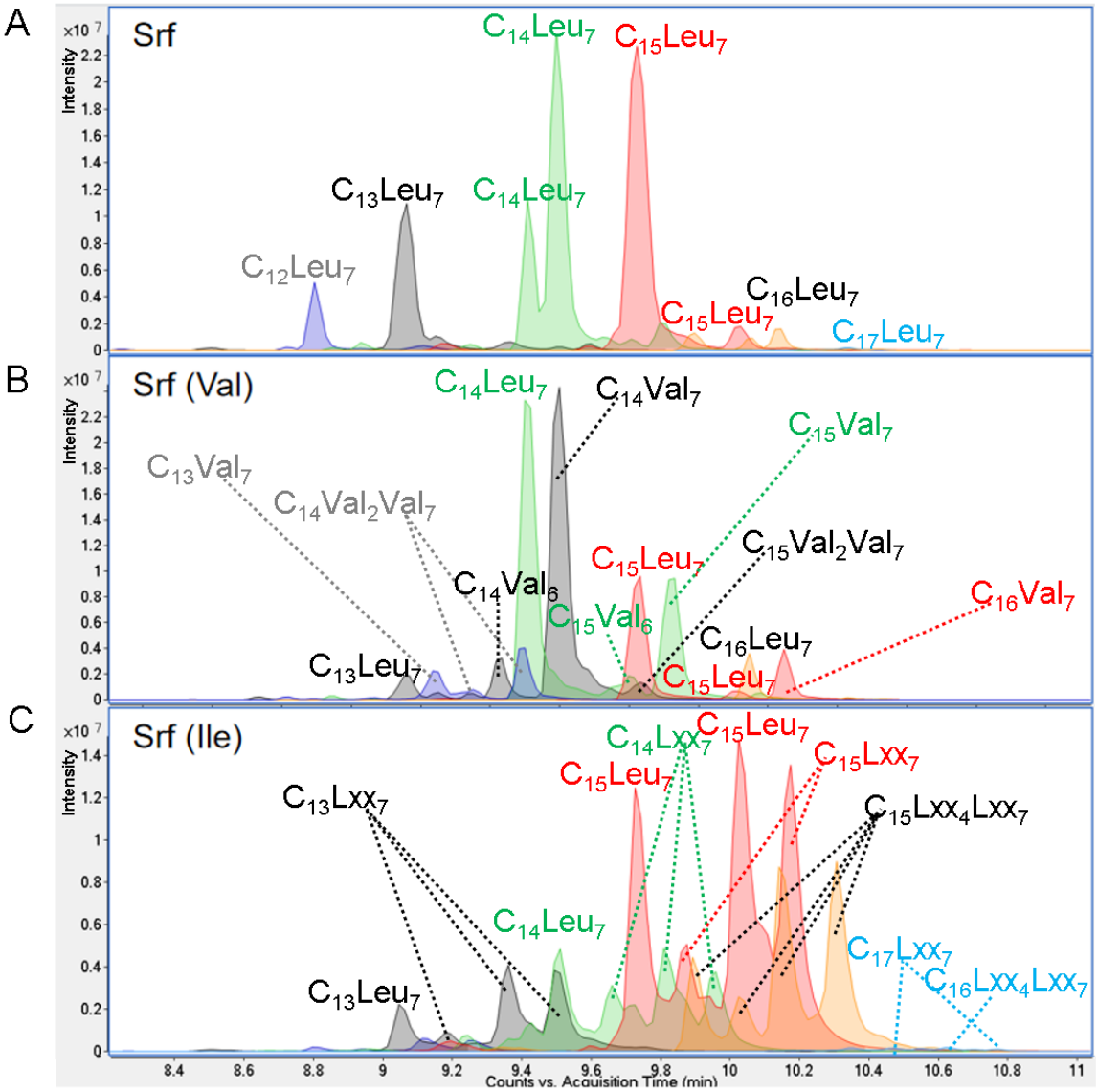

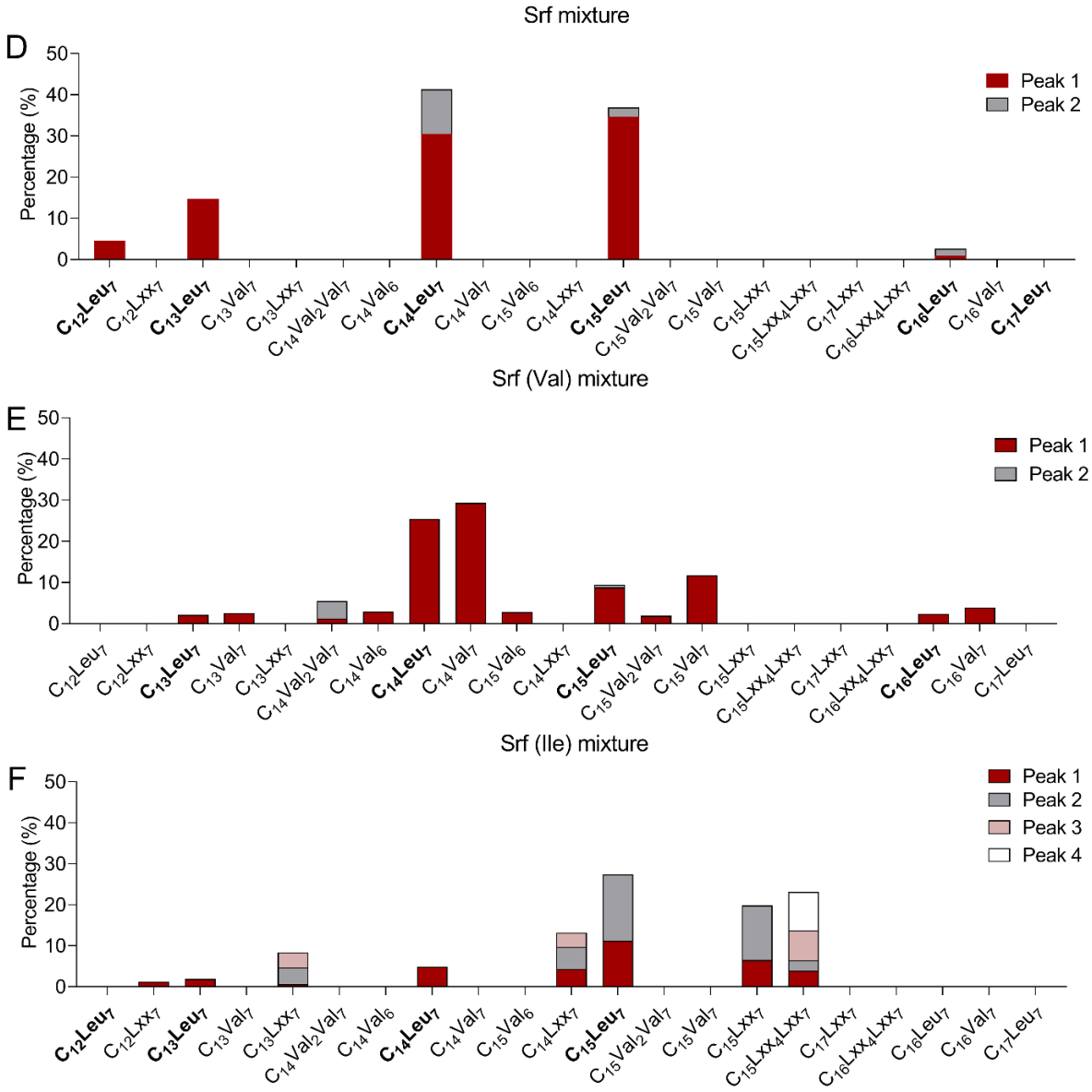

Figure 2-2 Structures of Srf variants.

A, B, **C.** Chromatograms of Srf, Srf (Val), Srf (Ile) mixture, respectively. Different colors refer to corresponding masses detailed in Table A1-1. The dotted lines show the new CLPs; **D, E, F.** Profile of the Srf, Srf (Val), Srf (Ile) mixture, respectively. Bold letters represent the existing canonical CLPs in each CLP mixture. In this study, each purified CLP component was collected and mixed into a single CLP mixture.

In the Liche (Val) mixture, comparison between Figure 2-3E and Figure 2-3D shows that the amount of most Val_7 ($C_{15}Val_7$, $C_{16}Val_7$) variants increased, while most Ile_7 decreased ($C_{14}Ile_7$ to $C_{16}Ile_7$ decreased, $C_{17}Ile_7$, the first peak of $C_{12}Ile_7$, $C_{13}Ile_7$, and $C_{15}Ile_7$ disappeared). In the Liche (Val) mixture (Figure 2-3B), we also noticed the replacement of Leu_2 by Val_2 compared with canonical Liche sample (Figure 2-3A), leading to the production of new molecules: $C_{14}Val_2Val_7$. The function of new CLP molecules need more attention.

In the Liche (Leu) mixture, comparison between Figure 2-3F and Figure 2-3D elucidates that except the first peak of $C_{15}Ile_7$, whose amount increased (compared to that of canonical Liche), the amount of other Ile_7 decreased ($C_{13}Ile_7$, $C_{14}Ile_7$ decreased, $C_{12}Ile_7$, $C_{16}Ile_7$ disappeared); the amount of Val_7 also decreased ($C_{15}Val_7$ decreased, C_{14}, C_{16} and $C_{17}Val_7$ disappeared). In the Liche (Leu) mixture (Figure 2-3C), we also noticed the replacement of Val_4 by Leu_4 or Ile_4, compared with standard Liche sample (Figure 2-3A), leading to the detection of new molecules: $C_{15}Lxx_4Lxx_7$. Due to its first AA to be Gln instead of Glu, this molecule is surely not C_{15}Pumi, but the exact structure needs further characterization.

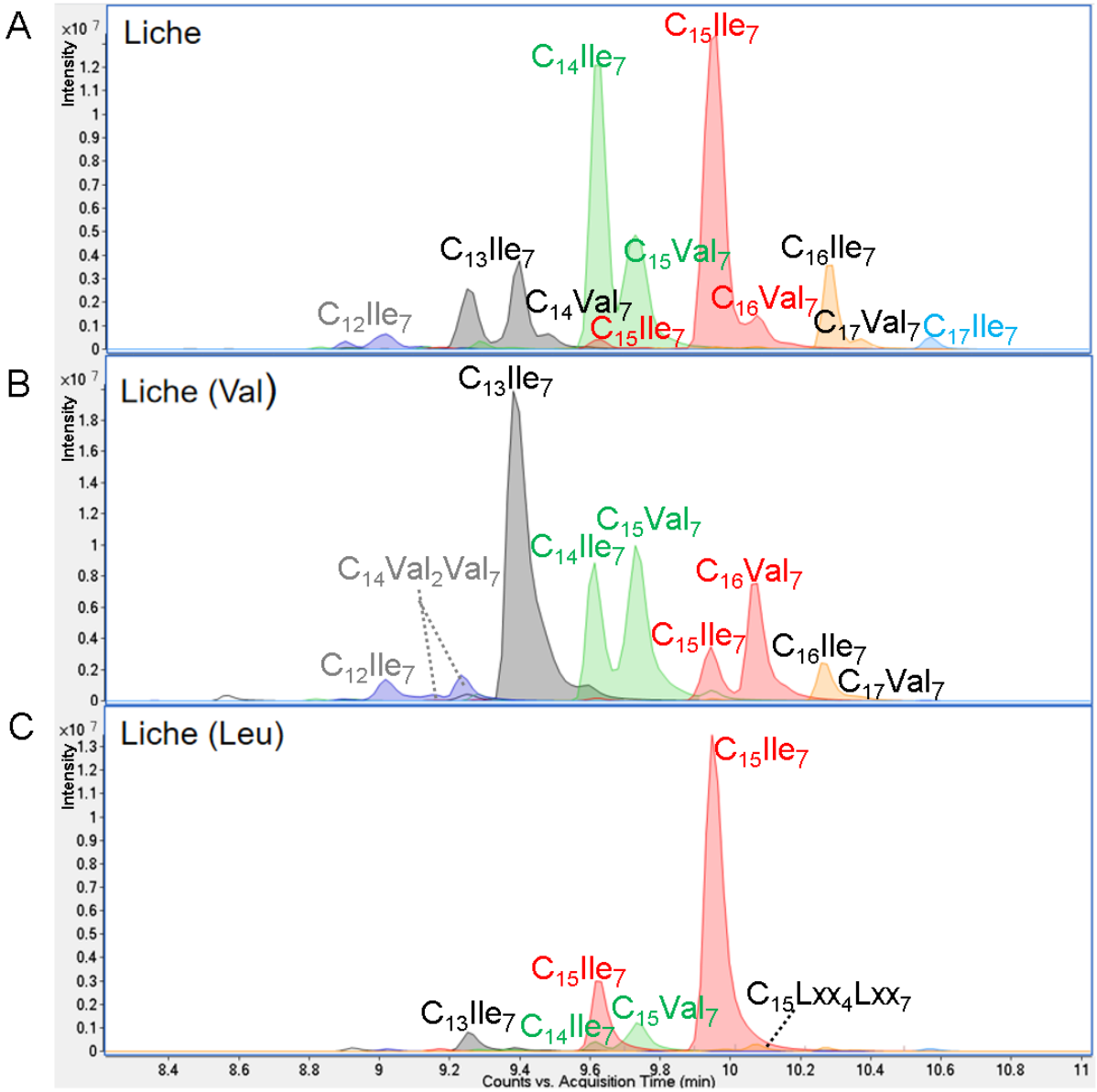
A
Liche
Intensity
x10 7
C15Ile7
C14Ile7
C13Ile7
C15Val7
C16Ile7
C12Ile7
C14Val7
C16Val7
C15Ile7
C17Val7
C17Ile7
B
Liche (Val)
C13Ile7
C15Val7
C14Ile7
C14Val2Val7
C16Val7
C15Ile7
C16Ile7
C12Ile7
C17Val7
C
Liche (Leu)
C15Ile7
C15Ile7
C13Ile7
C14Ile7
C15Val7
C15Lxx4Lxx7
8.4
8.6
8.8
9
9.2
9.4
9.6
9.8
10
10.2
10.4
10.6
10.8
11
Counts vs. Acquisition Time (min)

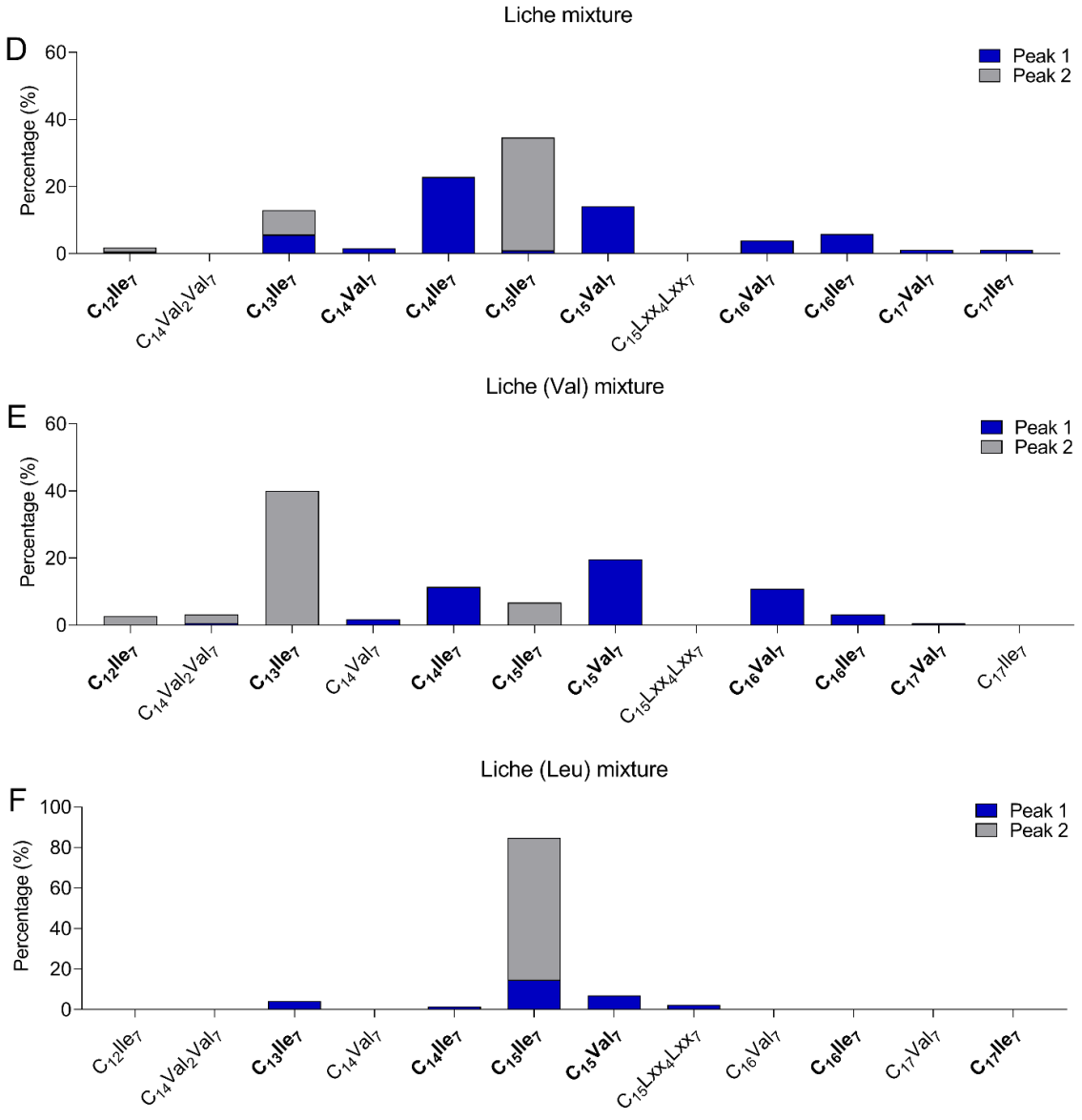

Figure 2-3 Structures of Liche variants.

A, B, **C.** Chromatograms of Liche, Liche (Val), Liche (Leu) mixture, respectively. The different colors refer to corresponding masses detailed in Table A1-2. The dotted lines show the new CLPs; **D, E, F.** Profile of the Liche, Liche (Val), Liche (Leu) mixture, respectively. Bold letters represent the existing canonical CLPs in each CLP mixture. Each purified CLP component was collected and mixed into a single CLP mixture used in this study.

In the Pumi (Val) mixture, comparison between Figure 2-4E and Figure 2-3D shows that except the amount of $C_{14}Val_7$ increased, most the amount of Val_7 decreased ($C_{17}Val_7$ and the second peak of $C_{15}Val_7$ decreased, $C_{13}Val_7$, the first peak of $C_{14}Val_7$ and $C_{15}Val_7$ disappeared); the amount of Ile_7 also decreased ($C_{16}Ile_7$ decreased, C_{15} and the third peak of $C_{17}Ile_7$ disappeared). In the Pumi (Val) mixture (Figure 2-4B), we noticed the replacement of Leu_4 by Val_4, compared with canonical Pumi sample (Figure 2-4A), leading to the detection of Val_4Val_7 (C_{15} to C_{17}). Likewise, we also detected the production of new molecules: $C_{18}Val_7$ and $C_{16}Val_3Val_4Val_7$. Additionally, C_{15} and $C_{16}Val_4Val_7$ detected in the Pumi (Val) mixture share the same retention times with C_{15} and $C_{16}Val_4Val_7$ in the Srf (Val) mixture, making it interesting to detect their importance in the Pumi (Val) mixture.

In the Pumi (Leu) mixture, when comparing Figure 2-4F to Figure 2-4D, except a few decreases (the third peak of $C_{16}Ile_7$ and the second peak of $C_{17}Ile_7$ decreased, $C_{13}Ile_7$ diseapered) most Ile_7 variants increased ($C_{15}Ile_7$, the first two peaks of $C_{16}Ile_7$ and the first peak of $C_{17}Ile_7$ increased) and Val_7 variants decreased (C_{17} and the second peak of $C_{15}Val_7$ decreased, $C_{16}Val_7$ disappeared). No new molecules were detected in the Pumi (Leu) mixture (Figure 2-4C).

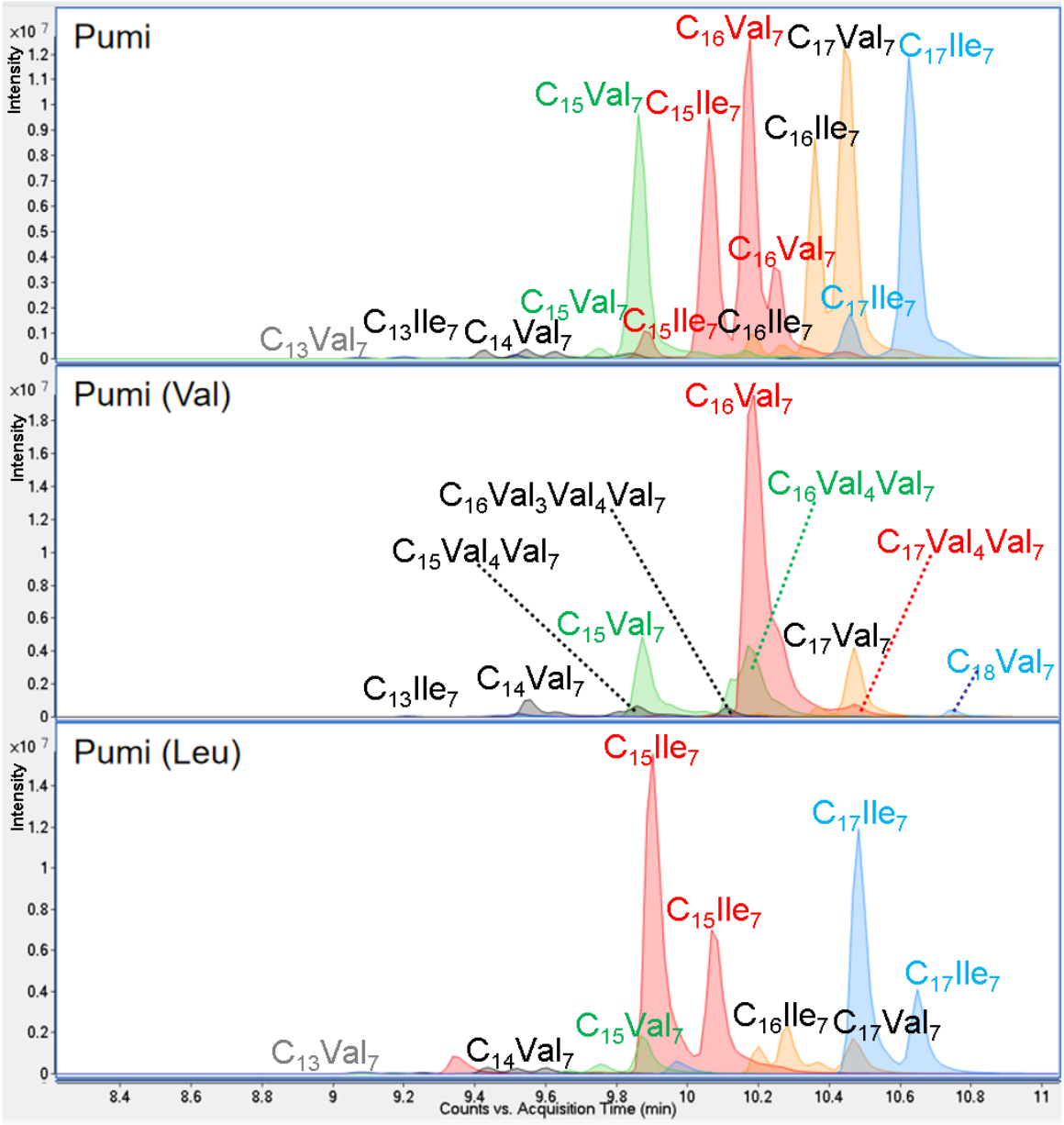
A
Pumi
Intensity
×10 7
C16Val7
C17Val7
C17Ile7
C15Val7
C15Ile7
C16Ile7
C16Val7
C17Ile7
C15Val7
C15Ile7
C16Ile7
C13Val7
C13Ile7
C14Val7
B
Pumi (Val)
C16Val7
C16Val4Val7
C16Val3Val4Val7
C17Val4Val7
C15Val4Val7
C15Val7
C17Val7
C18Val7
C13Ile7
C14Val7
C
Pumi (Leu)
C15Ile7
C17Ile7
C15Ile7
C17Ile7
C15Val7
C16Ile7
C17Val7
C13Val7
C14Val7
8.4
8.6
8.8
9
9.2
9.4
9.6
9.8
10
10.2
10.4
10.6
10.8
11
Counts vs. Acquisition Time (min)

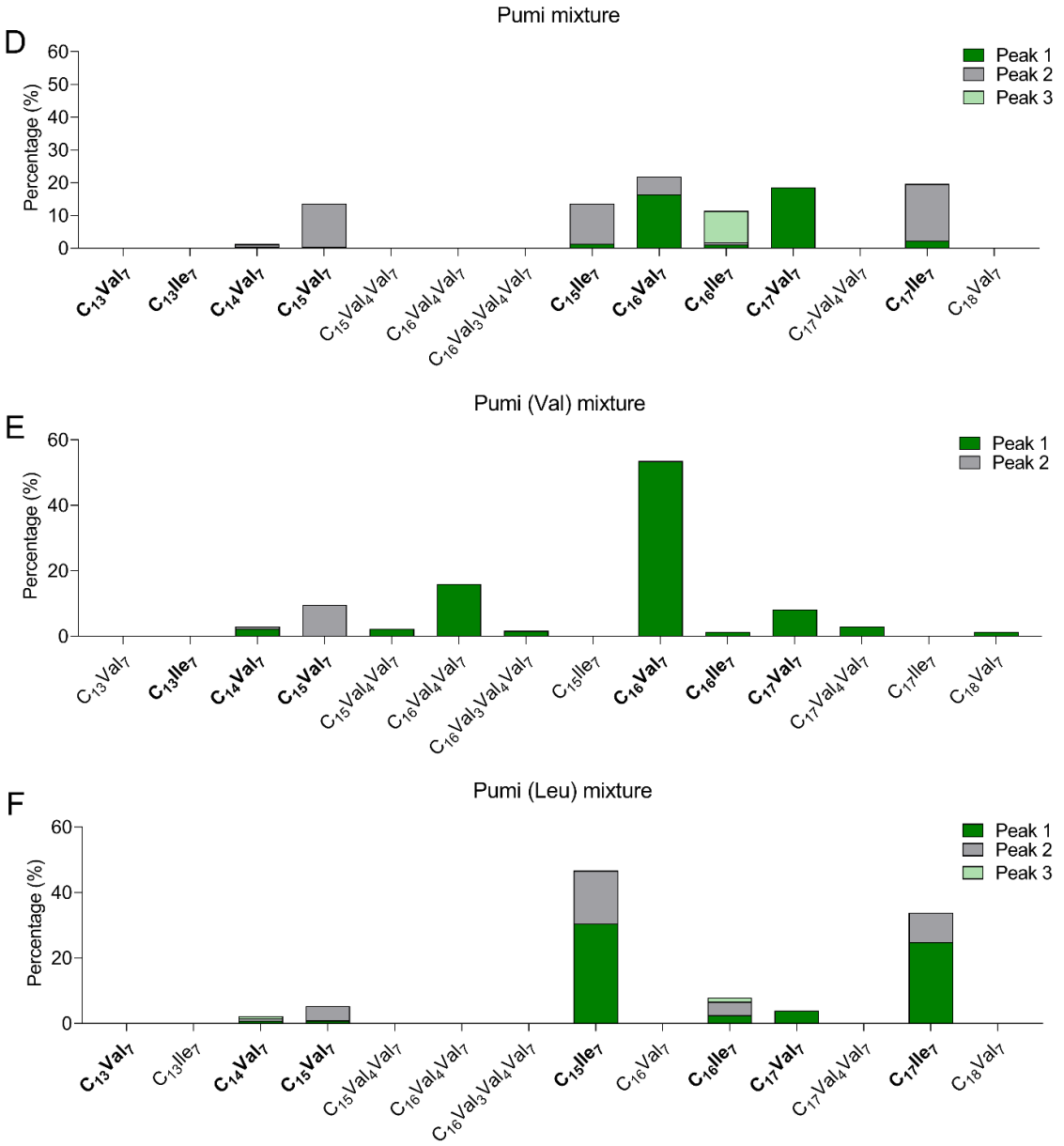

Figure 2-4 Structures of Pumi variants.

A, B, **C.** Chromatograms of Pumi, Pumi (Val), Pumi (Leu) mixture, respectively. The different colors refer to corresponding masses detailed in Table A1-3. The dotted lines show the new CLPs; **D, E, F.** Profile of the Pumi, Pumi (Val), Pumi (Leu) mixture, respectively. Bold letters

represent the existing canonical CLPs in each CLP mixture. In this study, each purified CLP component was collected and mixed into a single CLP mixture.

3.2.1. Identification of new CLP variants

As described above, new CLP molecules were detected from BCAA precursor-directed CLPs, using UPLC-ESI-QTOF MS/MS method. We listed the new molecules mentioned above in Table 2-1. Since most of them are minor within the CLP mixture, we also presented the main CLP homologs from each CLP variant mixture in the same table. CLP structures were confirmed by tandem MS/MS, as presented in Figure 2-5, using the same method as mentioned in section 3.1 of this chapter.

Table 2-1 Basic information on new and main CLP molecules generated from BCAA precursor-directed CLP mixtures.

Name		New CLP homologues	FA chain length of new CLP homologues / percentage	Main CLP homologues / percentage
Srf variants	Srf	/	/	$C_{14}Leu_7$, $C_{15}Leu_7$ / 41.3%, 36.9%
	Srf (Val)	Val_2Val_7 Val_6 Val_7	C_{14}-C_{15} / 5.5%, 1.9% C_{14}-C_{15} / 2.9%, 2.8% C_{13}-C_{16} / 2.5%, 29.3%, 11.7%, 3.9%	$C_{14}Leu_7$, $C_{14}Val_7$ / 25.4%, 29.3%
	Srf (Ile)	Lxx_4Lxx_7 Lxx_7	C_{15}-C_{16} / 23.1%, 0.01% C_{12}-C_{15}, C_{17} / 1.2%, 8.2%, 13.2%, 19.8%, 0.01%	$C_{15}Leu_7$, $C_{15}Lxx_7$, $C_{15}Lxx_4Lxx_7$ / 27.4%, 19.8%, 23.1%
Pumi variants	Pumi	/	/	$C_{16}Val_7$, $C_{17}Val_7$, $C_{17}Ile_7$ / 21.9%, 18.6%, 19.6%
	Pumi (Val)	Val_7 Val_4Val_7 $Val_3Val_4Val_7$	C_{18} / 1.3% C_{15}-C_{17} / 2.3%, 16%, 3% C_{16} / 1.7%	$C_{16}Val_7$ / 53.5%
	Pumi (Leu)	-	-	$C_{15}Ile_7$, $C_{17}Ile_7$ / 46.7%, 33.8%
Liche variants	Liche	/	/	$C_{14}Ile_7$, $C_{15}Ile_7$ / 22.8%, 34.6%
	Liche (Val)	Val_2Val_7	C_{14} / 3.3%	$C_{13}Ile_7$, $C_{15}Val_7$ / 40%, 19.6%
	Liche (Leu)	Lxx_4Lxx_7	C_{15} / 2.4%	$C_{15}Ile_7$ / 84.8%

A

C_{14}Srf Val_2Val_7 from Srf (Val) mixture

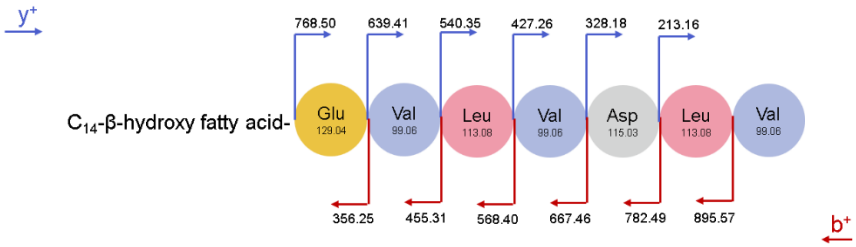

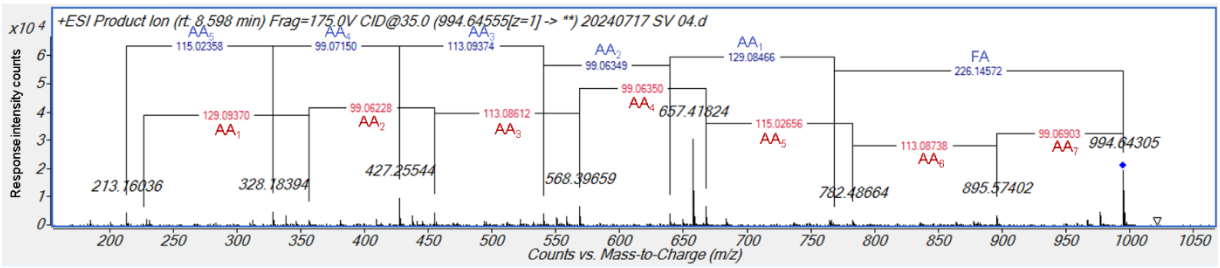

C_{14}Srf Val_6 from Srf (Val) mixture

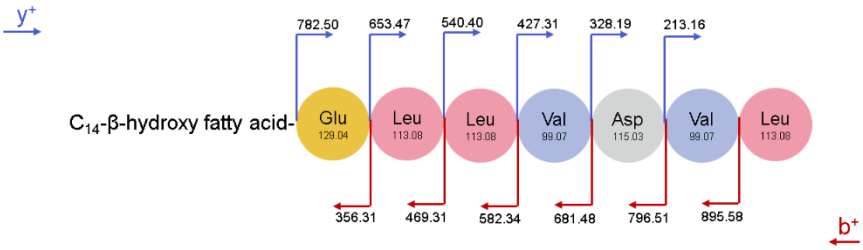

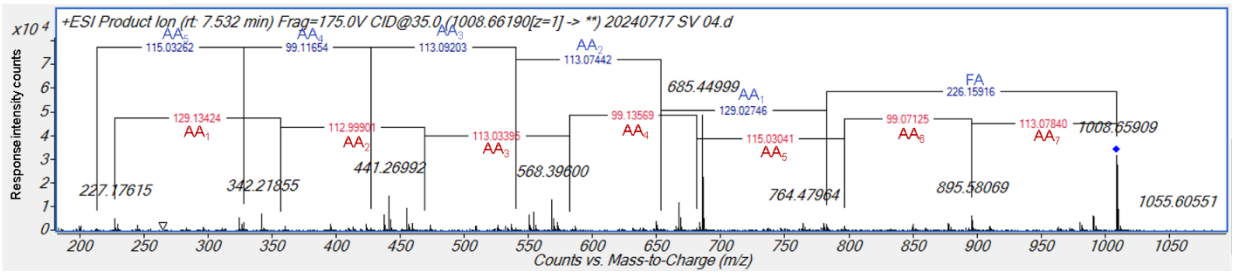

C_{15}Srf Lxx_7 from Srf (Ile) mixture

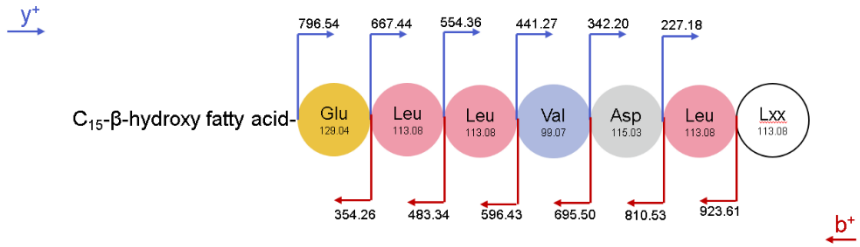

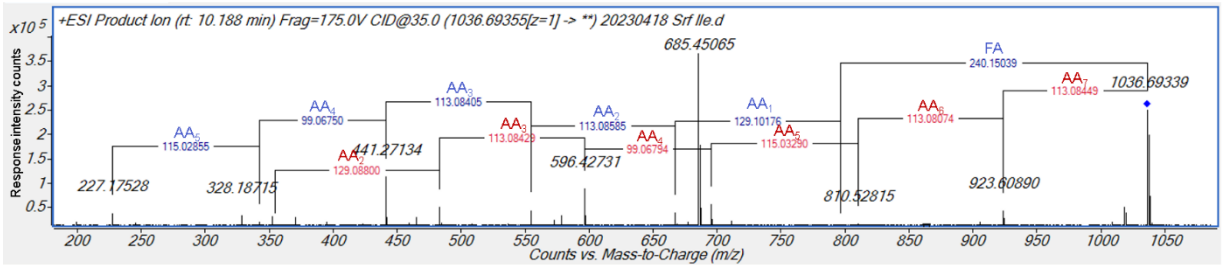

C_{15}Srf Lxx_4Lxx_7 from Srf (Ile) mixture

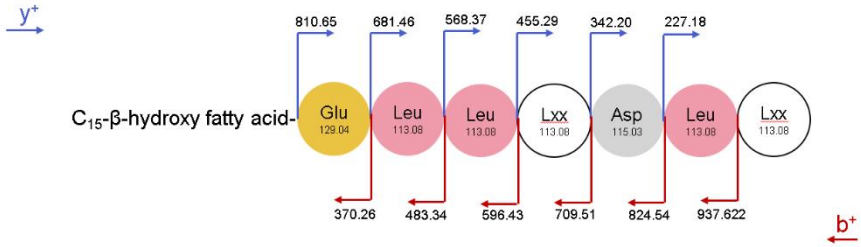

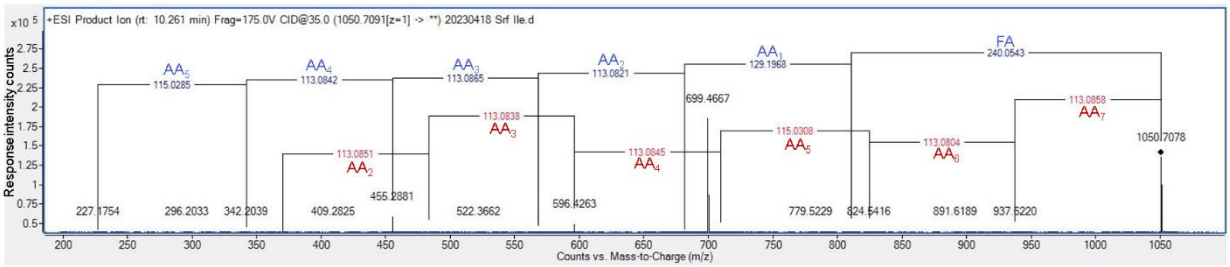

B

C_{18}Pumi Val_7 from Pumi (Val) mixture

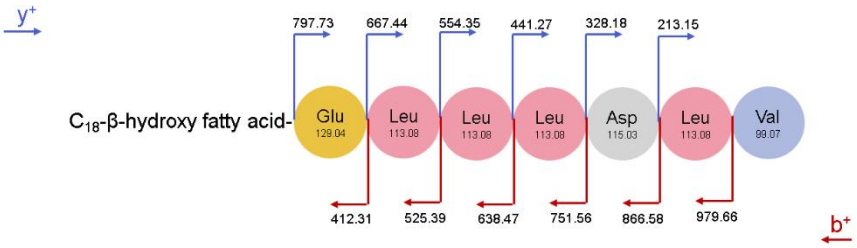

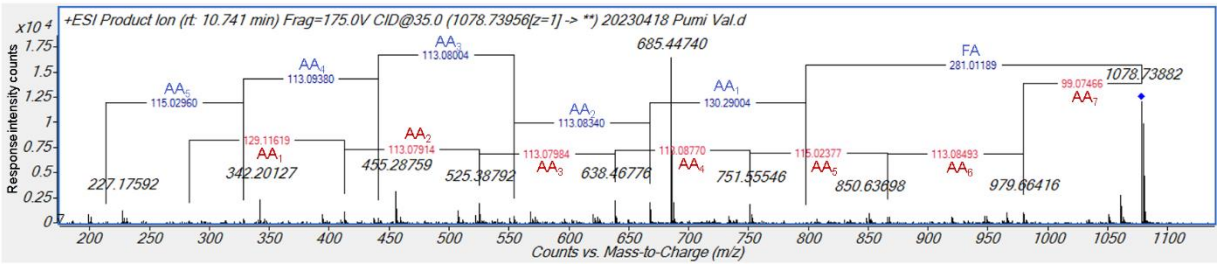

C_{15}Pumi Val_4Val_7 from Pumi (Val) mixture

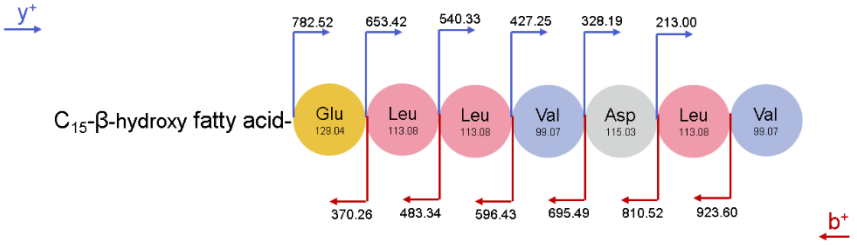

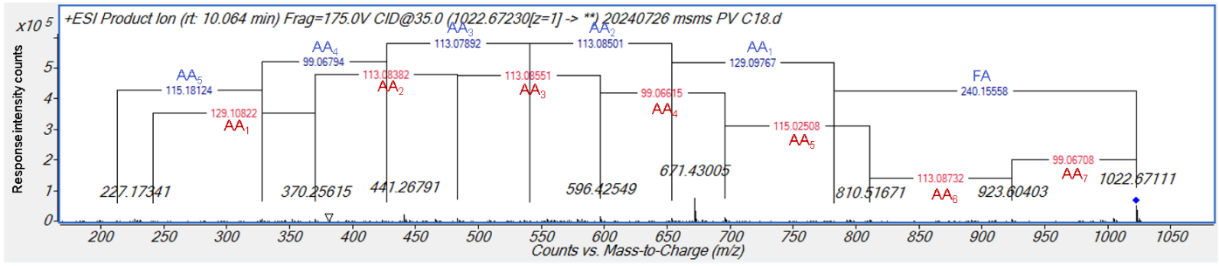

C_{16}Pumi $Val_3Val_4Val_7$ from Pumi (Val) mixture

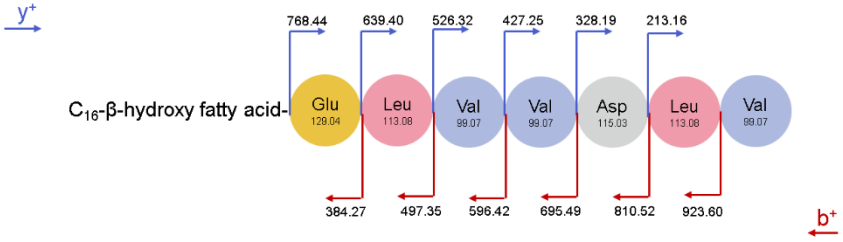

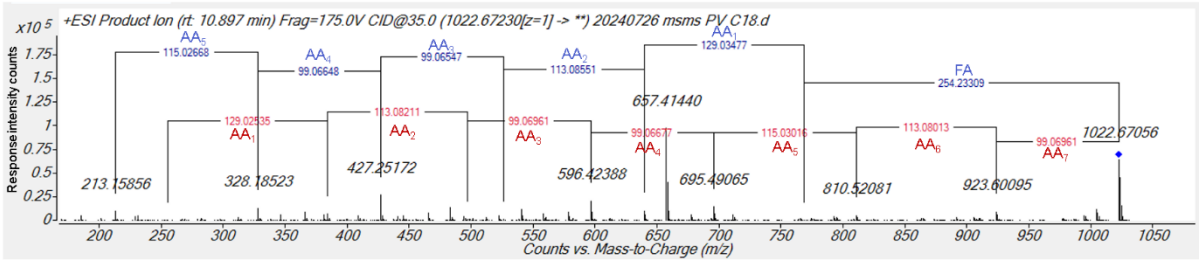

C

C_{14}Liche Val_2Val_7 from Liche (Val) mixture

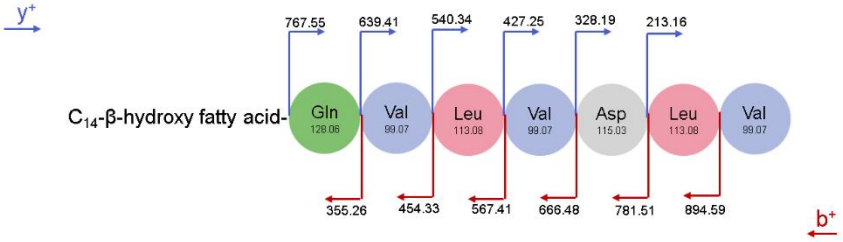

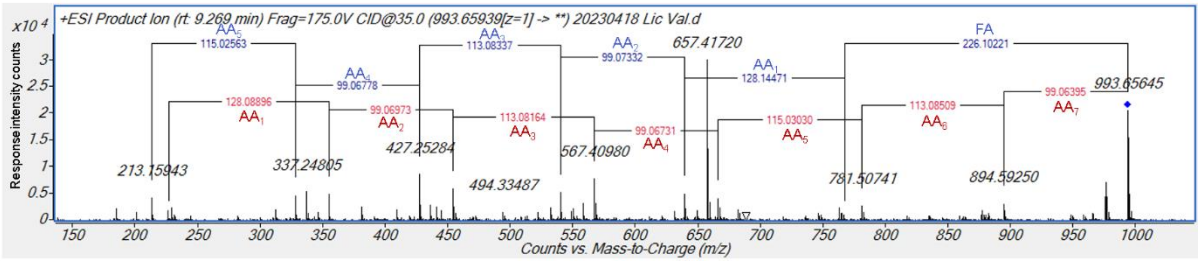

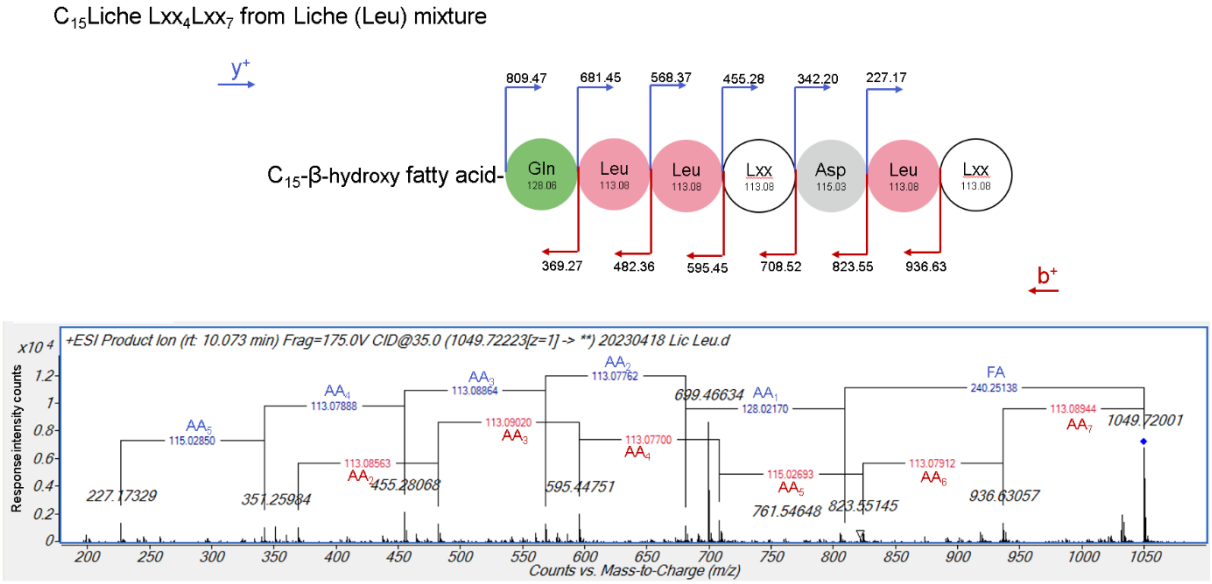

Figure 2-5 New CLP molecules structures generated from BCAA precursor-directed CLPs.

A, B, C represent the structures of new CLP molecules from CLP variants of Srf, Pumi, and Liche respectively (produced in Landy medium with BCAAs supplementation) via UPLC-ESI-QTOF MS/MS spectra. The red and blue arrows show the b^+ and y^+, respectively. FAs and AAs are marked with red or blue color in the MS/MS spectra accordingly.

4. Summary

In this chapter, firstly, we produced and purified canonical CLPs: Srf, Liche, and Pumi, and compared the hydrophobicity among them. Secondly, we generated BCAA-directed CLPs and compared their structures with canonical CLPs using UPLC-MS/MS: Srf and Liche variants production follow similar tendencies with minor differences, which differs to Pumi variants production.

Upon Val supplementation, the amount of Val_7 increases for Srf variants, Liche variants and only even-FA Pumi (C_{14}, C_{16}, C_{18}). The amount of Leu_7/Ile_7 decreases for Srf variants, most Liche variants and most Pumi variants. L-Val supplementation allows Val to replace the original AA not only at position 7; but also at position 2 or 4, leading to Val_2Val_7 (for variants of Srf or Liche), or Val_4Val_7 (for Pumi variants). Moreover, $Val_3Val_4Val_7$ Pumi variants as new molecules were detected. Interestingly, new molecules from Srf variants or Liche variants tend to have FA lengths shorter

than C_{15}, while Pumi variants tend to have FA lengths longer than C_{16}. The canonical CLPs and their variants mentioned in this chapter are all listed in Figure 2-6.

Leu supplementation did not result in new molecules in Pumi (Leu) mixture. For variants of Srf or Liche, the BCAA L-Ile or L-Leu supplementation allows Lxx_7 (for Srf variants) or Lxx_4Lxx_7 (for variants of Srf or Liche) to happen. As expected, L-Ile or L-Leu supplementation decreases the amounts of homologs with Leu_7 (Srf variants) or Ile_7 (most variants of Liche or Pumi), and Val_7 (Liche variants and most Pumi variants).

We further compared the retention times between certain CLP molecules and their canonical CLPs, leading to the hypothesis of a switch between Srf and Pumi: C_{15} and $C_{16}SrfVal_7$ in Pumi (Val) mixture, as well as C_{15}Pumi in Srf (Ile) mixture, which needs further characterization. Our results elucidate the differential impact of the nutritional environment on CLP producers. This finding may be critical for its agricultural efficacy and warrants further investigation. Figure 2-6 summarizes the canonical CLPs and their variants described in this chapter.

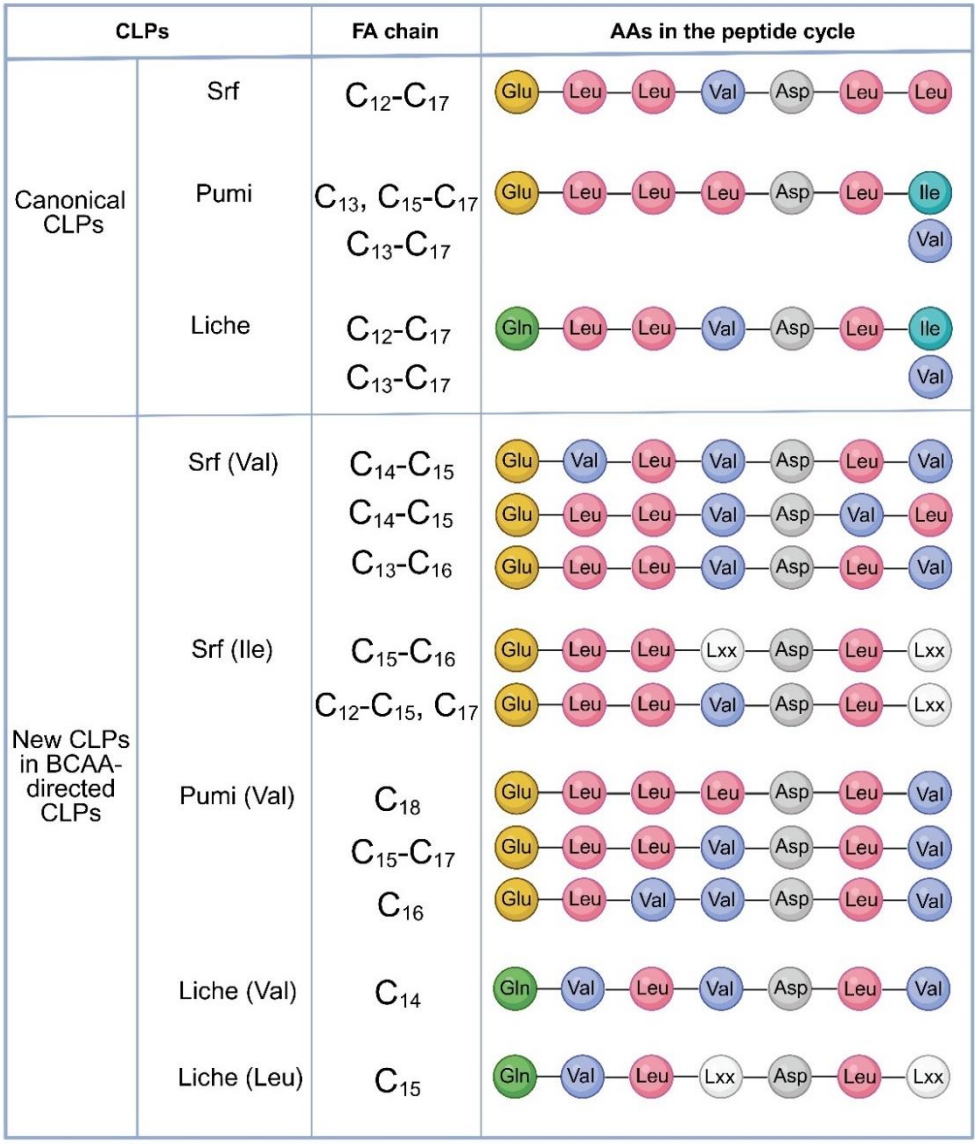

Figure 2-6 Canonical CLPs and their variants.

This figure shows the characteristic structural features of both canonical CLPs (Srf, Pumi, Liche) and the newly identified CLP variants produced in response to L-Val, L-Leu, or L-Ile supplementation in bacterial cultures.

Chapter 3

Plant immunity triggered by CLPs in *Arabidopsis*

Part of the results presented in this chapter have been published in: Ding, N.; Dong, H.; Thomas, R.; Gilliard, G.; Pršić, J.; Ongena, M. Surfactin Structural Variants Differentially Modulate Plant Immune Responses. *Biomolecules* 2025, *15*, 1479. https://doi.org/10.3390/biom15101479. The main findings are summarized but a comprehensive interpretation of these results, together with all data generated in this thesis work is provided in the General discussion.

1. Introduction

Plants have a multilayered defence system to counteract fungal pathogens, beginning with preformed physical and biochemical barriers such as cuticular waxes, cell wall fortifications, antimicrobial enzymes, and specialized metabolites (Ali et al., 2024; Piasecka et al., 2015; Reina-Pinto & Yephremov, 2009). Pathogen recognition is initiated through the detection of conserved PAMPs by PRRs, triggering PTI and associated defence signaling cascades (Tripathi et al., 2024). When pathogens evolve mechanisms to suppress PTI, plants activate a more robust ETI in response to specific pathogen effector proteins. This heightened defence response often includes localized PCD through the HR, effectively restricting pathogen spread in resistant plants (Nguyen et al., 2021).

Early immune responses associated with PTI include the rapid accumulation of extracellular ROS in the apoplast generated mainly by the plasma membrane-located NADPH oxidase RBOHD or by cell wall peroxidases (Waszczak et al., 2018). The elevation of cytoplasmic hydrogen peroxide concentration ($[ROS]_{intra}$) also emerges as an early defence response and could originate from various organelles as reported for ETI or in response to abiotic stresses or other small microbial compounds (Arnaud et al., 2023; Kadota et al., 2015; Waszczak et al., 2018). ROS burst is thus among the earliest measurable immune-related events and functions as dual-purpose agents, exhibiting direct antimicrobial activity while simultaneously acting as signaling compounds. Together with ROS, the production of RNS such as NO is also an important immune-related early event in plants and occurs in the apoplast or across multiple subcellular compartments including the cytosol, mitochondria, chloroplasts, or peroxisomes (Jedelská et al., 2021; Khan et al., 2023). The main way for NO to act is by post-translationally modifying proteins involved in immunity through S-nitrosylation, which impacts their conformation, activity and/or localization, a process highly ubiquitous in the different kingdoms of life (Astier et al., 2018). Additionally, NO can interfere with hormonal signaling, further emphasizing its role in plant immunity (Freschi, 2013). Ca^{2+} influx in plant cells is also typically associated with PTI and in response to many other stresses (Köster et al., 2022), and it is well-established in defence pathway activation (Meng & Zhang, 2013). Plasma membrane Ca^{2+}-permeable channels and intracellular Ca^{2+} sensors function in close coordination during plant immune responses, forming an intricate regulatory network (Zhang et al., 2024).

Plant systemic immunity activated through localized plant-microbe interactions is categorized as either SAR or ISR, distinguished by both the infection site and the nature of the inducing microorganism (Vlot et al., 2021). SAR typically originates from foliar interactions with pathogenic microbes, while ISR is initiated through root colonization by beneficial microorganisms (Vlot et al., 2021). Like pathogens, PBB also trigger early immune events mentioned above, which occur in the early stage of

the induction of ISR (Nie et al., 2017; Yu et al., 2022). Generally, PBB triggering plant immunity is not as well documented, let alone the plant immunity triggered by their metabolites.

Plants could decode molecular messages from their environment to mount defences. Among these messages, CLPs produced by PBB *Bacillus* stand out as multifaceted signals that blur the line between microbial warfare and diplomatic communication. While their antimicrobial properties (such as Srf against bacterial pathogen *Candidatus Liberibacter asiaticus*, fungal pathogens *Rhizoctonia solani*, *Botryosphaeria dothidea*, *Fusarium graminearum*) are well documented (Chowdhury et al., 2015; Chen et al., 2023; Nan et al., 2021; Pang et al., 2021), their role as evolutionarily honed plant immune primers suggests a deeper, symbiotic dimension: CLPs may serve as biochemical triggers that prepare plants for impending threats, while minimizing collateral damage to beneficial microbiota. There is the principle of on-demand CLP production, wherein bacterial synthesis of these metabolites is dynamically regulated, either enhanced or suppressed, depending on physiological requirements and the nature of the interacting organism (Balleux et al., 2024). Among CLPs, Srf production is enhanced when grown on root exudates, with this lipopeptide playing a critical role in facilitating biofilm formation, motility, and early root colonization by the bacterium (Hoff et al., 2021).Within this particular nutritional environment, the bacterium also adjusts the composition of coproduced Srf homologs, preferentially generating variants that exhibit heightened efficacy in inducing plant immune responses (Hoff et al., 2021). Other previous works from the laboratory have shown that changes in the surfactin molecule may impact its potential to trigger immune-related responses in tobacco cells (Henry et al., 2011; Jourdan et al., 2009), but globally, information on the structure-activity relationship underpinning immune activation by this molecule remains limited.

In this work, we investigated three structurally distinct Surfactin-family lipopeptides Srf, Liche and Pumi, along with their media-derived CLP variants, to decipher the molecular basis of their immune-eliciting efficacy in plants. Using *Arabidopsis* as a model, we evaluated their potential as root-applied foliar biofungicides through a multi-tiered approach: quantifying early immune markers ($[ROS]_{intra}$, NO, and Ca^{2+}) in root tissues and root cell protoplasts; analyzing concentration-dependent immune induction via $[ROS]_{intra}$ kinetics; assessing membrane remodeling using generalized polarization in root protoplasts. These experiments mechanistically linked root-localized CLP perception to distal leaf resistance, revealing how specific structural features govern immune activation.

2. Materials and methods

2.1. Plant growth conditions

All *Arabidopsis* seeds were kept at 4°C, in a dark environment, prior to sterilization by ethanol (70%) for 3 minutes and then by a bleach solution (17% bleach, 0.2% tween-80) for 6 minutes, later washed by sterile water for at least 3 times. After sterilization, seeds were planted in Petri dishes with MS (1% sucrose) solid culture medium, which were vertically placed at 22°C, under 12/12 hours of light and dark environment.

2.2. Protoplast extraction

Two-week-old *Arabidopsis* seedling roots (from 27 mg seeds) were collected and put into a new Petri dish with 1 mL of fresh enzymatic solution (400 mM mannitol, 20 mM KCl, 10 mM $CaCl_2$, 0.1% BSA, 1.5% cellulase, 0.4% macerozyme, 10 mM MES, pH=5.7), and cut by a clean scalpel into pieces. 3 mL extra fresh enzymatic solution were applied, and then to incubate in dark at room temperature for 4 hours. After incubation, 1 mL solution A (154 mM NaCl, 5 mM KCl, 125 mM $CaCl_2$, 4 mM MES, pH=5.7) was added inside. The suspension was agitated gently and filtered by gauze to remove extra roots tissues The Petri dish was rinsed by 2 mL solution A and then the former step was repeated to collect more protoplasts. Filtered suspension was centrifuged at 850 g for 6 min at room temperature and the sediment was kept to be washed by 5 mL solution A at 850 g for 6 min at room temperature. 2 mL solution B (500 mM mannitol, 20 mM KCl, 2 mM $CaCl_2$, 4 mM MES, pH=5.7) was used to collect protoplasts. The concentration of root protoplasts was counted with Bürker, while $1\text{-}2\times10^5$ root protoplasts per mL was required for the further fluorescence detection.

2.3. ROS measurements

For cytoplasmic hydrogen peroxide (reflecting cytosolic/intracellular ROS and referred hereafter as $[ROS]_{intra}$) measurement in roots, 15 mm long *Arabidopsis thaliana* root segments, isolated from different two-week-old plants, were placed in a well (one root/well) of a microplate (96 Flat Black–Greiner Bio-One™ CellStar™, Fischer Scientific) filled with sterile water. After overnight incubation, roots were treated with 50 µM DCFH-DA (dichloro-dihydro-fluorescein diacetate; ACROS Organics) for 10 minutes in the dark, rinsed with PBS and next, wells were filled with CLP/mock solution. Fluorescence measurements (excitation wavelength 492 nm, emission wavelength 530 nm) were conducted by a Spark® (Tecan) microplate reader by using nine readings per well. Data expressed as relative fluorescence increase were obtained

by subtracting the fluorescence measured at the first time point from the fluorescence measured at each time point (the first time point was taken as 0). The fluorescence fold increase was defined for each repetition as the ratio between the fluorescence increase obtained at one time point for treatments and the mean fluorescence increase obtained at the same time point in mock treated tissues.

For $[ROS]_{intra}$ measurements in protoplasts, protoplasts isolated from roots of *Arabidopsis thaliana* Col-0 plants were incubated for 10 minutes with 5 µM of DCFH-DA. Then, wells of black 96-well microplates (96 Flat Black - Greiner Bio-One™ CellStar™, Fischer Scientific) were loaded with 150 µL of protoplasts solution per well. After the addition of 50 µL of four times concentrated CLP treatment, the fluorescence was recorded every minute using a microplate reader with excitation filter at 485 ± 20 nm and emission filter at 535 ± 25 nm. The data were processed in the same way as in roots.

2.4. RNS measurements

For the detection of intracellular NO, roots were processed as described above and 200 µL sterile water was replaced by 200 µL 5 µM DAF-DA in buffered solution (10 mM Tris/HCl, pH = 7.4). Roots were incubated at room temperature for 1 hour in the absence of light and then washed 3 times with Tris/HCl (10 mM, pH=7.4). The fluorescence emitted by DAF-DA was detected by excitation at 495 nm and emission at 515 nm. Experiments where NO was measured after pre-treatment with the calcium channel blocker or calcium chelator included an additional step where $LaCl_3$ (10 mM; Sigma-Aldrich) or EGTA (1 mM; Sigma-Aldrich) respectively, were added three minutes before treatments. Data were processed in the same way as described above for ROS. For NO measurements in protoplasts, the suspension was incubated in the same conditions before being distributed (50 µL) in microplate wells and treated with the CLPs at 10 µM final concentration or with 0.1% DMSO as mock.

2.5. Calcium influx measurements

Calcium measurements were also performed on protoplasts with the Fluo-4 AM probe. Protoplasts isolated from roots of Arabidopsis thaliana Col-0 were incubated for 1 hour with 5 µM of Fluo-4 AM (ThermoFischer) (from a 5 mM stock solution in DMSO). The suspension was then centrifuged at 750 g and the supernatant was discarded to eliminate the remaining free fluo-4 AM. The protoplasts were resuspended in fresh solu-tion C and were incubated for 1 hour. Microplates (96 Flat Black-Greiner Bio-One™ CellStar™, Fischer Scientific) were loaded with 150 µL of protoplasts solution per well. After the addition of 50 µL of 4 times concentrated treatment, the fluorescence was rec-orded every 15 seconds using a Spark® microplate

reader (Tecan) with an excitation filter at 485 ± 20 nm and an emission filter at 535 ± 25 nm. The values obtained were then converted as normalized fluorescence increase (F/F0) by dividing the fluorescence meas-ured at each time point (F) by the fluorescence measured at the first time point (F0).

2.6. Laurdan measurements

To detect Laurdan polarization in *Arabidopsis* root protoplasts, we firstly prepared fresh protoplasts as described above. Afterwards, we added 1 µM Laurdan into protoplasts suspension with the number atround 2×10^5 /mL for 1h 30 min and applied this solution into 96-well flat-bottomed plate (Greiner Bio-One™), then used the SPARK® multimode microplate reader to detect the fluorescence with emission wavelength between 410 nm and 500 nm, with the excitation wavelength at 360 nm. After adding more concentrated CLP to make sure final concentration at 10 µM, the fluorescences were recorded for more than 20 min. The generalized polarization (GP) was calculated by $(I_{440nm}-I_{490nm})/(I_{440nm}+I_{490nm})$, of which I_{440nm} represents the blank subtracted fluorescences intensities with emission wavelength at 440 nm and I_{490nm} at 490 nm.

2.7. ISR in Arabidopsis triggered by CLPs

Plants were grown for 4 weeks in hydroponic conditions in Araponics systems containing nutrient solution (0.25% (v/v) FLORAMICRO®, 0.25% (v/v) FLORABLOOM®, 0.25% (v/v) FLORAGRO®; General Hydroponics®), in volume ratio 1:1:1, as recommended by the manufacturer, with a photoperiod of 12 hours and a temperature of 22°C. Plants were then transferred in 10 mL vials filled with fresh nutrient solution and treated at the root level with CLPs or ethanol (mock treatment) to obtain final concentrations of 10 µM and 0.1% respectively. After incubation for 24 h, plants were inoculated with *Botrytis cinerea* as conidia solution. Spores were collected from *B. cinerea* grown on PDA plates for four weeks using solution composed of 1.75 g/L KH_2PO4, 0.74 g/L $MgSO_4$, 4 g/L glucose and 0.02 % (v/v) Tween 20. After spore collection the concentration was adjusted to $5x10^5$ spores per mL, and spores were incubated at 30°C for eight hours. Inoculation was conducted by inoculating a drop of 3 µL of conidia solution onto seven leaves per plant and fifteen plants per treatment. The number of spreading lesions was evaluated 96 h post infection.

2.8. Statistical analysis

Statistical analyses were conducted using GraphPad Prism 8.0.2. Differences between groups were assessed using two tailed t-test. The notation “ns” denotes a lack

of statistical significance, while *, **, *** and **** indicate levels of significance corresponding to $p < 0.05$, $p < 0.01$, $p < 0.001$ and $p < 0.0001$, respectively.

3. Results

3.1. Early immune events triggered by canonical CLPs in Arabidopsis

3.1.1. Defence responses in root tissues

In this study, we used the $[ROS]_{intra}$ burst as initial proxy to compare the immune activation potential of the various CLPs in *Arabidopsis thaliana* roots when treated with a 10 µM solution, which was previously determined to be the minimal active concentration (Cawoy et al., 2014). CLPs were used as a mix of homologs (Figure 2-1) in all subsequent experiments. Results showed that Srf and Liche significantly increased $[ROS]_{intra}$ production compared to mock-treated plant roots, while Pumi did not exhibit significant triggering activity (Figure 3-1 A, B). Treatment of roots with Srf at 10 µM induces a rapid accumulation of NO compared to the control as revealed by staining with the DAF-DA fluorescence probe (Figure 3-1 C, D). A similar fluorescence increase was observed upon treatment with Liche whereas Pumi had no impact on this marker of immunity.

Our results suggest that, Srf stimulates RNS, which can act in concert with ROS as redox regulators during plant immune responses, although the exact pathway remains to be determined. Elevated NO levels typically correlate with increased ROS production, and their interaction can enhance defence responses (Shah et al., 2023). This reciprocal relationship is maintained through dual feedback mechanisms where ROS promotes NO generation, and NO modulates antioxidant defences to prevent oxidative damage and sustain cellular redox homeostasis (Shah et al., 2023).

To test the integration of ionic and redox signaling upon Srf perception, we examined NO burst after pretreatment of *Arabidopsis thaliana* roots with the Ca^{2+} chelator EGTA and the Ca^{2+} channel blocker $LaCl_3$. In both cases, Srf-induced RNS was abolished (Figure 3-1 E, F), indicating that NO synthesis of is Ca^{2+} dependent as previously reported for immune activation in other systems (Courtois et al., 2008). Intracellularly, NO can be produced by nitrate reductases [NADH] 1 (NIA1) and NIA2 as triggered upon infection by the pathogen *Pseudomonas syringae* pv. *maculicola* (Modolo et al., 2005). Using the *Arabidopsis thaliana nia1nia2* double mutant in response to Srf treatment, we observed a fully conserved induction of NO production (Figure 3-1 G). This indicates that Srf-induced RNS burst is mediated via another pathway, similar to that reported upon lipopolysaccharide elicitation involving NO synthase (Mur et al., 2006; Zeidler et al., 2004).

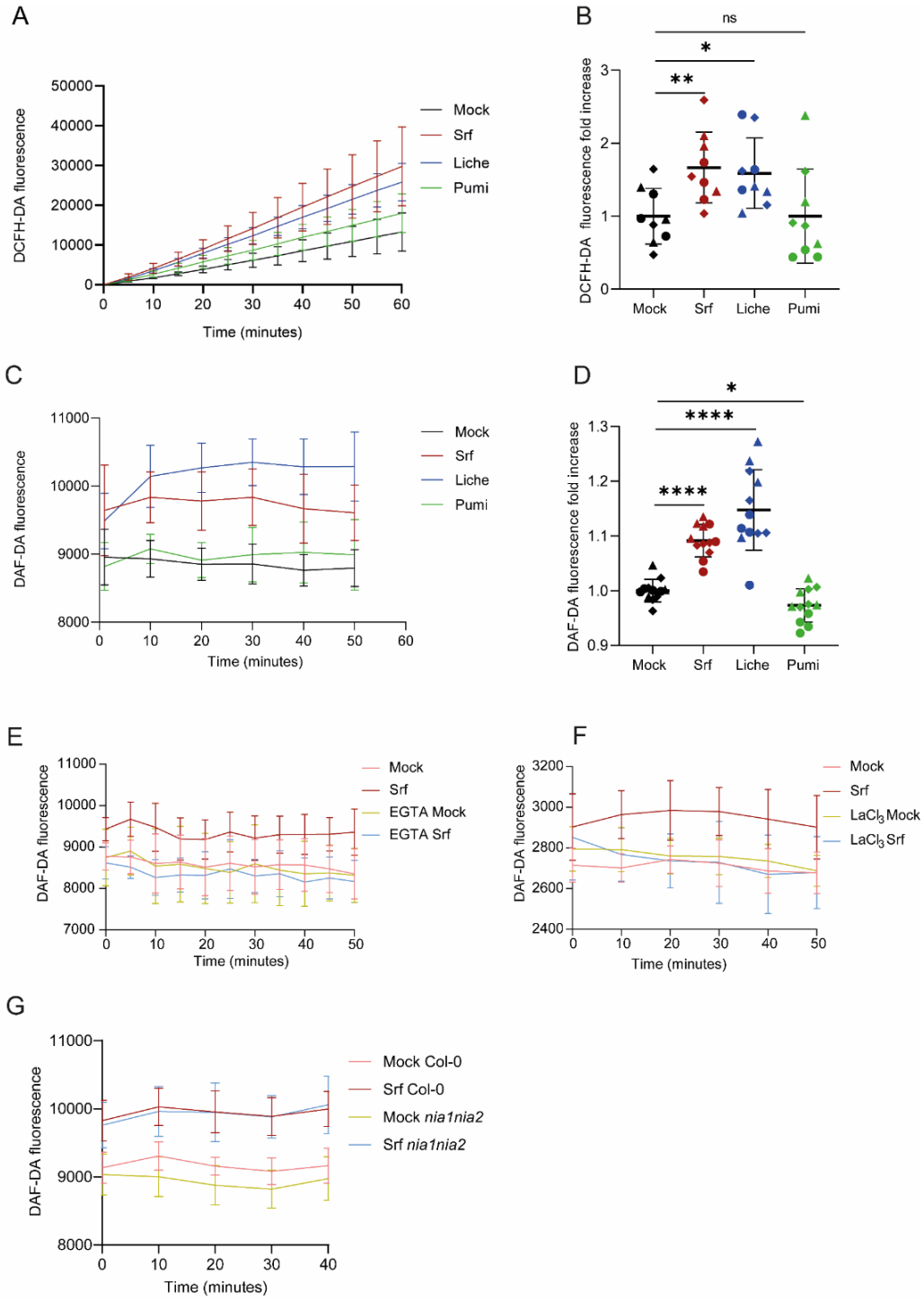

Figure 3-1 Detection of early immune events in *Arabidopsis* roots triggered by CLPs.

A. $[ROS]_{intra}$ production; **C**. NO production ± SD measured 60 minutes following treatment in *Arabidopsis* roots; **B**, **D**. Fold change calculated at 20 min by using values obtained from the mock-treated roots. The three shapes of dots in panels B and D represent values obtained from three independent experiments (n=9 and n=12, respectively). Asterisks indicate statistically significant differences compared with the mock plants (two tailed t-test, $^{*}P < 0.05$, $^{**}P < 0.01$, $^{****}P < 0.0001$). (**E, F**) Fluorescence increase reflecting RNS bursts, measured in roots over 50 minutes following Srf treatment with or without pre-incubation using the calcium channel blocker $LaCl_3$ (C) or the Ca^{2+} ion chelator EGTA (D). Data are the mean ± SD with n=8 from two independent experiments. **G**. Srf-induced NO independent of NR activity in *Arabidopsis thaliana* Col-0 or *nia1nia2* mutant roots. Fluorescence ± SD was measured 40 minutes after Srf treatment in roots. N=12 from three independent experiments.

3.1.2. Defence responses in protoplasts from root cells

We also wanted to evaluate the response of ROS to CLPs in individual root cells. To that end, we used protoplasts derived from root tissues, which have been reported to be an interesting and relevant tool for studying plant stress signaling and plant defence mechanisms. First, we tested ROS-triggering activity and observed a very similar trend to that seen in roots with Srf and Liche at 10 µM, which displayed significant boosting activity, while Pumi was inactive (Figure 3-2A). These results strongly support the relevance of these isolated cells as a study system for early immune activation, as domonstrated with various other elicitors. A similar trend in NO signaling was also observed when protoplasts of root cells were treated with 10 µM Srf or Liche (Figure 3-2B). To further analyze the impact of CLP structural differences on Ca^{2+} production in *Arabidopsis thaliana*, we monitored $[Ca^{2+}]_{cyt}$ production in root protoplasts using a specific Fluo4-AM fluorescent probe. We observed a fast increase in $[Ca^{2+}]_{cyt}$ within minutes of treating with Srf and Liche at 10 µM, but not with Pumi. Integrating data from independent assays showed that the slight increase in $[Ca^{2+}]_{cyt}$ production induced by Pumi is not significant (Figure 3-2C).

To further evaluate the effects of CLPs on plant cell membranes, an environmentally sensitive fluorescent probe Laurdan, was used to assess the packing and dynamics of membrane lipids in *Arabidopsis* root protoplasts. Our data revealed the capacity of CLPs influence to alter plasma membrane fluidity in *Arabidopsis* root protoplasts is influenced by structural variations among CLPs, as evidenced by changes in GP values. Srf and Liche at 10 µM showed the most pronounced lipid-ordering effects, while Pumi at the same concentration did not affect the physical state of the plant membrane in protoplasts (Figure 3-2D).

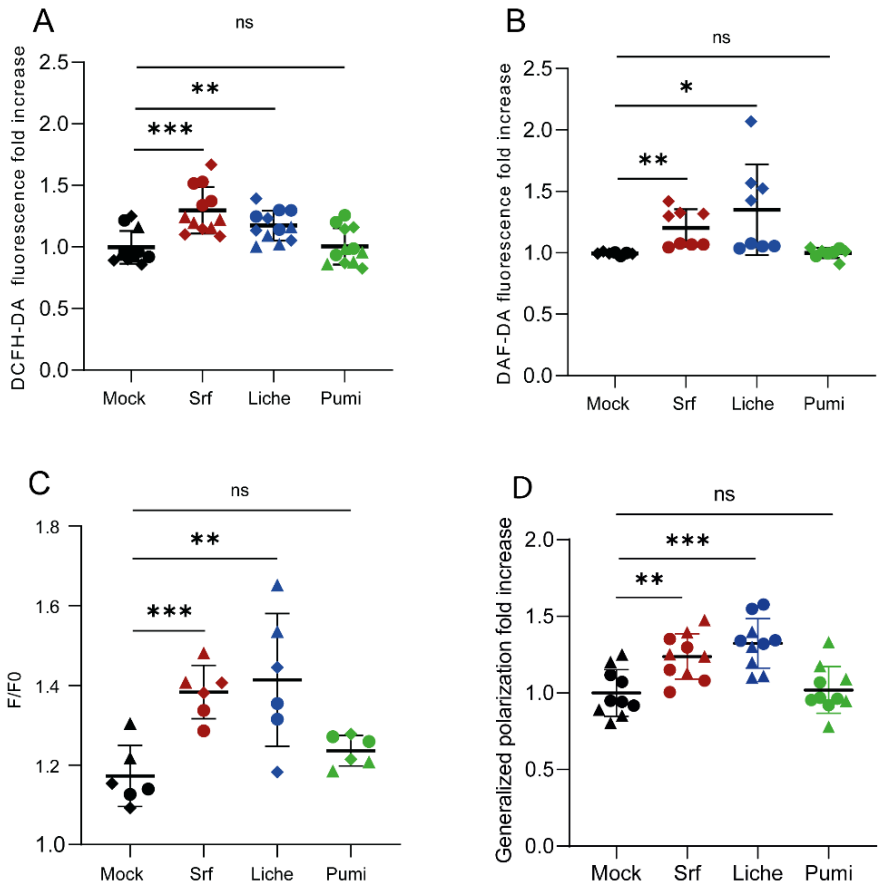

Figure 3-2 Detection of early immune events in *Arabidopsis* root protoplasts by CLPs.

Quantification of CLP-induced $[ROS]_{intra}$ (**A**) or NO burst (**B**) in roots protoplasts represented as fold changes calculated by using values obtained upon CLP treatment at 20 min divided by the average values of the mock-treated roots or root protoplasts in each experiment. N=9 or 12 respectively, from three independent experiments presented by three shapes of dots. **C**. Ca^{2+} influx in Col-0 protoplasts measured by Fluo-4 fluorescence after CLP treatment (10 µM). Mean ± SD; n=6 from three independent experiments. **D**. Fold change of Laurdan GP in mock or CLP variants at 10 µM treated *Arabidopsis* protoplasts of root cells. Graphs show the means ± SD calculated from ten biological replicates (n=10) collected from two independent experiments. Asterisks indicate statistically significant differences compared with the mock treatment (two tailed t-test, $^{*}P < 0.05$, $^{**}P < 0.01$, $^{***}P < 0.001$, ns=not significant).

3.1.3. ROS response triggered by CLPs at different concentrations

All of the mentioned CLP-*Arabidopsis* experiments only focused on 10 µM CLPs (a decision based on previous tests with Srf, in which Pumi did not show any responses). We also wanted to test the effect of each CLP at concentrations of 2 µM, 10 µM and 40 µM on the $[ROS]_{intra}$ response. Data collected from two independent experiments confirmed that unlike Srf and Liche, Pumi is not active at intermediate and high concentrations. Interestingly, the three CLPs efficiently trigger an $[ROS]_{intra}$ burst but at the lower dose of 2 µM (Figure 3-3). The higher activity of Pumi should be tested with other early events.

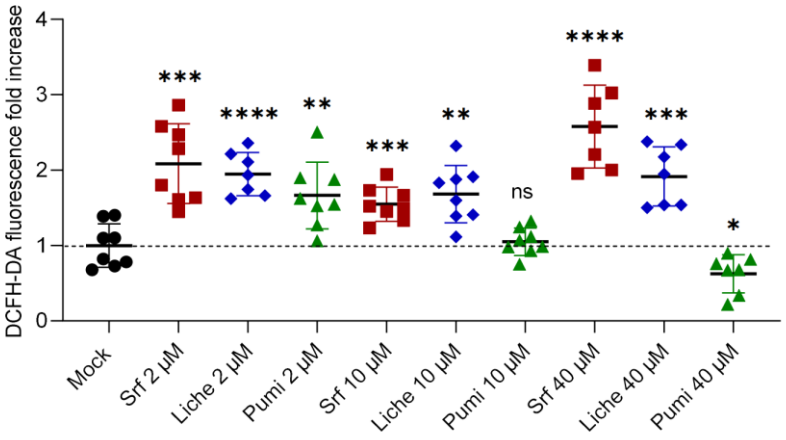

Figure 3-3 ROS production in *Arabidopsis* roots treated by CLPs at various concentrations.

Fold change in $[ROS]_{intra}$ production by CLPs compared to the mock treatment after 20 min in *Arabidopsis* roots. The graphs show the means ± SD, which were calculated from eight biological replicates collected from two independent experiments. Asterisks indicate statistically significant differences compared to the mock plants (two tailed t-test, $^{*}P < 0.05$, $^{**}P < 0.01$, $^{***}P < 0.001$, $^{****}P < 0.0001$, ns=not significant).

3.1.4. ISR triggered in *Arabidopsis* by CLPs against *Botrytis cinerea* in *Arabidopsis*

Early immune-related events initiate signaling and transcriptional reprogramming, which ultimately lead to the local and systemic accumulation of defence compounds and pathogen resistance (DeFalco & Zipfel, 2021). The most important functional outcome, is the ability to stimulate systemic resistance in *Arabidopsis thaliana*, so we wanted to determine the potential of Liche and Pumi in comparison to Srf. In these assays, CLPs were applied at a concentration of 10 µM via root treatment in a hydroponic setup 24 h prior to the infection of leaves with the necrotrophic

phytopathogen *B. cinerea*. Four days post infection (dpi), the disease level was determined by counting lesion numbers, as illustrated in Figure 3-4A, which shows representative symptoms typically observed. Root treatment with Srf and Liche significantly reduced leaf infection by the gray mold pathogen; however, no disease reduction compared to controls was observed with Pumi (Figure 3-4). Thus, there is thus a strong correlation between the ability of a CLP to trigger early immune events and its efficiency as an elicitor of systemic resistance.

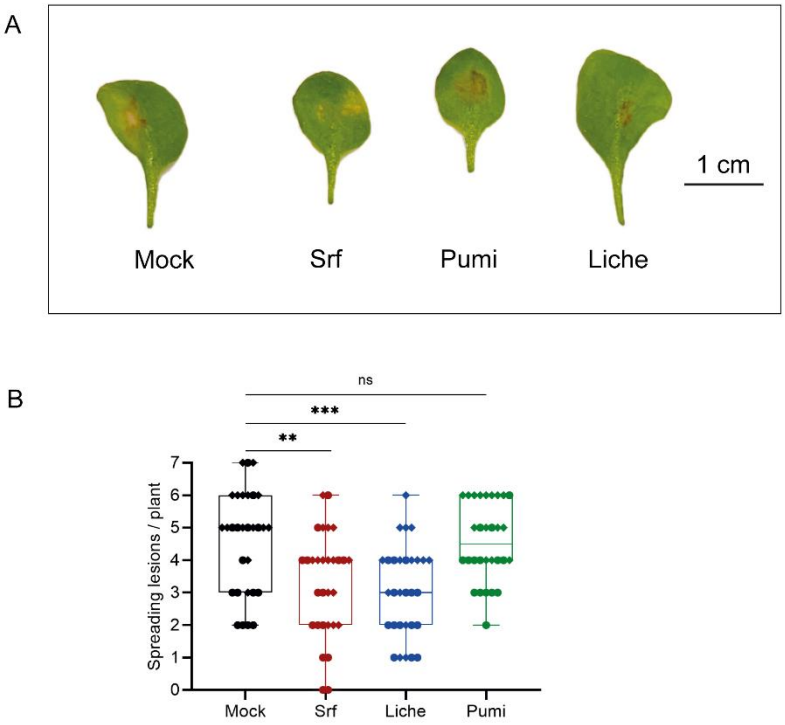

Figure 3-4 The ISR in *Arabidopsis* treated by CLPs.

Representative symptoms of lesions that are typically observed on the leaves of hydroponically grown *Arabidopsis thaliana* Col-0 plants 4 dpi by *Botrytis cinerea*; **B**. Disease incidence in *Arabidopsis thaliana* Col-0 pre-treated with 10 µM CLP or a mock treatment (0.1% EtOH) prior to *B. cinerea* infection (n=30 from two independent experiments). Boxplots encompass the first and third quartiles and bars extend from the lower to the higher values. Asterisks indicate statistically significant differences compared with the mock treatment (two tailed t-test, $^{**}P < 0.01$, $^{***}P < 0.001$, ns=not significant).

3.2. Early immune events triggered by precursor-directed CLPs

3.2.1. In root tissues

To further investigate how structural variations among CLPs influence their immune-eliciting activity, we selected six distinct variants that differ maximally from canonical CLP structures: Srf (Val), Srf (Ile), Pumi (Val), Pumi (Leu), Liche (Val), and Liche (Leu). These compounds were applied as mixtures of congeners (described in Chapter 2) to *Arabidopsis* roots at a concentration of 10 µM to monitor early immune signaling events. Using the fluorescent probes DCFH-DA for $[ROS]_{intra}$ and DAF-DA for NO, we quantified reactive species production in root tips (1.5 cm from the apex) following treatment.

The results (Figure 3-5) from two independent experiments of each show that all tested CLP variants induced $[ROS]_{intra}$ and NO production 20 minutes aftr treatment compared to the mock controls. Production increased by between 1.1 times and 1.8 times. Only Pumi failed to trigger significant $[ROS]_{intra}$ or NO accumulation. This should also be detected in protoplasts of root cells.

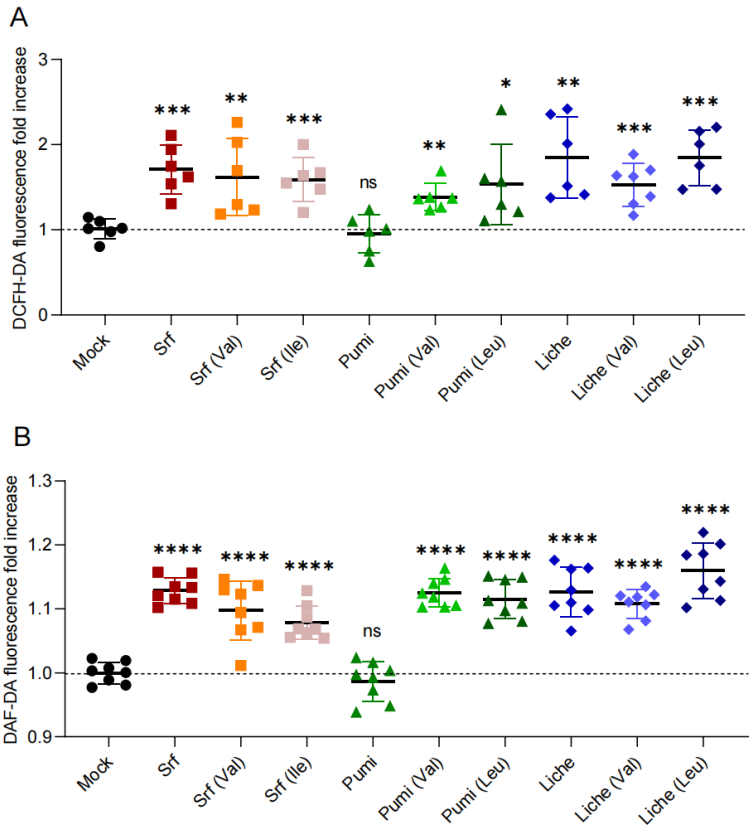

Figure 3-5 Induction of oxidative species burst in *Arabidopsis* roots treated by CLP variants.

The fold change of **A**. $[ROS]_{intra}$ production, and **B**. NO production was calculated at 20 min compared to the mock-treated *Arabidopsis* roots. The four shapes of the dots represent the four types of treatment: mock, Srf variants, Pumi varaints, and Liche variants. The graphs show the means ± SD, which were calculated from eight or six biological replicates (n=8 or 6) from two independent experiments. Asterisks indicate statistically significant differences compared with the mock plants (two tailed t-test, $^{*}P < 0.05$, $^{**}P < 0.01$, $^{***}P < 0.001$, $^{****}P < 0.0001$).

3.2.2. In protoplasts

Following the detection of the early immune events in *Arabidopsis* after CLP variant treatment, we further detected ROS and NO bursts as well as $[Ca^{2+}]_{cyt}$ in *Arabidopsis* root cell protoplasts treated with 10 µM CLP. Our comprehensive analysis (Figure 3-6) from two independent experiments revealed three tiers of activity. Srf, Srf (Ile), Pumi (Leu), and Liche triggered the complete triad of $[ROS]_{intra}$, NO, and $[Ca^{2+}]_{cyt}$ fluxes; Liche (Val) induced $[ROS]_{intra}$ and NO (but not $[Ca^{2+}]_{cyt}$). Srf (Val), Pumi (Val), and Liche (Leu) elicited only singular responses (either $[ROS]_{intra}$ or NO). Pumi

failed to activate any signals. While prior research has emphasized the importance of the plant cell membrane in ISR induction (Gilliard et al., 2026), our synthesis of findings from *Arabidopsis* roots and root cell protoplasts highlights the critical role of the cell wall in CLP-induced plant early immune responses in plants. However, the mechanistic link between these early events and ISR remains to be fully elucidated.

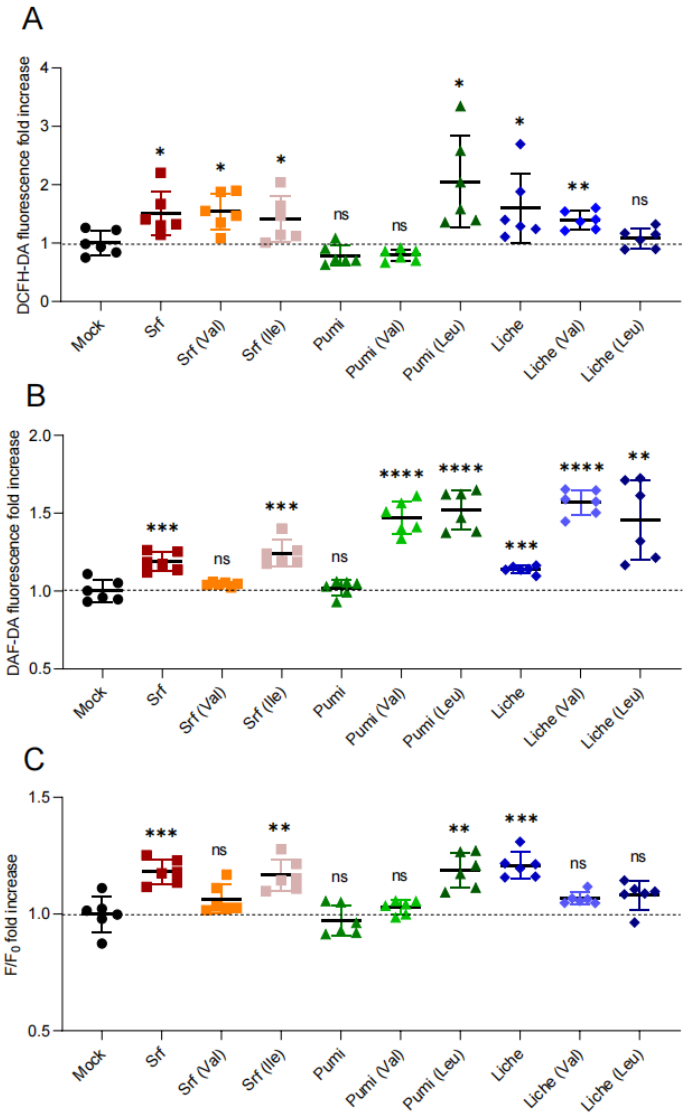

Figure 3-6 Induction of oxidative species and Ca^{2+} bursts in *Arabidopsis* root protoplasts treated by CLP variants.

The fold change of **A.** $[ROS]_{intra}$ production, **B.** NO production, and **C**. $[Ca^{2+}]_{cyt}$ production treated by CLPs compared to the mock treatment after 20 min in *Arabidopsis* root protoplasts. The four shapes of the dots represent the four types of treatments: mock, Srf variants, Pumi varaints, and Liche variants. The graphs show the means ± SD, which were calculated from six biological replicates (n=6) collected from two independent experiments. Asterisks indicate statistically significant differences compared to the mock plants (two tailed t-test, $^{*}P < 0.05$, $^{**}P < 0.01$, $^{***}P < 0.001$).

3.2.3. ISR triggered in *Arabidopsis* by CLPs

To evaluate the correlation between early immune responses and upcoming systemic resistance, we selected two structurally distinct CLP variants: Srf (Val) and Pumi (Leu), based on their different immune-triggering activity compared to the canonical CLP, for *Botrytis cinerea* challenge assays in *Arabidopsis*. The lower disease incidence (decreased lesion numbers) upon 10 µM Srf (Val) treatment (Figure 3-7B) in contrast to with 10 µM Pumi (Leu) treatment (Figure 3-7B) across three independent experiments highlights the structural specificity of CLP peptides in triggering plant ISR. This finding contrasts with the data observed for early immune events in Figure 3-5. Although 10 µM Srf (Val) treatment is relatively inefficient at inducing early immune-related events, it significantly reduced lesion numbers. Conversely, 10 µM Pumi (Leu) treatment triggered robust early defence signaling but did not reduce lesion incidence. These results suggest that the core molecular pattern necessary for ISR is conserved in BCAA-precursor-generated CLP variants.

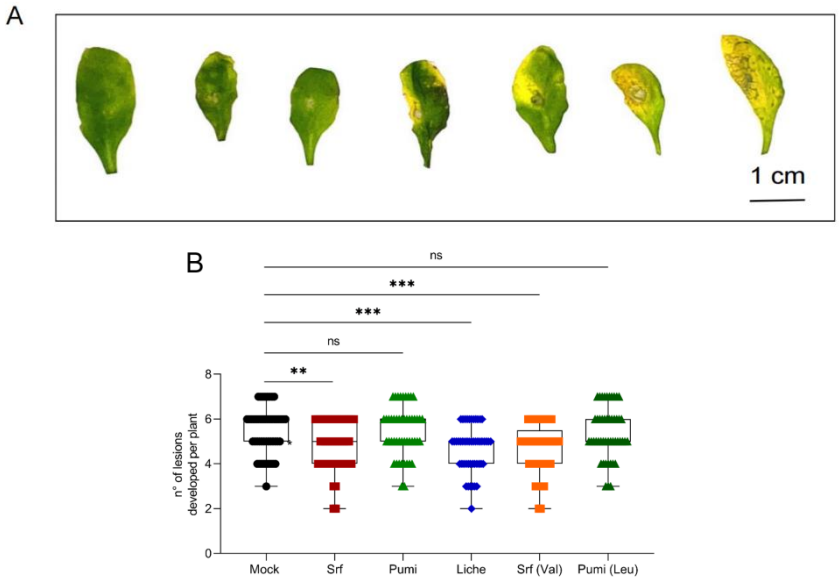

Figure 3-7 The ISR in *Arabidopsis* triggered by CLPs.

A. Disease severity in *Arabidopsis* leaves infected by *Botrysis cinerea*, increasing from left to right. **B.** Lesions were counted in ISR experiments treated with different CLPs. The data represent the mean number of lesions ± SD on leaves infected with *B. cinerea* (n= 48 from three independent experiments), counted 96 hours after CLP pretreatment of the roots. Asterisks indicate statistically significant differences compared with the mock plants (two tailed t-test, $^{*}P < 0.05$, $^{***}P < 0.001$, $^{****}P < 0.0001$).

4. Summary

In Chapter 3, we examined the relationship between the CLP structure and its role in activating plant immunity. Our study successfully evaluated the early root cell signaling events, such as ROS, NO, and Ca^{2+} in *Arabidopsis* treated with 10 µM Srf or Liche, as well as ISR against subsequent pathogen infection. These results support the potential of Liche for future field application as a biopesticide. We hypothesize that the ability of Srf and Liche to induce ISR, unlike Pumi, stems from their distinct interactions with host membrane components. Additionally, CLP concentration plays an important role in Pumi triggering early events; further experiments are needed to better this phenomenon.

Preliminary investigations into early immune signaling and ISR, conducted with CLPs generated via BCAA precursor-directed synthesis, reveal the significant complexity of the CLP structure-function relationship. While the core ISR-triggering pattern is conserved in BCAA-derived CLPs, the efficacy of systemic resistance is decoupled from the intensity of early immune signaling. A conclusive mechanistic understanding will require direct comparisons among purified single CLP homologs. To further investigate CLP structure and function in plant protection besides ISR ability, CLP variants could be examined for other properties, such as antimicrobial function.

Chapter 4

Molecular aspects of ISR triggered by CLPs

1. Introduction

Plant immunity is coordinately regulated by an intricate signaling network centered on two key defence phytohormones SA and JA, which is further modulated through crosstalk with additional hormonal pathways, including auxin, ET, ABA, cytokinins, brassinosteroids, and gibberellin signaling, to enable precise tuning of plant defence responses to diverse biotic challenges (Yu et al., 2019). Molecular crosstalk between mentioned defence-related phytohormones and abiotic stress signaling pathways, such as ABA-mediated regulation can modulate plant immunity (Teixeira et al., 2019).

The induction of ISR in *Arabidopsis* mediates a dual protective function: it enhances host resistance against soil-borne root pathogens while simultaneously modulating rhizosphere microbial community composition (Vlot et al., 2021). For example, ISR activation leads to root exudation of the coumarin derivative scopoletin in *Arabidopsis*, which exhibits selective antimicrobial activity. Notably, this compound demonstrates differential effects on microbial growth, while remaining ineffective against ISR-promoting rhizobacteria, such as *Pseudomonas simiae* or *Pseudomonas capeferrum*, but significantly inhibits pathogenic fungi, such as *Fusarium oxysporum* and *Verticillium dahliae* (Stringlis et al., 2018). Additionally, the biosynthesis of coumarin-type secondary metabolites has recently emerged as a distinct defence pathway activated in plants in response to *Bacillus* species (Bai et al., 2024). Accordingly, Srf, a representative metabolite of this genus, previously demonstrated in Chapter 3 to prime immunity in *Arabidopsis thaliana* against subsequent pathogen attack, likely exerts its ISR function, through the modulation of coumarin-related pathways.

The transcription factor MYB72 plays a pivotal role in *Arabidopsis* ISR activation against both (hemi-)biotrophic and necrotrophic pathogens (Van der Ent et al., 2008; Vlot et al., 2021). Beneficial rhizobacteria *Pseudomonas*-induced systemic resistance upregulates fluorescent phenolic compound scopolin/scopoletin biosynthesis in a MYB72-dependent manner; while the *f6h'1* mutant is deficient in coumarin production, the *bglu42* mutant exhibits substantial intracellular accumulation of scopolin, resulting from a deficiency in its capacity to convert scopolin into antimicrobial scopoletin, and excrete the latter one into the rhizosphere (Stassen et al., 2021; Stringlis et al., 2018; Zamioudis et al., 2015). Genetic studies reveal MYB72 coregulation with iron homeostasis pathways, suggesting an integration of defence and nutrient acquisition mechanisms (Zamioudis et al., 2015). The enzymatic products of BGLU42, particularly scopoletin, are proposed to function as mobile signaling molecules that translocate from roots to shoots, potentially contributing to systemic ISR activation (Stassen et al., 2021). Endogenous scopolin can move from roots to shoots while in roots and leaves scopoletin concentration was negligible compared to scopolin, xylem sap contained more scopoletin than scopolin (Robe et al., 2021). Interestingly, it was found that scopoletin was effective against *B. cinerea* infection by inhibiting *B. cinerea* mycelial growth and conidial germination, disrupting cell

wall, cell membrane, as well as infection towards structure formation (Yuan et al., 2024).

Previous RNA-sequencing results of Srf treated *Arabidopsis* from this laboratory bring up four genes (*CYP71A12*, *ERF6*, *MYB51*, *CML37*) that draw our attention. *CYP71A12* encodes Cytochrome P450, which is responsible for the biosynthesis of phytoalexin camalexin (Millet et al., 2010), a kind of indole-containing compound that participates in plant defences and resistance against necrotrophic and biotrophic pathogens (Nguyen et al., 2022). The accumulation of camalexin was potentiated within ISR induced by PBB *Bacillus subtilis* or *Pseudomonas fluorescens*, against the pathogens *Botrytis cinerea* and *Pseudomonas syringae Pst* DC3000 (Nguyen et al., 2022). Therefore, camalexin might also play a role in CLP triggered ISR activity. Additionally, ERF6 is a transcription factor from ERFs, and it positively regulates defence gene expression as well as plant resistance to the necrotrophic fungal pathogen *Botrytis cinerea*, though its regulation in defensin gene activation is independent of ethylene (Meng et al., 2013). MYB51, as another transcription factor, is essential for the regulation of indole-glucosinolate biosynthesis that might lead to responses to biotic stress (Gigolashvili et al., 2007). CML37, as a Ca^{2+} sensor protein, is important in regulating responses to abiotic and biotic stresses (Heyer et al., 2022). Additionally, oxylipin azelaic acid (AZA) acts as a signaling metabolite in the induction of systemic resistance, with its pathway involving the lipid transfer proteins AZI1 and EARLI1 as key components (Cecchini et al., 2019). Transcriptional profiling of plant immune-related genes following CLP treatment will provide a foundational dataset essential for identifying and characterizing novel defence pathways integral to CLP induced immunity.

CLPs are potent elicitors of ISR in plants and Srf, the most extensively characterized CLP for that function, has demonstrated broad-spectrum protective effects across diverse plant-pathogen systems. However, the underlying molecular mechanisms remain poorly understood. In this chapter, we investigated some of the mechanisms potentially involved in CLP-mediated plant immunity using canonical Srf as model CLP. We focused our investigation on three distinct defence pathways. First, we examined the role of coumarin in CLP-triggered ISR by profiling the expression of coumarin biosynthesis-associated genes *MYB72* and *BGLU42*, and evaluating ISR induction in coumarin-deficient *Arabidopsis* mutants. Second, after detecting *CYP71A27* expression via RT-qPCR, we quantified the phytoalexin camalexin from *Arabidopsis* leaves and roots. Third, we analyzed possible modulation of phytohormone levels (ABA, JA and SA) in both leaves and roots following CLP root pretreatment and subsequent *Botrytis cinerea* pathogen infection. Additionally, we assessed the expression of some selected defence-related genes in *Arabidopsis* roots in response to CLP treatment. This multi-pathway approach was designed to provide a more integrated understanding of the molecular mechanisms by which CLPs prime systemic immunity in plants.

2. Materials and methods

2.1. Plant growth conditions

In this study, *Arabidopsis thaliana* wild type Col-0, reporter lines *pMYB72*: GFP and *pBGLU42*: GFP-GUS, mutants *f6h1-1*, *bglu42* (kindly provided by Christian Dubos, University of Montpellier, Montpellier, France) were used. All *Arabidopsis* seeds were kept at 4°C, in a dark environment, prior to sterilization by ethanol (70%) for 3 minutes and then by a bleach solution (17% bleach, 0.2% tween-80) for 6 minutes, later washed by sterile water for at least 3 times. After sterilization, seeds were planted in Petri dishes with MS (1% sucrose) solid culture medium, which were vertically placed at 22°C, under 12/12 hours of light and dark environment.

2.2. GFP reporter lines based analysis

Seedlings of the *Arabidopsis thaliana* reporter lines *pMYB72:GFP-GUS* and *pBGLU42:GFP-GUS* were germinated and cultivated for seven days under the aforementioned conditions. Uniform plantlets were then transferred to 96-well optical bottom black microplates (Greiner 96 µClear). Each well contained 150 µL of the hydroponic solution. Following transfer, the microplates were sealed and incubated in a growth chamber under controlled conditions (22°C with a 12-hour photoperiod). On the fifth day of this incubation, the plates were treated by adding 150 µL of either the CLP solution or a mock control to each well. Fluorescence measurements were subsequently acquired using a Spark microplate reader, configured with an excitation wavelength of 485 nm and an emission wavelength of 530 nm. Data were collected with nine measurement points acquired per well to ensure robustness.

2.3. ISR in Arabidopsis triggered by CLPs

Five-day-old *Arabidopsis* mutants *f6'h1-1, bglu42* seedlings were transferred in a sterile environment from MS plate into seed holders which were filled with 7.5 g/L sterile agar in a hydroponic system with 1.8 L sterile hydroponic medium (0.25% (v/v) FLORAMICRO®, 0.25% (v/v) FLORABLOOM®, 0.25% (v/v) FLORAGRO®; General Hydroponics®), in volume ratio 1:1:1, as recommended by the manufacturer, at 22°C, under 12/12 hours of light and dark environment until four weeks old. Plants were then transferred in 10 mL vials filled with fresh nutrient solution and treated at the root level with CLPs or mock treatment to obtain final concentrations of 10 µM and 0.1% respectively. After incubation for 24 h, plants were inoculated with *Botrytis cinerea* as conidia solution. Spores were collected from *B. cinerea* grown on PDA plates for four weeks using solution composed of 1.75 g/L KH_2PO4, 0.74 g/L $MgSO_4$, 4 g/L glucose and 0.02 % (v/v) Tween 20. After spore collection the concentration

was adjusted to $5x10^5$ spores per mL, and spores were incubated at 30°C for eight hours. Inoculation was conducted by inoculating a drop of 3 µL of conidia solution onto seven leaves per plant and fifteen plants per treatment. The number of spreading lesions was evaluated 96 h post infection.

2.4. RT-qPCR analysis

After roots of eight 12-day-old *Arabidopsis* Col-0 seedlings treated by 10 µM CLP for six hours, the seedlings were flash frozen by liquid nitrogen. Each CLP treatment contains eight seedlings. Frozen tissues were homogenized by using Eppendorf pestles before using Plant RNeasy Plant Mini Kit for RNA extraction according to the manufacturer's instructions. Afterwards, reverse transcription quantitative polymerase chain reaction (RT-qPCR) was conducted by using Luna Universal One-Step RT-qPCR Kit. The thermal cycling program was: 55°C for 10 min, and 95°C for 1 min; 95°C for 10 s and 60°C for 30 s, which lasted 40 cycles. This was followed by a melting curve: 95°C for 15 s, and 60°C for 1 min; 95°C for 15 s. Quantstudio Design and Analysis software was used for analysis via the $2^{-\Delta\Delta Ct}$ method. Housekeeping gene *UBQ5* was used to normalize mRNA levels in this study. The expression level of each gene was determined using the gene-specific primers listed in Table 4-1.

Table 4-1 List of primers used in this study.

Primer name	Gene	Primer sequence (5'-3')
*CYP71A12*_Fw	At2g30750	CGAAAGCGAGAAGAGTATTGGA
*CYP71A12*_Rev	At2g30750	TGTGGCCTAATGGTTGACCG
*ERF6*_Fw	At4g17490	GAAAACCGCCGTTGAAGATC
*ERF6*_Rev	At4g17490	CGGTTGCGAATTGAATCCA
*MYB51*_Fw	At1g18570	CTACAAGTGTTTCCGTTGACTCTGAA
*MYB51*_Rev	At1g18570	ACGAAATTATCGCAGTACATTAGAGGA
*CML37*_Fw	At5g42380	ACGAGCAGTAATAGTAGCGGAAGCA
*CML37*_Rev	At5g42380	CGCCTAAGAGACTAACGCAGCTTT
*EARLI1*_Fw	At4g12480	TGCAACCCAAGTCCTAAGCA
*EARLI1*_Rev	At4g12480	AACGTTCGCACATACACCGA
*AZI1*_Fw	At4g12470	CAAGCCGGTCCAATGTCCTC
*AZI1*_Rev	At4g12470	CAAACCTTGGATGAGCGAGC
*UBQ5*_Fw	At3g62250	GGAAGAAGAAGACTTACACC
*UBQ5*_Rev	At3g62250	AGTCCACACTTACCACAGTA

2.5. Extraction and quantification of phytohormones and camalexin

To extract camalexin and the phytohormones ABA, JA in *Arabidopsis* roots and rosette leaves, we firstly used three flash frozen independent samples each containing five *Arabidopsis* treated by CLPs in roots, around 100 mg of their leaves or roots after grinding with liquid nitrogen were used for extraction. Secondly, we started the first extraction by adding 1 mL 80% methanol to each sample and placing all the samples on bench rotating agitator in dark (covered by aluminium foil) at room temperature for two hours. Then, we centrifuged each sample at 15180 g for five minutes to collect the supernatant and transfer into another tube. The supernatant was transferred into a new tube and put in a rational vacuum concentrator speedvac (2-25 CD plus, Christ) at 50℃ to dry. Thirdly, we started second extraction by adding 1 mL 100% methanol into the first tube and suspended before applying it on bench rotating agitator in dark (covered by aluminium foil) at room temperature for one hour. Then each sample was centrifuged at 15180 g for five minutes to collect the new supernatant. This supernatant was mixed with previous dry sample, and the drying process continued with speedvac (2-25 CD plus, Christ) at 50℃. Once fully dry, each powder was resuspended with 1 mL 100% methanol to vortex until the total dissolution. 0.22 µM PTFE filters were used before LC-MS analyses.

To quantify the amount of camalexin from *Arabidopsis* roots or rosette leaves samples, we used Agilent 1290 Infinity II HPLC system with C18 reversed phase (waters acquity premier BEH C18 1.7µm 2.1 mm x 50 mm) was at a flow rate of 0.2 mL/min, a temperature of 40°C. The injection volume was 10 µL, and a gradient of acidified water containing 0.1% TFA (solvent A) and of ACN containing 0.1% TFA (solvent B) was used as mobile phase with a constant flow rate of 0.2 mL/min, and column temperature set at 40℃ with the min pressure at 0 bar, and the max pressure at 1k bar. Solvent B was kept at 25% for 1 min followed by an increase from 25% to 60% in 4 min. Then 100% solvent B was applied for 2.5 min before going back to initial conditions in 0.5 min and kept for 4 min. That was coupled with a mass detector (Agilent Technologies 6530 Accurate-Mass Q-TOF LC/MS) at positive mode with the parameters set up as follows: drying gas temperature of 300°C, drying gas of 8 L/min, nebulizer of 35 psi, sheath gas temperature of 350°C, flow rate of sheath gas of 11 L/min, capillary voltage of 3.5 kV, nozzle voltage (expt) of 1kV, fragmentor voltage of 175 V, skimmer voltage of 65 V, and octopole radiofrequency of 750 V. Accurate mass spectra were recorded in the m/z range of 100-500.

To quantify the amount of ABA and JA from *Arabidopsis* roots or rosette leaves samples, we used Agilent 1290 Infinity II HPLC system with C18 reversed phase (waters acquity premier BEH C18 1.7µm 2.1 mm x 50 mm) was at a flow rate of 0.3 mL/min, a temperature of 40 °C. The injection volume was 20 µL, and a gradient of acidified water containing 0.1% TFA (solvent A) and of ACN containing 0.1% TFA

(solvent B) was used as mobile phase with a constant flow rate of 0.3 mL/min, and column temperature set at 40°C with the min pressure at 0 bar, and the max pressure at 1k bar. Solvent B was from 5% to 30% in 0.5 min followed by an increase from 30% to 80% in 2.7 min. Then 100% solvent B was applied in 0.1min and was kept for 2.7 min before going back to initial conditions in 0.5 min and kept for 5.5 min. That was coupled with a mass detector (Agilent Technologies 6530 Accurate-Mass Q-TOF LC/MS) at negative mode with the parameters set up as follows: drying gas temperature of 250°C, drying gas of 8 L/min, nebulizer of 35 psi, sheath gas temperature of 300°C, flow rate of sheath gas of 8 L/min, capillary voltage of 3 kV, nozzle voltage (expt) of 200 V, fragmentor voltage of 100 V, skimmer voltage of 65 V, and octopole radiofrequency of 750 V. Accurate mass spectra were recorded in the m/z range of 50-500.

Quantification of camalexin and phytohormones was perfomed by comparing camalexin peak area in samples, to their calibration curve constructed by injection of gradient concentrations of commercial camalexin and phytohormone strandards, with MassHunter Workstation software (version B.09.00).

2.6. Statistical analysis

Statistical analyses were conducted using GraphPad Prism 8.0.2. Differences between groups were assessed using two tailed t-test. The notation "ns" denotes a lack of statistical significance, while *, **, *** and **** indicate levels of significance corresponding to $p < 0.05$, $p < 0.01$, $p < 0.001$ and $p < 0.0001$, respectively.

3. Results

3.1. Coumarin pathway

As outlined in the introduction of this chapter, *MYB72* and *BGLU42* are key regulators of coumarin biosynthesis. To investigate whether 10 µM Srf activates this pathway, we employed *Arabidopsis thaliana* reporter lines *pMYB72:GFP-GUS* and *pBGLU42:GFP-GUS*. Both experiments exhibited the significant induction following Srf treatment at 10 µM (Figure 4-1 A, B), demonstrating that Srf primes the coumarin biosynthetic pathway at the molecular level.

To further assess the dependency of Srf-triggered ISR on the coumarin pathway, we evaluated ISR responses in two *Arabidopsis* mutants *f6'h1* and *bglu42*. Data from two independent experiments demonstrated that the ISR-inducing capacity of 10 µM Srf was compromised in both mutants compared to wild type Col-0 (Figure 4-1C) that Srf fails to elicit ISR in *f6'h1-1* and *bglu42* mutants, suggesting that *F6'H1* and *BGLU42*

activation is necessary for Srf-mediated resistance against *B. cinerea*. To conclusively validate this mechanism, future work should directly measure coumarin accumulation in *Arabidopsis* roots and leaves following CLP treatment.

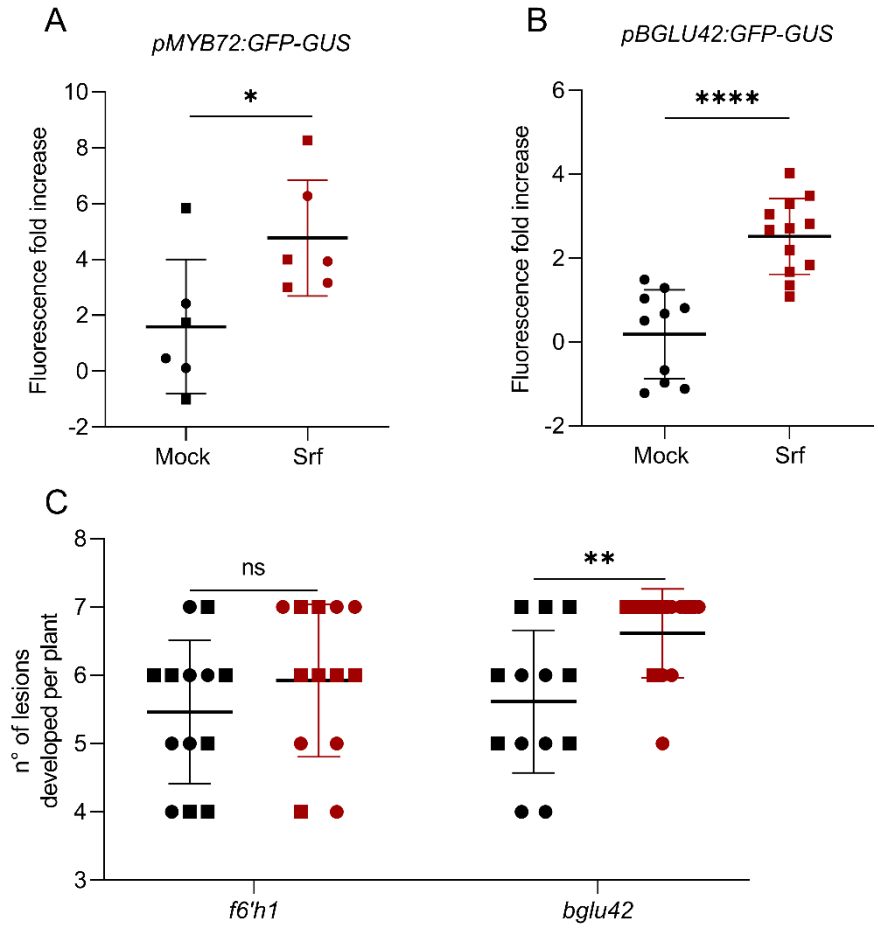

Figure 4-1 CLPs may prime immunity through the coumarin pathway.

A and **B** represent the mean fluorescence fold increases ± SD at 280 min, 220 min respectively, after following CLP treatment (Srf) in roots of *Arabidopsis* reporter lines *pMYB72:GFP* (n=6 from two independent experiments) and *pBGLU42:GFP-GUS* (n=9 from three independent experiments) respectively. **C**. After Srf treatment in roots of *Arabidopsis* muant *f6'h1-1* or *bglu42* overnight in araponic system, pathogen *Botrytis cinerea* was applied on leaves (n=7 or 6 from two independent experiments marked in two dot shapes). Mock is marked in black color, while Srf treatment is marked in red color. Mean lesions ± SD were counted at 72 h. Asterisks indicate statistically significant differences compared with the mock plants (two paired t-test, ns means no significance). Asterisks indicate statistically significant differences compared with the mock (two tailed t-test, *P <0.05, **P <0.01, ****P <0.0001, ns means no significance).

3.2. Camalexin pathway

In addition to findings indicating the involvement of the coumarin pathway in the CLP-ISR response, we further examined the potential role of the phytoalexin camalexin in CLP-triggered ISR. Camalexin dynamics were assessed through two approaches: first, by using with RT-qPCR to monitor the induction of *CYP71A12* gene expression in *Arabidopsis* roots six hours after 10 µM Srf treatment; second, by using UPLC-MS/MS to quantify camalexin accumulations in both roots and leaves following a 12-hour root pretreatment with CLP (T0), as well as after this pretreatment followed by a subsequent infection with *Botrytis cinerea* at 4 dpi (T96), when lesions were best observed (see Results section of Chapter 3 or 4).

After 10 µM Srf treatment, the upregulation of *CYP71A12* (Figure 4-2A) in *Arabidopsis* leaves and the accumulation of camalexin in both roots and leaves (Figure 4-2B) underscored the significance of camalexin in Srf-triggered plant immunity. While T96 root samples from Srf-pretreated plants are slightly lower than in T0 leaves or T0 roots, but still maintained high camalexin levels, T96 leaf tissues exhibited a marked reduction which is 1.5 times. This decrease in leaves may be attributable to the substantial consumption of camalexin during the active defence against *B. cinerea*. However, these experiments require more repetitions.

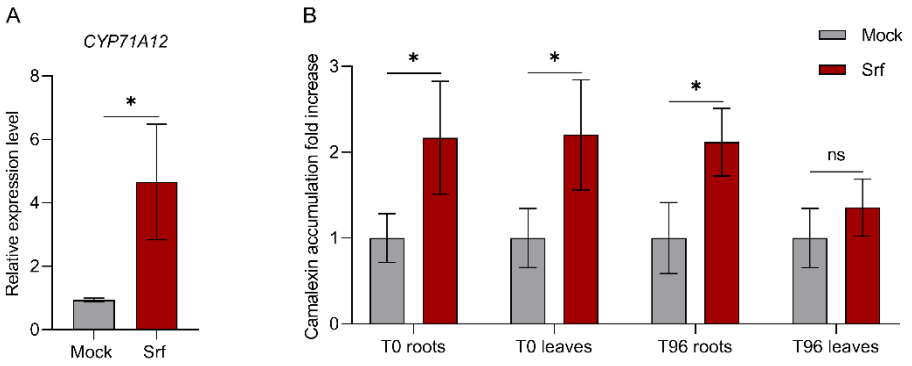

Figure 4-2 CLPs may prime immunity through the camalexin pathway.

A. *CYP71A12* relative expression in *Arabidopsis* roots, treated by 10 µM Srf for 6 hours. Relative expression was calculated using the $2^{-\Delta\Delta Ct}$ method and normalized to *UBQ5*. Graphs show the means ± SD calculated from three biological replicates and each involves eight plants. **B**. Fold increase of camalexin ± SD measured following Srf treatment in roots and leaves (n=3 from one independent experiment). Asterisks indicate statistically significant differences compared with the mock treated plants (two tailed t-test for A, $^{*}P < 0.05$; multiple t-test for B, $^{*}P < 0.05$, ns= not significant).

3.3. Other defence-related components

To further elucidate the mechanisms underlying plant immunity induced by CLPs in *Arabidopsis*, the expression of immunity-associated genes (see the Introduction section of this chapter) triggered by Srf treatment was analyzed by RT-qPCR, including *ERF6*, *MYB51*, *CML37*, *EARLI1*, and *AZI1*. Results indicated that *ERF6* and *CML37* are responsive to Srf treatment at 10 µM, and both are 1.4 times more than mock treatment, whereas the rest (*MYB51*, *EARLI1* and *AZI1*) showed no involvement under these experimental conditions (Figure 4-3A). Future investigations should include more experimental conditions and expand analysis to other key immune pathways.

Beyond phytoalexins, phytohormonal signaling pathways also fulfill critical functions in plant immunity by mediating defence responses against external threats. To explore additional regulatory mechanisms in Srf-primed plants, the levels of ABA, JA, and SA were measured in *Arabidopsis* following root pretreatment with Srf for 12 hours (T0) and subsequent infection with *B. cinerea* in leaves at 96 hours post-inoculation (T96). As depicted in Figure 4-3B and C, ABA signaling was not significantly activated at T0, but was significantly activated at T96 in the leaves. Figure 4-3C is from one independent experiment, so further repetitions are required; it might be interesting to include root samples at T96 and other time points. In contrast, Figure 4-3D shows no induction of JA in response to treatment with Srf. This should be confirmed with additional repetitions. Similarly, it might be interesting to include root samples at different time points. It is worth mentioning that SA signal was not detected from mentioned samples. Future investigations should incorporate a broader array of CLP structural variants to assess response specificity.

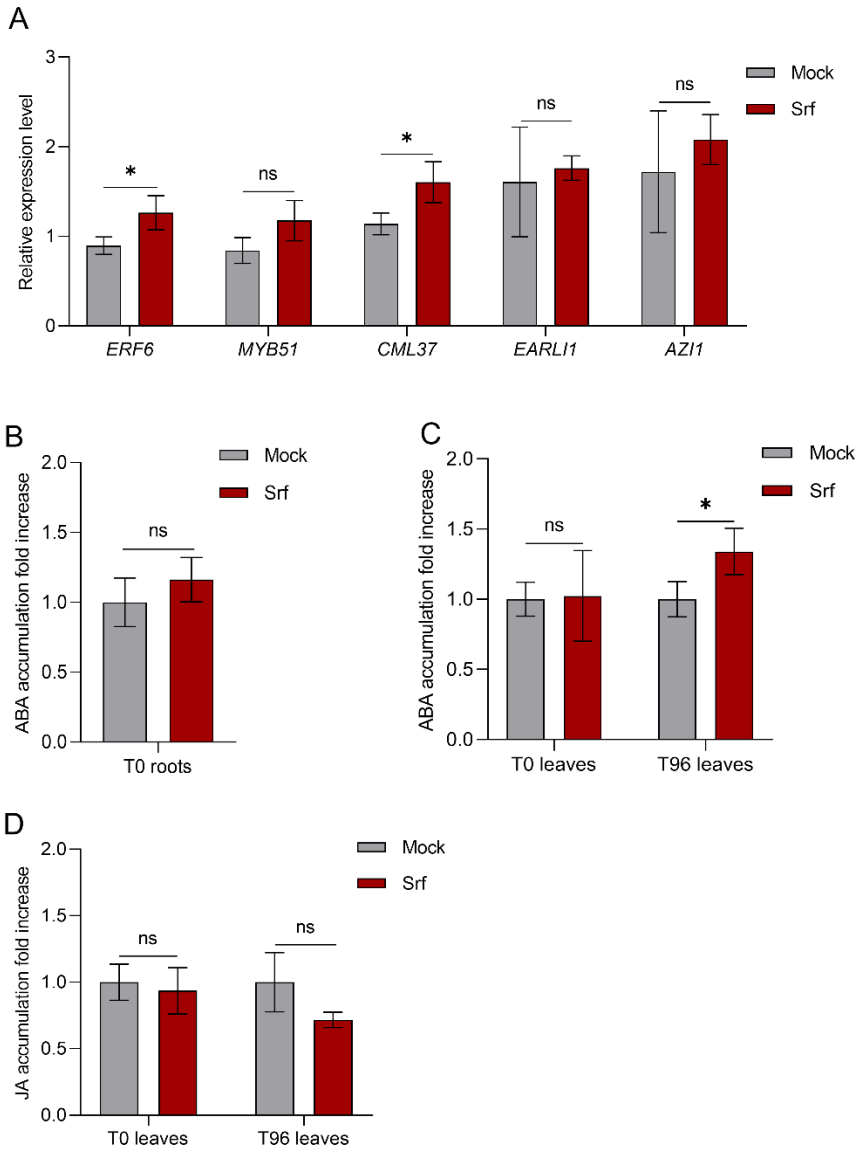

Figure 4-3 CLPs as immune primers: other defence gene regulation and phytohormonal shifts in *Arabidopsis.*

A. Stimulation of plant immunity genes *ERF6*, *MYB51*, *CML37*, *EARLI1*, *AZI1* expression in *Arabidopsis* roots, treated by Srf at 10 µM for 6 hours. Relative expression was calculated using the $2^{-\Delta\Delta Ct}$ method and normalized to *UBQ5*. **B.C.D.** Fold increase of hormonal signaling in roots (B. ABA) or leaves (C. ABA, D. JA) ± SD measured following Srf treatment in roots (B.D. n=6 from two independent experiments; C. n=3 from one independent experiment).

Asterisks indicate statistically significant differences compared with the mock treated plants (multiple t-test, $^{*}P < 0.05$, ns= not significant).

4. Summary

In this chapter, the mechanisms underpinning CLP-triggered plant immunity are investigated using Srf as an example, encompassing the spectrum from phytoalexin biosynthesis to phytohormonal signaling. Our findings indicate that both coumarin and camalexin contribute significantly to ISR induced by 10 µM Srf, with ABA potentially playing an ancillary role. To advance this field, future research should delineate the distinct ISR mechanisms elicited by other CLP variants to clarify their individual signaling pathways and evaluate potential synergistic effects in compound mixtures. Furthermore, experimental designs should be extended to include other plant species to assess the broader applicability of these defence mechanisms.

Chapter 5

General discussion and future perspectives

1. Current overview of CLPs

CLPs produced by PBB *Bacillus* are characteristically low molecular weight secondary metabolites that exhibit amphiphilic properties, comprising both hydrophilic cyclic peptide heads and hydrophobic FA tails (Ongena & Jacques, 2008). CLPs could trigger biofilm formation of the producing strains (Balleux et al., 2025), and the associated reduction in surface tension facilitates passive motility by diminishing surface adhesion (Markelova & Chumak, 2025). Interestingly, exposure of Srf non-producing strain *B. subtilis* to Srf at concentrations of 350 μg/mL and 650 μg/mL induced concentration-dependent growth arrest, followed by resumed growth at a modified rate (Uttlová et al., 2016). This adaptation may be attributed to alterations in the phospholipid composition of *B. subtilis* membranes, which could confer self-tolerance against the membrane-active properties of Srf (Uttlová et al., 2016).

The unique molecular architecture of CLPs confers membrane-active and surface-active properties, enabling significant reductions in surface and interfacial tension across liquid-solid-gas phase boundaries, as well as high aqueous dispersibility and a remarkably low CMC. These characteristics give rise to several valuable functional properties for human society, including emulsification capacity, pore-forming activity, foam generation, viscosity modulation, dispersion enhancement, solubilization potential, and mobilization efficacy (Dini et al., 2024).

Additionally, *Bacillus* CLPs are promising candidates for the development of new biocontrol agents against plant-pathogenic microbes (Balleux et al., 2025). The antimicrobial ability allows CLPs suppress competing microorganisms, thereby conferring a competitive advantage to the producing strains during habitat colonization (Markelova & Chumak, 2025). The most well-established antimicrobial function of CLPs is their direct antifungal activity against phytopathogenic fungi, with iturins and fengycins representing the CLPs of greatest antifungal potency (Théatre et al., 2022). Within the Iturin family, mycosubtilins have been specifically shown to inhibit *Botrytis cinerea* and *Zymoseptoria tritici* (Farace et al., 2015; Mejri et al., 2018), while iturins more broadly suppress a diverse array of fungal pathogens including *Colletotrichum demiatium*, *Penicillium roqueforti*, *Aspergillus flavus* and *Rhizoctonia solani* (Raaijmakers et al., 2010). Fengycins also inhibitory activity against a wide range of fungi such as *Fusarium graminearum*, *Podosphaera fusca*, *Alternaria brassicicola* and *Botrytis cinerea* (Raaijmakers et al., 2010; Wu et al., 2021; Gilliard et al., 2024; Magwebu et al., 2023).

Co-evolutionary pressures acting on CLP-producing bacteria and their host plants have refined the capacity of CLPs to activate plant innate immunity and facilitate ISR against phytopathogens, positioning these CLPs as a distinct class of immunity-based biocontrol agents. Building upon this framework, our study investigated CLP-mediated plant immune activation with the dual aim of advancing mechanistic

understanding of this process and elucidating the underlying structure-activity relationships that determine CLP immune-eliciting efficacy.

2. The panoply of surfactin structural variants

Although previous research has investigated how culture conditions affect total Srf yields (Bartal et al., 2018), their specific influence on the compositional distribution of Srf variants within the lipopeptide mixture remains poorly characterized. Indeed, exogenous AAs influence both the peptide ring composition and the hydroxyl FA structure of the resulting lipopeptide (Liu et al., 2012). Our study demonstrates that supplementation with different BCAAs selectively directs the biosynthesis of CLP analogs. L-Val supplementation increased the proportion of Val_7-containing analogs of Srf, Pumi, and Liche while decreasing other analogs containing Leu or Ile. This supports previous research, which showed that supplementation with L-Val selectively increases $SrfVal_7$ production, in contrast to the supplementation with L-Leu (Peypoux & Michel, 1992). L-Ile supplementation reduced Srf Leu_7 analogs and enhanced those with Lxx at position 7 as well as at both positions 4 and 7, no Val_7 was detected in this condition. This differs from the previously reported finding that L-Ile supplementation acts similarly to L-Val in increasing $SrfVal_7$ production (Peypoux & Michel, 1992). This discrepancy may be attributable to strain-specific differences, as the present study used *B. velezensis* GA1, whereas the earlier findings were derived from *B. subtilis* S499. The differential incorporation efficiency of specific BCAA residues across strains therefore warrants further systematic investigation. L-Leu supplementation decreased most Val_7 analogs, contributed a minor proportion of Liche $C_{15}Lxx_4Lxx_7$, but did not promote Leu_7 incorporation in Pumi variants. Instead, the proportion of Pumi Ile_7 analogs was increased. Notably, among the production of other Ile_7 analogs that are decreased, Liche $C_{15}Ile_7$ was elevated to 84.8% of its mixture, which is 2.45 times more than canonical $C_{15}Ile_7$. The distinct analog profiles observed among Srf, Pumi, and Liche variants suggest that NRPS domain flexibility in response to BCAA precursors is species-dependent, a relationship that remains poorly characterized in the existing literature. This knowledge gap necessitates systematic investigation to establish the mechanistic basis of BCAA precursor-directed CLP analog generation and to determine how this relationship varies across CLP-producing species.

In addition to the previously reported Srf and Liche variants with AA substitutions at positions 2, 4, or 7 (Grangemard et al., 1999), our findings also demonstrate that the Leu residues at positions 3 or/and 6 can be substituted with Val in Srf and Pumi variants, and the L- or D-form requires further elucidation. The observed dose-dependent increase in Val_7-Srf production with elevated Val concentrations in the culture medium suggests a concentration-responsive influence of this AA on the enzymatic biosynthesis machinery (Peypoux & Michel, 1992). This might be the

reason why AA substitution in Srf producing strain was not observed from the previous report (Youssef et al., 2005), which could be attributed to the lower supplementation concentration used (1 g/L versus 5 g/L in the present study). This study also reveals that supplementation of L-Val in Pumi biosynthesis can introduce an extended FA chain (C_{18}), a previously underreported aspect of Pumi assembly. Although these novel CLP variants are present in low abundance within the CLP mixture, they still offer a new perspective on biosynthetic flexibility and expand the structural repertoire for investigating structure-function relationships.

In our study, the addition of L-Val, L-Ile, and L-Leu to the medium markedly altered the CLP composition. Some CLP analogs were written in the same way but with different retention time (Figure 2-2, Figure 2-3, Figure 2-4**)**. This mainly corresponds to the previous report that the addition Val preferentially increased Srf variants containing even-numbered β-hydroxy iso-FA chains, while Ile, Leu supplementation selectively enriched Srf with odd-numbered β-hydroxy FAs (anteiso- and iso- respectively) (Hu et al., 2019; Liu et al., 2012), although this conclusion remains uncharacterized for other CLPs. In the future, the FA chain configurations of CLP analogs presented in this study should be further confirmed by GC-MS and NMR spectroscopy. Notably, we also applied L-Ala in the Landy medium for the new profile of CLPs. However, the difference was not as significant as BCAAs supplementation mentioned above (Figure A1-1, Table A1-1). Still, expanding the scope of precursor AAs represents an interesting direction for future work, that could lead to the discovery of new CLPs and an enrichment of the overall CLP repertoire.

Additionally, Bartal et al. examined the influence of carbon sources and metal ions on Srf production in *Bacillus subtilis* (Bartal et al., 2018). Fructose and xylose emerged as the most impactful carbon sources, altering variant ratios through modifications in both peptide sequences and FA chain lengths. Supplementation with Mn^{2+}, Cu^{2+}, or Ni^{2+} induced substantial compositional shifts, including the emergence of methyl-esterified Srf forms and novel variants with short FA chains ($\leq C_{11}$) (Bartal et al., 2018). Srf structural diversification has also been achieved through chemical, cultural, and genetic approaches. Future strategies could employ site-directed mutagenesis of FA 3-hydroxylases to engineer biosurfactants with customized functionalities via precise modification of 3-hydroxy FA composition (Youssef et al., 2011).

3. Impact of CLP structure on immune elicitor function

Within the *Bacillus* CLPs, Srf stands out as the most extensively characterized immune elicitor, exhibiting the broadest and most consistently documented ISR-inducing activity across plant species, particularly in dicots, relative to structurally distinct *Bacillus* CLPs including fengycin and iturin. For instance, the functional

specificity of this eliciting capacity is illustrated by findings in melon plants, where the absence of fengycin and iturin production does not impair ISR against *Podosphaera fusca*, implying that Srf alone is sufficient for ISR induction in this pathosystem (García-Gutiérrez et al., 2013). Recent evidences have also established that *Pseudomonas*-derived CLPs elicit ISR in a pathosystem-dependent manner, with their immunostimulatory efficacy varying as a function of the specific plant host and pathogen combination involved (Tran et al., 2007; Ma et al., 2016; Omoboye et al., 2019).

Previous research has demonstrated that CLP structural properties are critical determinants of plant immune elicitation efficacy, as illustrated by the contrasting immune responses observed following surfactin and fengycin treatments: although both CLPs induced significant Ca^{2+} accumulation at 10 µM, the response elicited by Srf was significantly greater than that triggered by fengycin (Gilliard et al., 2024). In contrast, root pretreatment with 10 µM Srf amplified the ROS response to chitin in *Arabidopsis*, while pretreatment with fengycin at the same concentration did not differ from the control solution (Gilliard et al., 2024). These findings collectively underscore that CLP-mediated ISR activation depends critically on precise molecular recognition events between specific CLP structures and particular plant-pathogen combinations.

To further elucidate the structural determinants underlying CLP-mediated plant immune elicitation, we used a panel of Srf variants and their BCAA-directed variants as model compounds to systematically investigate the relationship between CLP molecular architecture and immunostimulatory potency. Our results demonstrated that both Srf and Liche could trigger plant early immune signaling events including ROS, NO and Ca^{2+} in both *Arabidopsis* roots and protoplasts of root cells, which eventually triggers ISR in *Arabidopsis* against *B. cinerea*. Conversely, Pumi treatment showed no detected early response signals, also failed to induce ISR in *Arabidopsis*. The structural alterations observed in the GP assay (Figure 3-2) indicate that the deficient Pumi-membrane interaction, a consequence of its structure, underpins the impaired initiation of immune signals and the consequent attenuation of the ISR.

Previous studies from the lab have shown that both the FA chain lengths and AA positions in the peptide chain influence the eliciting potential of Srf in cultured tobacco cells (Henry et al., 2011; Jourdan et al., 2009). The linear, methylated, and linear/methylated derivatives C_{14}Srf lost their eliciting activity, which was attributed to the finding that the presence of two acidic residues in the Srf peptide is critical for elicitor activity in tobacco cells (Henry et al., 2011). However, in our study, Liche carrying only one charge yet demonstrated equally strong efficacy in inducing plant immunity in *Arabidopsis*. This discrepancy may stem from differences between the experimental plant systems (tobacco versus *Arabidopsis*). Alternatively, the mechanism by which the net charge is altered, specifically, through methylation in Srf versus direct AA substitution, could result in distinct 3D conformations of the final CLP, thereby influencing its biological activity. Furthermore, the observation that

Pumi carries two charges yet does not enhance plant immunity challenges the notion that the presence of two acidic residues is a key determinant of the elicitor activity of CLPs at least in *Arabidopsis*.

Variations in FA tail length and composition can markedly alter biological potency, with studies revealing that an increased proportion of BCAAs correlates with diminished surface activity (Yakimov et al., 1995). Lipid tails play equally critical roles in governing CLP functionality alongside the peptide moiety. Among Srf homologs, those with longer FA chains stimulate better immune capacity in tobacco cells compared to Srf with shorter chains; $C_{15}Leu_4$ and C_{15}Ile had three times lower activity, while $C_{15}Val_7$ retained only half of the natural C_{15} homolog's activity (Henry et al., 2011). The structural alterations observed in early immune events (Figure 3-5, 3-6) and ISR (Figure 3-7) induced by different precursor-directed CLPs reveal the complexity of CLP structure-function relationships. However, since the purified CLP mixtures used in these studies only bring the general information, future studies employing purified CLP homologs that share the same peptide cycle or FA chain could provide greater insight into the differences in bioactivity among structurally similar CLP variants. A better understanding of the 3D conformation of surfactin and its variants in a lipid matrix would be precious as recently published for *Pseudomonas* CLPs (Kovács et al., 2025). Establishing the impact of small structural changes in the variants on this spatial conformation would certainly provide additional insights in the relationship between structure and immune-eliciting functions.

Beside the intricate structure-activity relationship, concentration also defines CLP efficacy. In this work, Srf variants were mainly compared when applied to *Arabidopsis* roots or protoplasts at 10 µM, the well documented effective concentration. At such dose, Pumi triggered neither early immune events nor ISR against subsequent *B. cinerea* infection. However, some data strongly suggest that it may be active at lower concentration as it triggered a $[ROS]_{intra}$ response at 2 µM. We hypothesized that it can be due to different CMC values for Pumi compared with Srf or Liche and that Pumi may form micelles (aggregates of CLP molecules) at lower concentration. Still, this is not clear based on published data because the reported CMC values for the three CLPs are difficult to compare. The pH value of the medium is crucial in determining CMC but is not always explicitely specified (Deleu et al., 2013; Yakimov et al., 1995; Dasgupta et al., 2023). In our work, all tested CLP concentrations (2-40 µM) fell below the mentioned CMC of Pumi, so the observed lack of activity at 10 or 40 µM is unlikely due to micelle formation. Still, this highlights the need for further characterization of the CMC of the CLP samples used in this study under the specific pH conditions tested. More recently, however, *Bacillus pumilus* strain JM79 was reported to activate local and systemic resistance in wheat plants against the necrotrophic soil-borne fungal pathogen *Fusarium graminearum*, possibly due to the production of Pumi (Ballot et al., 2025). This bioactivity of Pumi may be contingent upon the structural composition of its analog mixture, the applied concentration, and the specificity of the plant-pathogen system under investigation,

collectively suggesting that its immune-eliciting outcomes are highly context-dependent. To systematically resolve the relative contributions of these variables, future research should employ multivariate factorial experimental designs that independently manipulate analog composition, concentration, plant species, pathogen identity, and environmental conditions, while quantifying both early immune signaling events and downstream disease resistance outcomes.

4. Mechanisms of *Bacillus* CLPs eliciting plant immunity

Recent findings from our lab demonstrate that canonical Srf is perceived by *Arabidopsis* root cells via remodelling of the plasma membrane structure through specific insertion into sphingolipid-enriched nano-domains. This interaction does not compromise membrane integrity nor inducing electrolyte loss, and thereby potentiates host defense and resistance to *Botrytis cinerea* independently of classical PRR-mediated PTI (Gilliard et al., 2026). We assume that Srf also interacts with PM lipids in other dicot plant species such as tomato (Hoff et al., 2021) or tobacco (Henry et al., 2011) but generalization of this perception mechanism requires further experiments. Still, the failure of Pumi to trigger ISR in *Arabidopsis* under conditions effective for Srf and Liche, supported by GP analysis (Figure 3-2), suggests that Pumi engages plasma membrane sphingolipids less effectively than these structurally related CLPs. This hypothesis requires validation through isothermal titration calorimetry and molecular dynamics simulation approaches as established by Gilliard. Furthermore, the known divergence in sphingolipid composition between monocot and dicot species provides a plausible mechanistic basis for the reduced ISR-eliciting capacity of Srf in monocots, and renders the investigation of Pumi activity on monocot membranes a scientifically compelling priority. Importantly, the observation that Liche, bearing one fewer net charge than Srf, retains comparable ISR-eliciting efficacy indicates that net molecular charge is insufficient as a sole predictor of CLP elicitor function, redirecting investigative focus toward the 3D structural determinants of selective sphingolipid recognition.

The plasma membrane remodeling by Srf elevates lateral membrane tension, leading to the activation of PM-localized mechanosensitive channels and the consequent initiation of downstream ion fluxes, such as Ca^{2+} and $[ROS]_{intra}$ (Gilliard et al., 2026). Here, we additionally characterized NO production as part of the early immune signaling events (Figure 3-1, 3-2), followed by upregulation of immunity-related genes such as *CYP71A12*, *ERF6*, *CML37* (Figure 4-2A and Figure 4-3A). Furthermore, Srf appears to trigger additional signaling pathways, potentially including ABA-mediated routes, which may contribute to the biosynthesis of phytoalexins such as coumarin and camalexin (Figure 4-1, 4-2), resulting in ISR against *Botrytis cinerea* in *Arabidopsis* (Figure 3-4). Plants synthesize phytoalexins

as a defense response against pathogen attack; however, fungi such as *B. cinerea* can enzymatically degrade these compounds, including camalexin (Pedras et al., 2005; Pedras et al., 2011). Our camalexin levels in T96 leaves (Figure 4-2B) showed no significant difference between the mock and Srf treatments, possibly because camalexin was being degraded during its deployment by the plant as a defense response against *B. cinerea*. The importance of the camalexin pathway was also confirmed by the loss of Srf-triggered ISR in the *pad3* mutant, which is impaired in camalexin synthesis (Gilliard et al., 2026). The lipid-dependent $[ROS]_{intra}$ induction has also been documented for other CLPs from *Pseudomonas* that trigger ISR, including orfamide, and WLIP (Gilliard et al., 2026). Our study demonstrated that CLP variants elicited divergent early immune events but yet converged on comparable ISR phenotypes compared to canonical CLPs. It indicates that early immune signal intensity does not universally predict ISR competence. The mechanistic framework developed in our study for characterizing CLP structure-function relationships should be extended to encompass a structurally broader repertoire of CLPs, providing a comparative foundation for understanding the molecular determinants of differential immune-eliciting potency across the CLP structural landscape. Concurrently, definitively resolving the dissociation between early immune signal magnitude and ISR competence, a central finding of the present study, will require systematic quantification of additional mechanistically informative immune or defense mechanisms. This includes stomatal closure as a measure of guard cell immune activation, MAPK cascade activation (MPK3 and MPK6) as indicators of PTI-associated kinase signaling, and callose deposition as a marker of structural defence reinforcement. Collectively, this would enable a more precise delineation of the signaling nodes essential for CLP-mediated ISR induction.

Generally, SA-mediated signaling pathways are primarily associated with resistance against biotrophic pathogens, while JA/ET-dependent responses are typically linked to defence against necrotrophic pathogens (Ballot et al., 2025). Preinoculation of wheat collars at the soil surface interface with *Bacillus pumilus* JM79 prior to *Fusarium graminearum* challenge induced upregulation of host defence genes associated with both JA/ET and SA-dependent signaling pathways (Ballot et al., 2025). However, the induction of defence-related gene expression in the host plant following bacterial treatment differs from the response observed upon treatment with its metabolite CLP (Gond et al., 2015). In our study, although SA was not detected and JA levels were statistically insignificant, these outcomes may reflect the relatively short CLP pretreatment duration used. Future studies employing extended pretreatment periods and more sensitive detection methods such as spectroscopy, biosensors, electrochemical sensors should be applied to re-examine both SA and JA levels while simultaneously monitoring ET.

Pathogenic infection stimuli induced scopolin accumulation in leaves (Döll et al., 2018; Stringlis et al., 2019), which represents an integrated response involving both local biosynthesis and root-sourced metabolite allocation (Robe, Izquierdo, et al.,

2021). The systemic translocation of coumarins from root to shoot tissues was established through reciprocal grafting of wild type and *f6'h1* mutant seedlings (Robe, Conejero, et al., 2021). Coumarins, including scopoletin, are postulated to translocate from the root to the shoot, where they play important roles in the induction of ISR (Stassen et al., 2021). Moreover, the coumarin scopoletin also appears to be a key component in CLP-ISR against *Botrytis cinerea*, functioning as an effective phytoalexin in tomato leaves (Yuan et al., 2024). However, when exploring further, we detected fluorescent phenolic compounds in root exudates at multiple time points within 12 hours of Srf treatment, without any statistically significant increase being observed (data not shown). This result implies that exposure to Srf did not specifically promote coumarin secretion at the root level during the observation period. To acquire more direct evidence, future analyses should quantify coumarin timecourse accumulation within *Arabidopsis* root and leaf tissues, both with and without subsequent pathogen challenge.

Liche and Srf exhibit superior surface tension reduction compared to Pumi (Théatre et al., 2022), which likely reflects the adaptations to their producers' ecological niches. The distinct properties of these CLPs may correlate with their producers' lifestyles: whereas *B. pumilus* (Pumi producer, mostly endophytic) (Melo et al., 2009) inhabits internal plant tissues, the epiphytic *B. velezensis* (Srf producer) (Wilson et al., 2023) is best known to colonize plant surfaces. So, from an ecological perspective, the lack of immunogenic activity of Pumi can be interpreted as an adaptation to the lifestyle of the producer, which would avoid triggering strong immune-related responses that are detrimental for population establishment and persistence inside the plant tissues. These observations highlight the need for co-evolutionary studies of CLP-producing bacteria and their host plants, which could reveal fundamental principles of microbial-plant interactions and adaptive specialization in secondary metabolite production.

5. Perspective of CLPs for agricultural application

Within the current biological control agent's registry, PBB *Bacillus* spp. are the most prevalent taxon, followed by *Trichoderma* spp. and *Pseudomonas* spp (De Pessemier et al., 2026). The commercial dominance of *Bacillus* is primarily attributable to its endospore-forming ability, which underpins superior desiccation tolerance and formulation stability, properties critical for commercial biopesticide development and shelf-life (Tabassum et al., 2017). For instance, RhizoVital®, Botrybel, Serenade®, Kodiak™, Taegro® are *Bacillus velezensis*-based commercial biocontrol agents for agricultural applications (Fazle Rabbee & Baek, 2020).

However, despite their considerable promise as biocontrol solutions, PBBs are subject to significant limitations that constrain their widespread agricultural adoption. Their performance is frequently inconsistent and difficult to reproduce, owing to the

inherent complexity of biological interactions among biocontrol agents, host plants, pathogens, and associated microbiota, compounded by the influence of fluctuating environmental conditions (Haskett et al., 2021; Rutledge & Challis, 2015; Wang et al., 2024). These inherent biological constraints highlight the complementary potential of CLPs as more chemically defined and reproducible biocontrol agents. The amphiphilic architecture of CLPs underlies a suite of unique and ecologically relevant biological functions, particularly within the complex chemical milieu of the soil and phyllosphere. Among these, the antifungal activity of specific CLP is well established, enabling effective suppression of a broad spectrum of plant-pathogenic fungi. The direct application of purified CLPs as bio-based crop protection products is therefore preferable to deployment of the producing bacterial strains, as these molecules exhibit inherent chemical stability and relative resistance to environmental degradation even if they can be degraded by other microbes (Rigole et al., 2024; Hansen et al., 2024; Lozano-Andrade et al., 2026). Moreover, CLPs demonstrate selective bioactivity against plant-pathogenic fungi with minimal disruption to non-target soil organisms and plant-associated microbial communities, while additionally functioning as elicitors of plant innate immunity capable of inducing ISR, a dual-mode action that substantially broadens their biocontrol utility beyond direct antifungal antagonism.

Translation to agricultural applications will require optimization of industrial-scale CLP production through strain selection and culture condition refinement, and rigorous field trials to evaluate efficacy under real-world conditions. These advances will bridge the gap between mechanistic understanding and practical implementation of CLP-based crop protection strategies. Extensive studies have demonstrated that culture parameters, including pH, temperature, and agitation rate, significantly modulate Srf biosynthesis through their effects on microbial growth (Chen et al., 2015). Moreover, medium composition optimization, particularly through strategic supplementation with carbon sources, biosynthetic precursors, and production enhancers, represents one of the most efficient approaches for maximizing Srf yield (Xia & Wen, 2023). Metabolic engineering approaches, encompassing molecular cloning and targeted DNA recombination to modify biosynthetic pathway regulation and metabolite transport, provide a precision-based strategy for optimizing CLP yields (Wang et al., 2024). Guez et al. demonstrated this through a dual metabolic engineering approach combining transcriptomic and bioinformatic analyses to guide targeted genetic modifications, achieving selective production of mycosubtilin isoforms and specifically enriching the C_{17}-anteiso isoform (Guez et al., 2022). Additionally, economic optimization may additionally be achieved through the utilization of low-cost, carbohydrate- and lipid-rich substrates as fermentation feedstocks, substantially reducing production input costs. At the process level, established engineering techniques including foam fractionation, countercurrent extraction, rotating disk contactors, and circulating microfiltration offer practical means of further improving CLP recovery efficiency and reducing overall manufacturing expenditure (Wang et al., 2024). The engineering of synthetic microbial consortia for CLP co-production would represent an emerging and largely

unexplored strategy that may expand manufacturing potential and broaden application scope. Furthermore, the design and implementation of novel foam-suppressing bioreactors could optimize fermentation processes, improving both efficiency and stability in lipopeptide production.

Existing methodological limitations have contributed to knowledge gaps in the application of CLPs as biocontrol agents. Most of the studies have been conducted under controlled healthy soil conditions, with only one exception (Lam et al., 2021) considering the complex interplay between CLPs and environmental stressors. Future research must incorporate biotic and abiotic variables to better predict field performance. Given that phytoalexins such as coumarin and camalexin can exhibit cytotoxic properties at elevated concentrations, the levels of CLP-induced phytoalexins in field settings require quantification to confirm they remain within thresholds considered safe for human health.

Synergistic effects should also be taken into consideration. *Bacillus* isolated from rice spikelets demonstrated broad-spectrum antimicrobial activity against key rice pathogens (including *Xanthomonas oryzae* pv. *oryzae*, *Burkholderia plantari* as well as *Burkholderia glumae*) mediated through the synergistic action of secondary metabolite bacitracin, Liche and fengycin (Zhan et al., 2023). “Mixture-induced” biological activity was reported when combining different CLP types, resulting in enhanced antimicrobial activity and the possible reason could be the formation of mixed micelles or chemical interaction of CLPs (Leconte et al., 2024). This synergistic activity encourages the further development and application of CLP mixtures as biopesticides. Additionally, the application of a mixture of CLPs and their producer strains is a comprehensive strategy to induce plant immunity, which is most effective when initiated prior to the final establishment of PBB in the field.

Scientific production related to this thesis

Publications

Ding, N.; Dong, H.; Ongena, M. Bacterial Cyclic Lipopeptides as Triggers of Plant Immunity and Systemic Resistance Against Pathogens. *Plants* 2025, *14*, 2644. https://doi.org/10.3390/plants14172644

Ding, N.; Dong, H.; Thomas, R.; Gilliard, G.; Pršić, J.; Ongena, M. Surfactin Structural Variants Differentially Modulate Plant Immune Responses. *Biomolecules* 2025, *15*, 1479. https://doi.org/10.3390/biom15101479

Poster communications in scientific congresses

Ning Ding, Jelena Pršić, Hansong Dong, and Marc Ongena (21-23 Septermber 2022). *EOS workshop– Bacterial lipopeptides: from (physico)chemistry to ecology*. Poster: structural features driving the plant immunity elicitor activity of beneficial bacteria lipopeptides. Liège, Belgium.

Ning Ding, Jelena Pršić, Hansong Dong, and Marc Ongena (20-25 August 2023). *The 12th International Congress of Plant Pathology*. Poster: structure-activity of the lipopeptide surfactin as elicitor of plant immunity. Lyon, France.

References

Aci, MM., Sidari, R., Araniti, F., & Lupini, A. (2022). Emerging trends in allelopathy: a genetic perspective for sustainable agriculture. *Agronomy*, *12*(9), 2043. https://doi.org/10.3390/agronomy12092043

Aftab, U., & Sajid, I. (2017). Antitumor peptides from *Streptomyces* sp. SSA 13, isolated from Arabian Sea. *Int J Pept Res Ther*, *23*, 199–211. https://doi.org/10.1007/s10989-016-9552-6

Ahuja, I., Kissen, R., & Bones, AM. (2012). Phytoalexins in defense against pathogens. *Trends Plant Sci*, *17*(2), 73–90. https://doi.org/10.1016/j.tplants.2011.11.002

Ali, N., Pang, Z., Wang, F., Xu, B., & El-Seedi, HR. (2022). Lipopeptide biosurfactants from *Bacillus* spp.: types, production, biological activities, and applications in food. *J. Food Qual*, *2022*, *1–19*. https://doi.org/10.1155/2022/3930112

Ali, S., Tyagi, A., & Mir, ZA. (2024). Plant immunity: at the crossroads of pathogen perception and defense response. *Plants*, *13*(11), 1434. https://doi.org/10.3390/plants13111434

Altrão, CS., Kaneko, M., Shiina, S., Kajikawa, A., Shinohara, H., & Yokota, K. (2022). Insights on suppression of bacterial leaf spot by *Bacillus* cyclic lipopeptides via induced resistance in *Arabidopsis thaliana*. *J. Gen. Plant Pathol*, *88*(4), 259–263. https://doi.org/10.1007/s10327-022-01062-9

Andrić, S., Meyer, T., Rigolet, A., Prigent-Combaret, C., Höfte, M., Balleux, G., Steels, S., Hoff, G., De Mot, R., McCann, A., De Pauw, E., Argüelles Arias, A., & Ongena, M. (2021). Lipopeptide interplay mediates molecular interactions between soil bacilli and pseudomonads. *Microbiol. Spectr*, *9*(3), e0203821. https://doi.org/10.1128/spectrum.02038-21

Annunziata, F., Pinna, C., Dallavalle, S., Tamborini, L., & Pinto, A. (2020). An overview of coumarin as a versatile and readily accessible scaffold with broad-ranging biological activities. *Int. J. Mol. Sci*, *21*(13), 4618. https://doi.org/10.3390/ijms21134618

Aranda, FJ., Teruel, JA., & Ortiz, A. (2023). Recent advances on the interaction of glycolipid and lipopeptide biosurfactants with model and biological membranes. *Curr. Opin. Colloid Interface Sci*, *68*, 101748. https://doi.org/10.1016/j.cocis.2023.101748

Arnaouteli, S., Bamford, NC., Stanley-Wall, NR., & Kovács, ÁT. (2021). *Bacillus subtilis* biofilm formation and social interactions. *Nat. Rev. Microbiol*, *19*(9), 600–614. https://doi.org/10.1038/s41579-021-00540-9

Arnaouteli, S., MacPhee, CE., & Stanley-Wall, NR. (2016). Just in case it rains: building a hydrophobic biofilm the *Bacillus subtilis* way. *Curr. Opin. Microbiol*, *34*, 7–12. https://doi.org/10.1016/j.mib.2016.07.012

Arnaud, D., Deeks, MJ., & Smirnoff, N. (2023). Organelle-targeted biosensors reveal distinct oxidative events during pattern-triggered immune responses. *Plant Physiol*, *191*(4), 2551–2569. https://doi.org/10.1093/plphys/kiac603

Arnaud, D., & Hwang, I. (2015). A sophisticated network of signaling pathways regulates stomatal defenses to bacterial pathogens. *Mol. Plant*, *8*(4), 566–581. https://doi.org/10.1016/j.molp.2014.10.012

Astier, J., Gross, I., & Durner, J. (2018). Nitric oxide production in plants: an update. *J. Exp. Bot*, *69*(14), 3401–3411. https://doi.org/10.1093/jxb/erx420

Balleux, G., Höfte, M., Arguelles Arias, A., Deleu, M., & Ongena, M. (2024). *Bacillus* lipopeptides as key players in rhizosphere chemical ecology. *Trends in Microbiol*, *33*(1), *80–95*. https://doi.org/10.1016/j.tim.2024.08.001

Balleza, D., Alessandrini, A., & Beltrán García, MJ. (2019). Role of lipid composition, physicochemical interactions, and membrane mechanics in the molecular actions of microbial cyclic lipopeptides. *J. Membr. Biol*, *252*, 131–157. https://doi.org/10.1007/s00232-019-00067-4

Ballot, A., Gaucher, M., Rey, M., Brisset, MN., Joly, P., Dreux-Zigha, A., Taïbi, A., Langin, T., & Prigent-Combaret, C. (2025). Strong elicitation of plant defense pathways by foliar and collar inoculations of wheat with the *Bacillus pumilus* strain JM79. *Curr. Plant Biol*, *43*, 100524. https://doi.org/10.1016/j.cpb.2025.100524

Bartal, A., Vigneshwari, A., Bóka, B., Vörös, M., Takács, I., Kredics, L., Manczinger, L., Varga, M., Vágvölgyi, C., & Szekeres, A. (2018). Effects of different cultivation parameters on the production of surfactin variants by a *Bacillus subtilis* strain. *Molecules*, *23*(10), 2675. https://doi.org/10.3390/molecules23102675

Béchet, M., Castéra-Guy, J., Guez, J. S., Chihib, NE., Coucheney, F., Coutte, F., Fickers, P., Leclère, V., Wathelet, B., & Jacques, P. (2013). Production of a novel mixture of mycosubtilins by mutants of *Bacillus subtilis*. *Bioresour. Technol*, *145*, 264–270. https://doi.org/10.1016/j.biortech.2013.03.123

Bender, KW., & Zipfel, C. (2023). Paradigms of receptor kinase signaling in plants. *Biochem. J*, *480*(12), 835–854. https://doi.org/10.1042/BCJ20220372

Berendsen, RL., Vismans, G., Yu, K., Song, Y., De Jonge, R., Burgman, WP., Burmølle, M., Herschend, J., Bakker, PAHM., & Pieterse, CMJ. (2018). Disease-induced assemblage of a plant-beneficial bacterial consortium. *ISME Journal*, *12*(6), 1496–1507. https://doi.org/10.1038/s41396-018-0093-1

Bigelow, CC. (1967). On the average hydrophobicity of proteins and the relation between it and protein structure. *J. Theor. Biol*, *16*(2), 187–211. https://doi.org/10.1016/0022-5193(67)90004-5

Boller, T., & Felix, G. (2009). A renaissance of elicitors: perception of microbe-associated molecular patterns and danger signals by pattern-recognition receptors. *Annu. Rev. Plant Biol*, *60*, 379–406. https://doi.org/10.1146/annurev.arplant.57.032905.105346

Bonmatin, JM., Labbé, H., Grangemard, I., Peypoux, F., Maget-Dana, R., Ptak, M., & Michef, G. (1995). Production, isolation and characterization of [Leu_4]-and [Ile_4]surfactins from *Bacillus subtilis*. *Lett. Peptide Sci*, *2*, 41–47. https://doi.org/10.1007/BF00122922

Bonnichsen, L., Svenningsen, NB., Rybtke, M., de Bruijn, I., Raaijmakers, JM., Tolker-Nielsen, T., & Nybroe, O. (2015). Lipopeptide biosurfactant viscosin enhances

dispersal of *Pseudomonas fluorescens* SBW25 biofilms. *Microbiology*, *161*(12), 2289–2297. https://doi.org/10.1099/mic.0.000191

Boro, M., Sannyasi, S., Chettri, D., & Verma, AK. (2022). Microorganisms in biological control strategies to manage microbial plant pathogens: a review. *Arch. Microbiol*, *204*(11), 666. https://doi.org/10.1007/s00203-022-03279-w

Boubsi, F., Hoff, G., Arguelles Arias, A., Steels, S., Andrić, S., Anckaert, A., Roulard, R., Rigolet, A., van Wuytswinkel, O., & Ongena, M. (2023). Pectic homogalacturonan sensed by *Bacillus* acts as host associated cue to promote establishment and persistence in the rhizosphere. *iScience*, *26*(10), 107925. https://doi.org/10.1016/j.isci.2023.107925

Ngou, BPM., Ding, P., & Jones, JDG. Thirty years of resistance: zig-zag through the plant immune system. (2022). *Plant Cell*, *34*(5):1447-1478. https://doi.org/10.1093/plcell/koac041

Cao, H., Glazebrook, J., Clarke, JD., Volko, S., & Dong, X. (1997). The *Arabidopsis NPR1* gene that controls systemic acquired resistance encodes a novel protein containing ankyrin repeats. *Cell*, *88*(1), 57–63. https://doi.org/10.1016/S0092-8674(00)81858-9

Cawoy, H., Mariutto, M., Henry, G., Fisher, C., Vasilyeva, N., Thonart, P., Dommes, J., & Ongena, M. (2014). Plant defense stimulation by natural isolates of *Bacillus* depends on efficient surfactin production. *MPMI*, *27*(2), 87–100. https://doi.org/10.1094/MPMI-09-13-0262-R

Cecchini, NM., Roychoudhry, S., Speed, DQJ., Steffes, K., Tambe, A., Zodrow, K., Konstantinoff, K., Jung, HW., Engle, NL., Tschaplinski, TJ., & Greenberg, JT. (2019). Underground azelaic acid–conferred resistance to *Pseudomonas syringae* in *Arabidopsis*. *MPMI*, *32*(1), 86–94. https://doi.org/10.1094/MPMI-07-18-0185-R

Cesa-Luna, C., Geudens, N., Girard, L., De Roo, V., Maklad, HR., Martins, JC., Höfte, M., & De Mot, R. (2023). Charting the lipopeptidome of nonpathogenic *Pseudomonas*. *mSystems*, *8*(1), e0098822. https://doi.org/10.1128/msystems.00988-22

Ceulemans, E., Ibrahim, HMM., De Coninck, B., & Goossens, A. (2021). Pathogen effectors: exploiting the promiscuity of plant signaling hubs. *Trends Plant Sci*, *26*(8), 780–795. https://doi.org/10.1016/j.tplants.2021.01.005

Charpe, AM., Aglave, B., & Ghosh, DK. (2025). Microbial-mediated induced resistance: interactive effects for improving crop health. *Front. Microbiol*, *16*, 1660944. https://doi.org/10.3389/fmicb.2025.1660944

Chen, WC., Juang, RS., & Wei, YH. (2015). Applications of a lipopeptide biosurfactant, surfactin, produced by microorganisms. *Biochem. Eng. J*, *103*, 158–169. https://doi.org/10.1016/j.bej.2015.07.009

Chen, L., Xu, XX., Sun, YX., Xin, QH., Lv, YY., Hu, YS., & Bian, K. (2023). Surfactin inhibits *Fusarium graminearum* by accumulating intracellular ROS and inducing apoptosis mechanisms. *World J Microbiol Biotechnol*, *39*(12), 340. https://doi.org/10.1007/s11274-023-03790-2

Chowdhury, SP., Uhl, J., Grosch, R., Alquéres, S., Pittroff, S., Dietel, K., Schmitt-Kopplin, P., Borriss, R., & Hartmann, A. (2015). Cyclic lipopeptides of *Bacillus amyloliquefaciens* subsp. plantarum colonizing the lettuce rhizosphere enhance plant

defense responses toward the bottom rot pathogen *Rhizoctonia solani*. *MPMI*, *28*(9), 984–995. https://doi.org/10.1094/MPMI-03-15-0066-R

Clements, T., Ndlovu, T., Khan, S., & Khan, W. (2019). Biosurfactants produced by *Serratia* species: classification, biosynthesis, production and application. *Appl. Microbiol. Biotechnol*, *103*(2), 589–602. https://doi.org/10.1007/s00253-018-9520-5

Cochrane, SA., & Vederas, JC. (2016). Lipopeptides from *Bacillus* and *Paenibacillus* spp.: a gold mine of antibiotic candidates. *Med. Res. Rev*, *36*(1), 4–31. https://doi.org/10.1002/med.21321

Courtois, C., Besson, A., Dahan, J., Bourque, S., Dobrowolska, G., Pugin, A., & Wendehenne, D. (2008). Nitric oxide signalling in plants: interplays with Ca^{2+} and protein kinases. *J. Exp. Bot*, *59*(2), 155–163. https://doi.org/10.1093/jxb/erm197

Dasgupta, A., Saha, S., Ganguli, P., Das, I., De, D., & Chaudhuri, S. (2023). Characterization of pumilacidin, a lipopeptide biosurfactant produced from *Bacillus pumilus* NITDID1 and its prospect in bioremediation of hazardous pollutants. *Arch. Microbiol*, *205*, 274. https://doi.org/10.1007/s00203-023-03619-4

De Lorenzo, G., & Cervone, F. (2022). Plant immunity by damage-associated molecular patterns (DAMPs). *Essays Biochem*, *66*(5), 459–469. https://doi.org/10.1042/EBC20210087

de Melo, FMP., Fiore, MF., de Moraes, LAB., Silva-Stenico, ME., Scramin, S., Teixeira, M de A., & de Melo, IS. (2009). Antifungal compound produced by the cassava endophyte *Bacillus pumilus* MAIIIM4a. *Sci. Agric*, *66*(5), 583–592. https://doi.org/10.1590/S0103-90162009000500002

de Oliveira, J., Williams, D., Andersen, R., Sarragiotto, M., & Baldoqui, D. (2020). Pumilacidins A-E from sediment-derived bacterium *Bacillus* sp. 4040 and their antimicrobial activity evaluation. *J. Braz. Chem. Soc*, *31*(2), 357-368. https://doi.org/10.21577/0103-5053.20190188

De Pessemier, C., Vandecasteele, M., Hamonts, K., Van Damme, D., & Goormachtig, S. (2026). Licensed to protect: microbial biocontrol challenges and opportunities. *Trends Plant Sci*. 1360-1385. https://doi.org/10.1016/j.tplants.2026.03.012

De Roo, V., Verleysen, Y., Kovács, B., De Vleeschouwer, M., Muangkaew, P., Girard, L., Höfte, M., De Mot, R., Madder, A., Geudens, N., & Martins, JC. (2022). An nuclear magnetic resonance fingerprint matching approach for the identification and structural re-evaluation of *Pseudomonas* lipopeptides. *Microbiol. Spectr*, *10*(4), e01261-22. https://doi.org/10.1128/spectrum.01261-22

Debois, D., Fernandez, O., Franzil, L., Jourdan, E., de Brogniez, A., Willems, L., Clément, C., Dorey, S., De Pauw, E., & Ongena, M. (2015). Plant polysaccharides initiate underground crosstalk with bacilli by inducing synthesis of the immunogenic lipopeptide surfactin. *Environ. Microbiol. Rep*, *7*(3), 570–582. https://doi.org/10.1111/1758-2229.12286

DeFalco, TA., & Zipfel, C. (2021). Molecular mechanisms of early plant pattern-triggered immune signaling. *Mol. Cell*, *81*(20), 4346. https://doi.org/10.1016/j.molcel.2021.09.028

Deleu M., Lorent J., Lins L., Brasseur R., Braun N., El Kirat K., Nylander T., Dufrêne YF., & Mingeot-Leclercq MP. (2013). Effects of surfactin on membrane models displaying lipid phase separation. *Biochim Biophys Acta*, *1828*(2), 801-815. https://doi:10.1016/j.bbamem.2012.11.007

Deleu, M., Paquot, M., & Nylander, T. (2005). Fengycin interaction with lipid monolayers at the air-aqueous interface - implications for the effect of fengycin on biological membranes. *J. Colloid Interface Sci*, *283*(2), 358–365. https://doi.org/10.1016/j.jcis.2004.09.036

Delmer, D., Dixon, RA., Keegstra, K., & Mohnen, D. (2024). The plant cell wall—dynamic, strong, and adaptable—is a natural shapeshifter. *Plant Cell*, *36*(5), 1257–1311. https://doi.org/10.1093/plcell/koad325

Dhali, D., Coutte, F., Arias, AA., Auger, S., Bidnenko, V., Chataigné, G., Lalk, M., Niehren, J., de Sousa, J., Versari, C., & Jacques, P. (2017). Genetic engineering of the branched fatty acid metabolic pathway of *Bacillus subtilis* for the overproduction of surfactin C_{14} isoform. *Biotechnol. J*, *12*, 1600574. https://doi.org/10.1002/biot.201600574

Dihazi, A., Jaiti, F., WafaTaktak, kilani-Feki, O., Jaoua, S., Driouich, A., Baaziz, M., Daayf, F., & Serghini, MA. (2012). Use of two bacteria for biological control of bayoud disease caused by *Fusarium oxysporum* in date palm (*Phoenix dactylifera* L) seedlings. *Plant Physiol. Biochem*, *55*, 7–15. https://doi.org/10.1016/j.plaphy.2012.03.003

Dimkić, I., Janakiev, T., Petrović, M., Degrassi, G., & Fira, D. (2022). Plant-associated *Bacillus* and *Pseudomonas* antimicrobial activities in plant disease suppression via biological control mechanisms - a review. *Physiol. Mol. Plant Pathol*, *117*, 101754. https://doi.org/10.1016/j.pmpp.2021.101754

Ding, LN., Li, YT., Wu, YZ., Li, T., Geng, R., Cao, J., Zhang, W., & Tan, XL. (2022). Plant disease resistance-related signaling pathways: recent progress and future prospects. *Int. J. Mol. Sci*, *23*(24), 16200. https://doi.org/10.3390/ijms232416200

Dini, S., Oz, F., Bekhit, AEDA., Carne, A., & Agyei, D. (2024). Production, characterization, and potential applications of lipopeptides in food systems: a comprehensive review. *Compr. Rev. Food Sci. Food Saf*, *23*(4), e13394. https://doi.org/10.1111/1541-4337.13394

Dobrzyński, J., Jakubowska, Z., Kulkova, I., Kowalczyk, P., & Kramkowski, K. (2023). Biocontrol of fungal phytopathogens by *Bacillus pumilus*. *Front. Microbiol*, *14*, 1194606. https://doi.org/10.3389/fmicb.2023.1194606

Döll, S., Kuhlmann, M., Rutten, T., Mette, MF., Scharfenberg, S., Petridis, A., Berreth, DC., & Mock, HP. (2018). Accumulation of the coumarin scopolin under abiotic stress conditions is mediated by the *Arabidopsis thaliana* THO/TREX complex. *Plant J*, *93*(3), 431–444. https://doi.org/10.1111/tpj.13797

Duban, M., Cociancich, S., & Leclère, V. (2022). Nonribosomal peptide synthesis definitely working out of the rules. *Microorganisms*, *10*(3). https://doi.org/10.3390/microorganisms10030577

Elbadry, M., Taha, RM., Eldougdoug, KA., & Gamal-Eldin, & H. (2006). Induction of systemic resistance in faba bean (*Vicia faba* L.) to bean yellow mosaic potyvirus (BYMV) via seed bacterization with plant growth promoting rhizobacteria. *J. Plant Dis. Prot*, *113*(6), 247-251. https://doi.org/10.1007/BF03356189

Etesami, H. (2024). Enhancing crop disease management through integrating biocontrol bacteria and silicon fertilizers: challenges and opportunities. *J. Environ. Manage*, *371*, 123102. https://doi.org/10.1016/j.jenvman.2024.123102

Etesami, H., Jeong, BR., & Glick, BR. (2023). Biocontrol of plant diseases by *Bacillus* spp. *Physiol. Mol. Plant Pathol*, *126*, 102048. https://doi.org/10.1016/j.pmpp.2023.102048

Farace, G., Fernandez, O., Jacquens, L., Coutte, F., Krier, F., Jacques, P., Clément, C., Barka, EA., Jacquard, C., & Dorey, S. (2015). Cyclic lipopeptides from *Bacillus subtilis* activate distinct patterns of defence responses in grapevine. *Mol. Plant Pathol*, *16*(2), 177–187. https://doi.org/10.1111/mpp.12170

Freschi, L. (2013). Nitric oxide and phytohormone interactions: current status and perspectives. *Front. Plant Sci*, *4*, 398. https://doi.org/10.3389/fpls.2013.00398

Ganley, JG., Carr, G., Ioerger, TR., Sacchettini, JC., Clardy, J., & Derbyshire, ER. (2018). Discovery of antimicrobial lipodepsipeptides produced by a *Serratia* sp. within mosquito microbiomes. *ChemBioChem*, *19*(15), 1590–1594. https://doi.org/10.1002/cbic.201800124

Gao, D., Sun, Q., Hu, B., & Zhang, S. (2020). A framework for agricultural pest and disease monitoring based on internet-of-things and unmanned aerial vehicles. *Sensors*, *20*(5), 1487. https://doi.org/10.3390/s20051487

García-Gutiérrez, L., Zeriouh, H., Romero, D., Cubero, J., de Vicente, A., & Pérez-García, A. (2013). The antagonistic strain *Bacillus subtilis* UMAF6639 also confers protection to melon plants against cucurbit powdery mildew by activation of jasmonate- and salicylic acid-dependent defence responses. *Microb. Biotechnol*, *6*(3), 264–274. https://doi.org/10.1111/1751-7915.12028

Ghelardi, E., Salvetti, S., Ceragioli, M., Gueye, S. A., Celandroni, F., & Senesi, S. (2012). Contribution of surfactin and SwrA to flagellin expression, swimming, and surface motility in *Bacillus subtilis*. *Appl. Environ. Microbiol*, *78*(18), 6540–6544. https://doi.org/10.1128/AEM.01341-12

Gigolashvili, T., Berger, B., Mock, HP., Müller, C., Weisshaar, B., & Flügge, UI. (2007). The transcription factor HIG1/MYB51 regulates indolic glucosinolate biosynthesis in *Arabidopsis thaliana*. *Plant J*, *50*(5), 886–901. https://doi.org/10.1111/j.1365-313X.2007.03099.x

Gilliard, G., Demortier, T., Boubsi, F., Jijakli, MH., Ongena, M., De Clerck, C., & Deleu, M. (2024). Deciphering the distinct biocontrol activities of lipopeptides fengycin and surfactin through their differential impact on lipid membranes. *Colloids Surf B Biointerfaces*, *239*, 113933. https://doi.org/10.1016/j.colsurfb.2024.113933

Gilliard, G., Furlan, AL., Smeralda, W., Pršić, J., & Deleu, M. (2022). Added value of biophysics to study lipid-driven biological processes: the case of surfactins, a class of

natural amphiphile molecules. *Int. J. Mol. Sci*, *23*(22), 13831. https://doi.org/10.3390/ijms232213831

Gilliard, G., Pršić, J., Crowet, J.-M., Chemotti, C., Ahmed, J., Lorent, J., Jolivet, M.-D., Egli, S., Egée, S., Bouyer, G., Race, G., van Buren, L., Van Den Berghe, A., Argüelles-Arias, A., Mathelié-Guinlet, M., Ibrahim, H., Genva, M., Fouillen, L., Mirande-Bret, C., Razin, O., Vue, B., Zupunski, M., Luzuriaga-Loaiza, W. P., Deboever, E., Nasir, M. N., Lins, L., Van Der Smissen, P., Boubsi, F., Eschrig, S., Germain, V., Höfte, M., Zipfel, C., Dufrêne, Y. F., Tyteca, D., Koutsioubas, A., Brocca, P., Grossman, G., Ranf, S., Dorey, S., De Coninck, B., Nürnberger, T., Mongrand, S., Gronnier, J., Rondelli, V., Deleu, M., & Ongena, M. (2026). Membrane remodelling mediates lipopeptide-induced immunity in *Arabidopsis*. *Nat. Plants*, *12*. https://doi.org/10.1038/s41477-026-02270-3

Gimenez, D., Phelan, A., Murphy, CD., & Cobb, SL. (2021). Fengycin A analogues with enhanced chemical stability and antifungal properties. *Org. Lett*, *23*(12), 4672–4676. https://doi.org/10.1021/acs.orglett.1c01387

Gogoi, K., Gogoi, H., Borgohain, M., Saikia, R., Chikkaputtaiah, C., Hiremath, S., & Basu, U. (2024). The molecular dynamics between reactive oxygen species (ROS), reactive nitrogen species (RNS) and phytohormones in plant's response to biotic stress. *Plant Cell Rep*, *43*(11), 263. https://doi.org/10.1007/s00299-024-03343-3

Gómez, A., Moreno, H., & Andújar, D. (2025). Intelligent inter- and intra-row early weed detection in commercial maize crops. *Plants*, *14*(6), 881. https://doi.org/10.3390/plants14060881

Gond, SK., Bergen, MS., Torres, MS., & White, JF. (2015). Endophytic *Bacillus* spp. produce antifungal lipopeptides and induce host defence gene expression in maize. *Microbiol. Res*, *172*, 79–87. https://doi.org/10.1016/j.micres.2014.11.004

Götze, S., & Stallforth, P. (2020). Structure, properties, and biological functions of nonribosomal lipopeptides from pseudomonads. *Nat. Prod. Rep*, *37*(1), 29–54. https://doi.org/10.1039/c9np00022d

Grady, EN., MacDonald, J., Liu, L., Richman, A., & Yuan, ZC. (2016). Current knowledge and perspectives of *Paenibacillus*: a review. *Microb. Cell Fact*, *15*(1), 203. https://doi.org/10.1186/s12934-016-0603-7

Grangemard, I., Peypoux, F., Wallach, J., Das, BC., Labbé, H., Caille, A., Genest, M., Maget-Dana, R., Ptak, M., & Bonmatin, JM. (1997). Lipopeptides with improved properties: structure by NMR, purification by HPLC and structure-activity relationships of new isoleucyl-rich surfactins. *J. Pept. Sci*, *3*(2), 145–154. https://doi.org/10.1002/(SICI)1099-1387(199703)3:2<145::AID-PSC96>3.0.CO;2-Y

Grangemard, I., Bonmatin, JM., Bernillon, J., Das, BC., & Peypoux, F. (1999). Lichenysins G, a novel family of lipopeptide biosurfactants from *Bacillus licheniformis* IM 1307: production, isolation and structural evaluation by NMR and mass spectrometry. *J. Antibiot*, *52*(4), 363–373. https://doi.org/10.7164/antibiotics.52.363

Groll, AH., De Lucca, AJ., & Walsh, TJ. (1998). Emerging targets for the development of novel antifungal therapeutics. *Trends Microbiol*, *6*(3), 117–124. https://doi.org/10.1016/S0966-842X(97)01206-7

Grossman, AD. (1995). Genetic networks controlling the initiation of sporulation and the development of genetic competence in *Bacillus subtilis*. *Annu. Rev. Genet*, *29*, 477–508. https://doi.org/10.1146/annurev.ge.29.120195.002401

Guan, Y., Bak, F., Hennessy, RC., Horn Herms, C., Elberg, CL., Dresbøll, DB., Winding, A., Sapkota, R., & Nicolaisen, MH. (2024). The potential of *Pseudomonas fluorescens* SBW25 to produce viscosin enhances wheat root colonization and shapes root-associated microbial communities in a plant genotype-dependent manner in soil systems. *mSphere*, *9*(7), e00294-24. https://doi.org/10.1128/msphere.00294-24

Guez, JS., Coucheney, F., Guy, J., Béchet, M., Fontanille, P., Chihib, NE., Niehren, J., Coutte, F., & Jacques, P. (2022). Bioinformatics modelling and metabolic engineering of the branched chain amino acid pathway for specific production of mycosubtilin isoforms in *Bacillus subtilis*. *Metabolites*. *12*(2), 107. https://doi.org/10.3390/metabo12020107

Hamley, IW. (2015). Lipopeptides: from self-assembly to bioactivity. *Chem. Commun*, *51*(41), 8574–8583. https://doi.org/10.1039/c5cc01535a

Hamrouni, R., Regus, F., Farnet Da Silva, AM., Orsiere, T., Boudenne, JL., Laffont-Schwob, I., Christen, P., & Dupuy, N. (2025). Current status and future trends of microbial and nematode-based biopesticides for biocontrol of crop pathogens. *Crit. Rev. Biotechnol*, *45*(2), 333–352. https://doi.org/10.1080/07388551.2024.2370370

Hancock, JT., & Neill, SJ. (2019). Nitric oxide: its generation and interactions with other reactive signaling compounds. *Plants*, *8*(2), 41. https://doi.org/10.3390/plants8020041

Hansen, ML., Dénes, Z., Jarmusch, SA., Wibowo, M., Lozano-Andrade, CN., Kovács, ÁT., Strube, ML., Andersen, AJC., & Jelsbak, L. (2024). Resistance towards and biotransformation of a Pseudomonas-produced secondary metabolite during community invasion. *ISME J.*, *18*(1), wrae105. https://doi.org/10.1093/ismejo/wrae105

Hashem, A., Tabassum, B., & Fathi Abd Allah, E. (2019). *Bacillus subtilis*: a plant-growth promoting rhizobacterium that also impacts biotic stress. *Saudi J. Biol. Sci*, *26*(6), 1291–1297. https://doi.org/10.1016/j.sjbs.2019.05.004

Haskett, TL., Tkacz, A., & Poole, PS. (2021). Engineering rhizobacteria for sustainable agriculture. *ISME, 15*(4), 949–964. https://doi.org/10.1038/s41396-020-00835-4

He, P., Cui, W., Munir, S., He, P., Huang, R., Li, X., Wu, Y., Wang, Y., Yang, J., Tang, P., He, Y., & He, P. (2023). Fengycin produced by *Bacillus subtilis* XF-1 plays a major role in the biocontrol of Chinese cabbage clubroot via direct effect and defense stimulation. *J. Cell. Physiol*, *239*, e30991. https://doi.org/10.1002/jcp.30991

Heath, EC., Hurwitz, J., Horecker, BL., Ginsburg, A., & Olsen, CW. (1961). Serratamolide, a metabolic product of *Serratia*. *J. A m. Chem. Sot*, *82*(7), 4107–4108. https://doi.org/10.1021/ja01480a046

Heerklotz, H., & Seelig, J. (2001). Detergent-like action of the antibiotic peptide surfactin on lipid membranes. *Biophys. J*, *81*(3), 1547–1554. https://doi.org/10.1016/S0006-3495(01)75808-0

Heerklotz, H., & Seelig, J. (2007). Leakage and lysis of lipid membranes induced by the lipopeptide surfactin. *Eur. Biophys. J*, *36*(4–5), 305–314. https://doi.org/10.1007/s00249-006-0091-5

Henry, G., Deleu, M., Jourdan, E., Thonart, P., & Ongena, M. (2011). The bacterial lipopeptide surfactin targets the lipid fraction of the plant plasma membrane to trigger immune-related defence responses. *Cell. Microbiol*, *13*(11), 1824–1837. https://doi.org/10.1111/j.1462-5822.2011.01664.x

Heyer, M., Scholz, SS., Reichelt, M., Kunert, G., Oelmüller, R., & Mithöfer, A. (2022). The Ca^{2+} sensor proteins CML37 and CML42 antagonistically regulate plant stress responses by altering phytohormone signals. *Plant Mol. Biol*, *109*(4–5), 611–625. https://doi.org/10.1007/s11103-021-01184-2

Hoff, G., Argüelles Arias, A., Boubsi, F., Pršic, J., Meyer, T., Ibrahim, HMM., Steels, S., Luzuriaga, P., Legras, A., Franzil, L., Lequart-Pillon, M., Rayon, C., Osorio, V., de Pauw, E., Lara, Y., Deboever, E., de Coninck, B., Jacques, P., Deleu, M., Wuytswinkel, OV., & Ongena, M. (2021). Surfactin stimulated by pectin molecular patterns and root exudates acts as a key driver of the *Bacillus*-plant mutualistic interaction. *mBio*, *12*(6), e01774-21. https://doi.org/10.1128/mBio.01774-21

Hu, F., Liu, Y., & Li, S. (2019). Rational strain improvement for surfactin production: enhancing the yield and generating novel structures. *Microb. Cell Fact*, *18*(1), 42. https://doi.org/10.1186/s12934-019-1089-x

Huang, E., Yang, X., Zhang, L., Moon, SH., & Yousef, AE. (2017). New *Paenibacillus* strain produces a family of linear and cyclic antimicrobial lipopeptides: cyclization is not essential for their antimicrobial activity. *FEMS Microbiol. Lett*, *364*(8), fnx049. https://doi.org/10.1093/femsle/fnx049

Huang, E., & Yousef, AE. (2014). The lipopeptide antibiotic paenibacterin binds to the bacterial outer membrane and exerts bactericidal activity through cytoplasmic membrane damage. *Appl. Environ. Microbiol*, *80*(9), 2700–2704. https://doi.org/10.1128/AEM.03775-13

Jautzus, T., van Gestel, J., & Kovács, ÁT. (2022). Complex extracellular biology drives surface competition during colony expansion in *Bacillus subtilis*. *ISME*, *16*(10), 2320–2328. https://doi.org/10.1038/s41396-022-01279-8

Jedelská, T., Luhová, L., & Petřivalský, M. (2021). Nitric oxide signalling in plant interactions with pathogenic fungi and oomycetes. *J. Exp. Bot*, *72*(3), 848–863. https://doi.org/10.1093/jxb/eraa596

Jeet, P., Hébrard, C., Deville, MA., Cordelier, S., Dorey, S., Aziz, A., & Crouzet, J. (2014). Deciphering the role of phytoalexins in plant-microorganism interactions and human health. *Molecules*, *19*(11), 18033–18056. https://doi.org/10.3390/molecules191118033

Jin, L., Garamus, VM., Liu, F., Xiao, J., Eckerlebe, H., Willumeit-Römer, R., Mu, B., & Zou, A. (2016). Interaction of a biosurfactant, surfactin with a cationic gemini

surfactant in aqueous solution. *J. Colloid Interface Sci*, *481*, 201–209. https://doi.org/10.1016/j.jcis.2016.07.044

Jones, JDG., Staskawicz, BJ., & Dangl, JL. (2024). The plant immune system: from discovery to deployment. *Cell*, *187*(9), 2095–2116. https://doi.org/10.1016/j.cell.2024.03.045

Jourdan, E., Henry, G., Duby, F., Dommes, J., Barthélemy, JP., Thonart, P., & Ongena, M. (2009). Insights into the defense-related events occurring in plant cells following perception of surfactin-type lipopeptide from *Bacillus subtilis*. *MPMI*, *22*(4), 456–468. https://doi.org/10.1094/MPMI

Kadota, Y., Shirasu, K., & Zipfel, C. (2015). Regulation of the NADPH oxidase RBOHD during plant immunity. *Plant Cell Physiol*, *56*(8), 1472–1480. https://doi.org/10.1093/pcp/pcv063

Kansman, JT., Jaramillo, JL., Ali, JG., & Hermann, SL. (2023). Chemical ecology in conservation biocontrol: new perspectives for plant protection. *Trends in Plant Science*, *28*(10), 1166–1177. https://doi.org/10.1016/j.tplants.2023.05.001

Kashif, A., Rehman, R., Fuwad, A., Shahid, MK., Dayarathne, N., Jamal, A., Aftab, MN., Mainali, B., & Choi, Y. (2022). Current advances in the classification, production, properties and applications of microbial biosurfactants – a critical review. *Adv. Colloid Interface Sci*, *306*, 102718. https://doi.org/10.1016/j.cis.2022.102718

Kawagoe, Y., Shiraishi, S., Kondo, H., Yamamoto, S., Aoki, Y., & Suzuki, S. (2015). Cyclic lipopeptide iturin A structure-dependently induces defense response in *Arabidopsis* plants by activating SA and JA signaling pathways. *Biochem. Biophys. Res. Commun*, *460*(4), 1015–1020. https://doi.org/10.1016/j.bbrc.2015.03.143

Kecskeméti, A., Bartal, A., Bóka, B., Kredics, L., Manczinger, L., Shine, K., Alharby, NS., Khaled, JM., Varga, M., Vágvölgyi, C., & Szekeres, A. (2018). High-frequency occurrence of surfactin monomethyl isoforms in the ferment broth of a *Bacillus subtilis* strain revealed by ion trap mass spectrometry. *Molecules*, *23*(9), 2224. https://doi.org/10.3390/molecules23092224

Khan, AR., Mustafa, A., Hyder, S., Valipour, M., Rizvi, ZF., Gondal, AS., Yousuf, Z., Iqbal, R., & Daraz, U. (2022). *Bacillus* spp. as bioagents: uses and application for sustainable agriculture. *Biology*, *11*(12), 1763. https://doi.org/10.3390/biology11121763

Khan, EA., Aftab, S., & Hasanuzzaman, M. (2023). Unraveling the importance of nitric oxide in plant-microbe interaction. *Plant Stress*, *10*, 100258. https://doi.org/10.1016/j.stress.2023.100258

Kim, CY., Song, H., & Lee, YH. (2022). Ambivalent response in pathogen defense: a double-edged sword? *Plant Commun*, *3*(6), 100415. https://doi.org/10.1016/j.xplc.2022.100415

Kitani, S., Yoshida, M., Boonlucksanawong, O., Panbangred, W., Anuegoonpipat, A., Kurosu, T., Ikuta, K., Igarashi, Y., & Nihira, T. (2018). Cystargamide B, a cyclic lipodepsipeptide with protease inhibitory activity from *Streptomyces* sp. *J. Antibiot*. *71*(7), 662–666. https://doi.org/10.1038/s41429-018-0044-0

Kloepper, JW., Ryu, CM., & Zhang, S. (2004). Induced systemic resistance and promotion of plant growth by *Bacillus* spp. *Phytopath*, *94*(11), 1259–1266. https://doi.org/10.1094/PHYTO.2004.94.11.1259

Kopp, F., & Marahiel, MA. (2007). Macrocyclization strategies in polyketide and nonribosomal peptide biosynthesis. *Nat. Prod. Rep*, *24*(4), 735. https://doi.org/10.1039/b613652b

Korangi Alleluya, V., Argüelles Arias, A., Ribeiro, B., De Coninck, B., Helmus, C., Delaplace, P., & Ongena, M. (2023). *Bacillus* lipopeptide-mediated biocontrol of peanut stem rot caused by *Athelia rolfsii*. *Front. Plant Sci*, *14*, 1069971. https://doi.org/10.3389/fpls.2023.1069971

Köster, P., DeFalco, TA., & Zipfel, C. (2022). Ca^{2+} signals in plant immunity. *EMBO J*, *41*(12), e110741. https://doi.org/10.15252/embj.2022110741

Kovács, B., Prasad, D., De Roo, V., Vanheede, M., Muangkaew, P., Madder, A., Höfte, M., De Mot, R., Geudens, N., & Martins, J. C. (2025). Higher-level structural classification of *Pseudomonas* cyclic lipopeptides through their bioactive conformation. *Adv. Sci*, *13*(12), e20365. https://doi.org/10.1002/advs.202520365

Kowall, M., Vater, J., Kluge, B., Stein, T., Franke, P., & Ziessow, D. (1998). Separation and characterization of surfactin isoforms produced by *Bacillus subtilis* OKB 105. *J. Colloid Interface Sci*, *204*(1), 1–8. https://doi.org/10.1006/jcis.1998.5558

Kügler, JH., Le Roes-Hill, M., Syldatk, C., & Hausmann, R. (2015). Surfactants tailored by the class *Actinobacteria*. *Front. Microbiol*, *6*, 212 https://doi.org/10.3389/fmicb.2015.00212

Kuiper, I., Lagendijk, EL., Pickford, R., Derrick, JP., Lamers, GEM., Thomas-Oates, JE., Lugtenberg, BJJ., & Bloemberg, GV. (2004). Characterization of two *Pseudomonas putida* lipopeptide biosurfactants, putisolvin I and II, which inhibit biofilm formation and break down existing biofilms. *Mol. Microbiol*, *51*(1), 97–113. https://doi.org/10.1046/j.1365-2958.2003.03751.x

Lahlali, R., Ezrari, S., Radouane, N., Kenfaoui, J., Esmaeel, Q., El Hamss, H., Belabess, Z., & Barka, EA. (2022). Biological control of plant pathogens: a global perspective. *Microorganisms*, *10*(3), 596. https://doi.org/10.3390/microorganisms10030596

Lam, VB., Meyer, T., Argüelles Arias, A., Ongena, M., Oni, FE., & Höfte, M. (2021). *Bacillus* cyclic lipopeptides iturin and fengycin control rice blast caused by *Pyricularia oryzae* in potting and acid sulfate soils by direct antagonism and induced systemic resistance. *Microorganisms*, *9*(7), 1441. https://doi.org/10.3390/microorganisms9071441

Landy, M., Warren, GH., RosenmanM, SB., & Colio, LG. (1948). Bacillomycin: an antibiotic from *Bacillus subtilis* active against pathogenic fungi. *Exp. Biol. Med*, *67*(4), 539–541. https://doi.org/10.3181/00379727-67-16367

Leconte, A., Jacquin, J., Duban, M., Deweer, C., Trapet, P., Laruelle, F., Farce, A., Compère, P., Sahmer, K., Fiévet, V., Hoste, A., Siah, A., Lounès-Hadj Sahraoui, A., Jacques, P., Coutte, F., Deleu, M., & Muchembled, J. (2024). Deciphering the mechanisms involved in reduced sensitivity to azoles and fengycin lipopeptide in

Venturia inaequalis. *Microbiol. Res*, *286*, 127816. https://doi.org/10.1016/j.micres.2024.127816

Li, B., Meng, X., Shan, L., & He, P. (2016). Transcriptional regulation of pattern-triggered immunity in plants. *Cell Host Microbe*, *19*(5), 641–650. https://doi.org/10.1016/j.chom.2016.04.011

Li, ZJ., Tang, SY., Gao, HS., Ren, JY., Xu, PL., Dong, WP., Zheng, Y., Yang, W., Yu, YY., Guo, JH., L, YM., Niu, DD., & Jiang, CH. (2024). Plant growth-promoting rhizobacterium *Bacillus cereus* AR156 induced systemic resistance against multiple pathogens by priming of camalexin synthesis. *Plant Cell Environ*, *47*(1), 337–353. https://doi.org/10.1111/pce.14729

Liu, JF., Yang, J., Yang, SZ., Ye, RQ., & Mu, BZ. (2012). Effects of different amino acids in culture media on surfactin variants produced by *Bacillus subtilis* TD7. *Appl. Biochem. Biotechnol*, *166*(8), 2091–2100. https://doi.org/10.1007/s12010-012-9636-5

Liu, J., He, Q., Zhou, G., Song, Y., Guan, Y., Xiao, X., Sun, W., Shi, Y., Zhou, K., Zhou, S., Wu, Y., Ma, S., & Wang, R. (2023). Effects of sowing date variation on winter wheat yield: conclusions for suitable sowing dates for high and stable yield. *Agronomy*, *13*(4), 991. https://doi.org/10.3390/agronomy13040991

Lozano-Andrade, CN., Pires Queiroz, JI., Jelsbak, L,. (2026). When neighbors control metabolite fate: consequences for plant pathogen virulence and biocontrol outcomes. *Appl Environ Microbiol*, *0*, e00149-26. https://doi.org/10.1128/aem.00149-26

Luo, C., Zhou, H., Zou, J., Wang, X., Zhang, R., Xiang, Y., & Chen, Z. (2015). Bacillomycin L and surfactin contribute synergistically to the phenotypic features of *Bacillus subtilis* 916 and the biocontrol of rice sheath blight induced by *Rhizoctonia solani*. *Appl. Microbiol. Biotechnol*, *99*(4), 1897–1910. https://doi.org/10.1007/s00253-014-6195-4

Ma, W., Smigel, A., Tsai, YC., Braam, J., & Berkowitz, GA. (2008). Innate immunity signaling: cytosolic Ca^{2+} elevation is linked to downstream nitric oxide generation through the action of calmodulin or a calmodulin-like protein. *Plant Physiol*, *148*(2), 818–828. https://doi.org/10.1104/pp.108.125104

Ma, Z., Hoang Hua, G. K. H., Ongena, M., & Höfte, M. (2016). Role of phenazines and cyclic lipopeptides produced by *Pseudomonas* sp. CMR12a in induced systemic resistance on rice and bean. *Environ. Microbiol. Rep*, *8*(5), 896–904. https://doi.org/10.1111/1758-2229.12454

Ma, Z., Ongena, M., & Höfte, M. (2017). The cyclic lipopeptide orfamide induces systemic resistance in rice to *Cochliobolus miyabeanus* but not to *Magnaporthe oryzae*. *Plant Cell Rep*, *36*(11), 1731–1746. https://doi.org/10.1007/s00299-017-2187-z

Magwebu, S., Meitz-Hopkins, JC., Pott, RWM., & Lennox, CL. (2023). Efficacy of the cyclolipopeptides fengycin and iturin A against postharvest pome fruit pathogens. *Front. Hortic*. *2*, 1175251. https://doi.org 10.3389/fhort.2023.1175251

Markelova, N., & Chumak, A. (2025). Antimicrobial activity of *Bacillus* cyclic lipopeptides and their role in the host adaptive response to changes in environmental conditions. *Int. J. Mol. Sci*, *26*(1), 336. https://doi.org/10.3390/ijms26010336

Matern, U. (1991). Coumarins and other phenylpropanoid compounds in the defense response of plant cells. *Planta Med*, *57*, S15–S20. https://doi.org/10.1055/s-2006-960224

Mejri, S., Siah, A., Coutte, F., Magnin-Robert, M., Randoux, B., Tisserant, B., Krier, F., Jacques, P., Reignault, P., & Halama, P. (2018). Biocontrol of the wheat pathogen *Zymoseptoria tritici* using cyclic lipopeptides from *Bacillus subtilis*. *Environ Sci Pollut Res*, *25*, 29822–29833. https://doi.org/10.1007/s11356-017-9241-9

Melotto, M., Underwood, W., Koczan, J., Nomura, K., & He, SY. (2006). Plant stomata function in innate immunity against bacterial invasion. *Cell*, *126*(5), 969–980. https://doi.org/10.1016/j.cell.2006.06.054

Meng, X., Xu, J., He, Y., Yang, KY., Mordorski, B., Liu, Y., & Zhang, S. (2013). Phosphorylation of an ERF transcription factor by *Arabidopsis* MPK3/MPK6 regulates plant defense gene induction and fungal resistance. *Plant Cell*, *25*(3), 1126–1142. https://doi.org/10.1105/tpc.112.109074

Meng, X., & Zhang, S. (2013). MAPK cascades in plant disease resistance signaling. *Annu. Rev. Phytopathol*, *51*, 245–266. https://doi.org/10.1146/annurev-phyto-082712-102314

Miljaković, D., Marinković, J., & Balešević-Tubić, S. (2020). The significance of *Bacillus* spp. in disease suppression and growth promotion of field and vegetable crops. *Microorganisms*, *8*(7), 1–19. https://doi.org/10.3390/microorganisms8071037

Millet, YA., Danna, CH., Clay, NK., Songnuan, W., Simon, MD., Werck-Reichhart, D., & Ausubel, FM. (2010). Innate immune responses activated in *Arabidopsis* roots by microbe-associated molecular patterns. *Plant Cell*, *22*(3), 973–990. https://doi.org/10.1105/tpc.109.069658

Modolo, LV., Augusto, O., Almeida, IMG., Magalhaes, JR., & Salgado, I. (2005). Nitrite as the major source of nitric oxide production by *Arabidopsis thaliana* in response to *Pseudomonas syringae*. *FEBS Lett*, *579*(17), 3814–3820. https://doi.org/10.1016/j.febslet.2005.05.078

Molina, A., Jordá, L., Torres, MÁ., Martín-Dacal, M., Berlanga, DJ., Fernández-Calvo, P., Gómez-Rubio, E., & Martín-Santamaría, S. (2024). Plant cell wall-mediated disease resistance: current understanding and future perspectives. *Mol. Plant*, *17*(5), 699–724. https://doi.org/10.1016/j.molp.2024.04.003

Molina-Santiago, C., Pearson, JR., Navarro, Y., Berlanga-Clavero, MV., Caraballo-Rodriguez, AM., Petras, D., García-Martín, ML., Lamon, G., Haberstein, B., Cazorla, FM., de Vicente, A., Loquet, A., Dorrestein, PC., & Romero, D. (2019). The extracellular matrix protects *Bacillus subtilis* colonies from *Pseudomonas* invasion and modulates plant co-colonization. *Nat. Commun*, *10*(1), 1919. https://doi.org/10.1038/s41467-019-09944-x

Mülner, P., Schwarz, E., Dietel, K., Junge, H., Herfort, S., Weydmann, M., Lasch, P., Cernava, T., Berg, G., & Vater, J. (2020). Profiling for bioactive peptides and volatiles of plant growth promoting strains of the *Bacillus subtilis* complex of industrial relevance. *Front. Microbiol*, *11*, 1432. https://doi.org/10.3389/fmicb.2020.01432

Mur, LAJ., Carver, TLW., & Prats, E. (2006). NO way to live; the various roles of nitric oxide in plant-pathogen interactions. *J. Exp. Bot*, *57*(3), 489–505. https://doi.org/10.1093/jxb/erj052

Nan, J., Zhang, S., & Jiang, L. (2021). Antibacterial potential of *Bacillus amyloliquefaciens* GJ1 against citrus huanglongbing. *Plants*, *10*(2), 261. https://doi.org/10.3390/plants10020261

Naruse, N., Tenmyo, O., Kobaru, S., Kamei, H., Miyaki, T., Konishi, M., & Oki, T. (1990). Pumilacidin, a complex of new antiviral antibiotics. *J. Antibiot*, *43*(3), 267–280. https://doi.org/10.7164/antibiotics.43.267

Nasir, MN., & Besson, F. (2012). Interactions of the antifungal mycosubtilin with ergosterol-containing interfacial monolayers. *Biochim. Biophys. Acta Biomembr*, *1818*(5), 1302–1308. https://doi.org/10.1016/j.bbamem.2012.01.020

Ngou, BPM., Ahn, HK., Ding, P., & Jones, JDG. (2021). Mutual potentiation of plant immunity by cell-surface and intracellular receptors. *Nature*, *592*(7852), 110–115. https://doi.org/10.1038/s41586-021-03315-7

Nguyen, NH., Trotel-Aziz, P., Clément, C., Jeandet, P., Baillieul, F., & Aziz, A. (2022). Camalexin accumulation as a component of plant immunity during interactions with pathogens and beneficial microbes. *Planta*, *255*, 116. https://doi.org/10.1007/s00425-022-03907-1

Nguyen, NH., Trotel-Aziz, P., Villaume, S., Rabenoelina, F., Clément, C., Baillieul, F., & Aziz, A. (2022). Priming of camalexin accumulation in induced systemic resistance by beneficial bacteria against *Botrytis cinerea* and *Pseudomonas syringae* pv. tomato DC3000. *J Exp Bot*, *73*(11), 3743–3757. https://doi.org/10.1093/jxb/erac070

Nguyen, Q-M., Iswanto, ABB., Son, GH., & Kim, SH. (2021). Recent advances in effector-triggered immunity in plants: new pieces in the puzzle create a different paradigm. *Int. J. Mol. Sci*, *22*(9), 4709. https://doi.org/10.3390/ijms22094709

Nie, P., Li, X., Wang, S., Guo, J., Zhao, H., & Niu, D. (2017). Induced systemic resistance against *Botrytis cinerea* by *Bacillus cereus* AR156 through a JA/ET- and NPR1-dependent signaling pathway and activates PAMP-triggered immunity in *Arabidopsis*. *Front. Plant Sci*, *8*, 238. https://doi.org/10.3389/fpls.2017.00238

Niu, DD., Liu, HX., Jiang, CH., Wang, YP., Wang, QY., Jin, HL., & Guo JH G. (2011). The plant growth–promoting rhizobacterium *Bacillus cereus* AR156 induces systemic resistance in *Arabidopsis thaliana* by simultaneously activating salicylate- and jasmonate/ethylene-dependent signaling pathways. *MPMI*, *24*(5), 533–542. https://doi.org/10.1094/MPMI-09-10-0213

Olishevska, S., Nickzad, A., & Déziel, E. (2019). *Bacillus* and *Paenibacillus* secreted polyketides and peptides involved in controlling human and plant pathogens. *Appl. Microbiol. Biotechnol*, *103*, 1189–1215. https://doi.org/10.1007/s00253-018-9541-0

Omoboye, OO., Oni, FE., Batool, H., Yimer, HZ., De Mot, R., & Höfte, M. (2019). *Pseudomonas* cyclic lipopeptides suppress the rice blast fungus *Magnaporthe oryzae* by induced resistance and direct antagonism. *Front. Plant Sci*, *10*, 901. https://doi.org/10.3389/fpls.2019.00901

Ongena, M., & Jacques, P. (2008). *Bacillus* lipopeptides: versatile weapons for plant disease biocontrol. *Trends Microbiol*, *16*(3), 115–125. https://doi.org/10.1016/j.tim.2007.12.009

Ongena, M., Jourdan, E., Adam, A., Paquot, M., Brans, A., Joris, B., Arpigny, JL., & Thonart, P. (2007). Surfactin and fengycin lipopeptides of *Bacillus subtilis* as elicitors of induced systemic resistance in plants. *Environ. Microbiol*, *9*(4), 1084–1090. https://doi.org/10.1111/j.1462-2920.2006.01202.x

Oni, FE., Esmaeel, Q., Onyeka, JT., Adeleke, R., Jacquard, C., Clement, C., Gross, H., Barka, EA., & Höfte, M. (2022). *Pseudomonas* lipopeptide-mediated biocontrol: chemotaxonomy and biological activity. *Molecules*, *27*(2), 372. https://doi.org/10.3390/molecules27020372

Pang, L., Xia, B., Liu, X., Yi, Y., Jiang, L., Chen, C., Li, P., Zhang, M., Deng, X., & Wang, R. (2021). Improvement of antifungal activity of a culture filtrate of endophytic *Bacillus amyloliquefaciens* isolated from kiwifruit and its effect on postharvest quality of kiwifruit. *J. Food Biochem*, *45*(1), e13551. https://doi.org/10.1111/jfbc.13551

Panpatte, DG., Jhala YK., & Vyas, RV. (2020). Chapter 10–Signaling pathway of induced systemic resistance. *Mol. Aspects Plant Benefic. Microbes Agric*. 133–141. https://doi.org/10.1016/B978-0-12-818469-1.00011-0

Park, K., Park, YS., Ahamed, J., Dutta, S., Ryu, H., Lee, SH., Balaraju, K., Manir, M., & Moon, SS. (2016). Elicitation of induced systemic resistance of chili pepper by iturin A analogs derived from *Bacillus vallismortis* EXTN-1. *Can. J. Plant Sci*, *96*(4), 564–570. https://doi.org/10.1139/cjps-2015-0199

Pedras, MSC., & Ahiahonu, PWK. (2005). Metabolism and detoxification of phytoalexins and analogs by phytopathogenic fungi. *Phytochemistry*, *66*(4), 391-411. https://doi:10.1016/j.phytochem.2004.12.032

Pedras, MSC., Hossain, S. & Snitynsky, RB. (2011). Detoxification of cruciferous phytoalexins in *Botrytis cinerea*: spontaneous dimerization of a camalexin metabolite. *Phytochemistry*, *72*(5), 199–207. https://doi.org/10.1016/j.phytochem.2010.11.018

Peypoux, F., Bonmatin, JM, Labbe, H., Grangemard, I., Das, BC., Ptak, M., Wallach, J., & Michel, G. (1994). [Ala_4]Surfactin, a novel isoform from *Bacillus subtilis* studied by mass and NMR spectroscopies. *Eur. J. Biochem*, *224*(1), 89–96. https://doi.org/10.1111/j.1432-1033.1994.tb19998.x

Peypoux, F., Bonmatin, JM., & Wallach, J. (1999). Recent trends in the biochemistry of surfactin. *Appl. Microbiol. Biotechnol*, *51*(5), 553–563. https://doi.org/10.1007/s002530051432

Peypoux, F., & Michel, G. (1992). Controlled biosynthesis of Val_7-and Leu_7-surfactins. *Appl Microbiol Biotechnol*, *36*, 515–517. https://doi.org/10.1007/BF00170194

Phelan, A., Cobb, S., Gimenez-Ibanez, D., & Murphy, CD. (2019). Production of fluorinated fengycins in *Bacillus* spp. *Access Microbial*, *1*. https://doi.org/10.1099/acmi.ac2019.po0049

Piasecka, A., Jedrzejczak-Rey, N., & Bednarek, P. (2015). Secondary metabolites in plant innate immunity: conserved function of divergent chemicals. *New Phytol*, *206*(3), 948–964. https://doi.org/10.1111/nph.13325

Pieterse, CMJ. (2025). The extended plant immune system. *MPMI*, *36*, 780–795. https://doi.org/10.1094/MPMI-10-25-0144-HH

Pieterse, CMJ., van Wees, SCM., van Pelt, JA., Knoester, M., Laan, R., Gerrits, H., Weisbeek, PJ., & van Loon, LC. (1998). A novel signaling pathway controlling induced systemic resistance in *Arabidopsis*. *Plant Cell*, *10*(9), 1571–1580. https://doi.org/10.1105/tpc.10.9.1571

Pilz, M., Cavelius, P., Qoura, F., Awad, D., & Brück, T. (2023). Lipopeptides development in cosmetics and pharmaceutical applications: a comprehensive review. *Biotechnol. Adv*, *67*, 108210. https://doi.org/10.1016/j.biotechadv.2023.108210

Platel, R., Lucau-Danila, A., Baltenweck, R., Maia-Grondard, A., Trapet, P., Magnin-Robert, M., Randoux, B., Duret, M., Halama, P., Hilbert, J-L., Coutte, F., Jacques, P., Hugueney, P., Reignault, P., & Siah A. (2023). Deciphering immune responses primed by a bacterial lipopeptide in wheat towards *Zymoseptoria tritici*. *Front Plant Sci*, *13*, 1074447. https://doi.org 10.3389/fpls.2022.1074447

Pozo, MJ., Van der Ent, S., Van Loon, LC., & Pieterse, CMJ. (2008). Transcription factor MYC2 is involved in priming for enhanced defense during rhizobacteria-induced systemic resistance in *Arabidopsis thaliana*. *New Phytol*, *180*(2), 511–523. https://doi.org/10.1111/j.1469-8137.2008.02578.x

Pršić, J., & Ongena, M. (2020). Elicitors of plant immunity triggered by beneficial bacteria. *Front. Plant Sci*, *11*, 594530. https://doi.org/10.3389/fpls.2020.594530

Qi, X., Liu, W., He, X., & Du, C. (2023). A review on surfactin: molecular regulation of biosynthesis. *Arch. Microbiol*, *205*(9), 313. https://doi.org/10.1007/s00203-023-03652-3

Qiao, J., Borriss, R., Sun, K., Zhang, R., Chen, X., Liu, Y., & Liu, Y. (2024). Research advances in the identification of regulatory mechanisms of surfactin production by *Bacillus*: a review. *Microb. Cell Fact*, *23*, 100. https://doi.org/10.1186/s12934-024-02372-7

Qin, WQ., Fei, D., Zhou, L., Guo, YJ., An, S., Gong, OH., Wu, YY., Liu, JF., Yang, SZ., & Mu, BZ. (2023). A new surfactin-C_{17} produced by *Bacillus subtilis* TD7 with a low critical micelle concentration and high biological activity. *New J. Chem*, *47*(16), 7604–7612. https://doi.org/10.1039/d3nj00123g

Qin, WQ., Liu, YF., Gang, HZ., Liu, JF., Zhou, L., Yang, SZ., & Mu, BZ. (2025). Structural diversity of surfactin lipopeptides and their molecular behaviors in solutions and at interfaces. *Adv. Colloid Interface Sci*, *343*, 103581. https://doi.org/10.1016/j.cis.2025.103581

Raaijmakers, JM., De Bruijn, I., & De Kock, MJD. (2006). Cyclic lipopeptide production by plant-associated *Pseudomonas* spp.: diversity, activity, biosynthesis, and regulation. *Mol Plant Microbe Interact*, *19*(7), 699–710. https://doi.org/10.1094/MPMI-19-0699

Raaijmakers, JM., de Bruijn, I., Nybroe, O., & Ongena, M. (2010). Natural functions of lipopeptides from *Bacillus* and *Pseudomonas*: more than surfactants and antibiotics. *FEMS Microbiol. Rev*, *34*(6), 1037–1062. https://doi.org/10.1111/j.1574-6976.2010.00221.x

Rabbee, MF., Hwang, BS., & Baek, KH. (2023). *Bacillus velezensis*: a beneficial biocontrol agent or facultative phytopathogen for sustainable agriculture. *Agronomy*, *13*(3). https://doi.org/10.3390/agronomy13030840

Rahman, FB., Sarkar, B., Moni, R., & Rahman, MS. (2021). Molecular genetics of surfactin and its effects on different sub-populations of *Bacillus subtilis*. *Biotechnol. Rep*, *32*, e00686. https://doi.org/10.1016/j.btre.2021.e00686

Ranf, S., Eschen-Lippold, L., Pecher, P., Lee, J., & Scheel, D. (2011). Interplay between calcium signalling and early signalling elements during defence responses to microbe- or damage-associated molecular patterns. *Plant J*, *68*(1), 100–113. https://doi.org/10.1111/j.1365-313X.2011.04671.x

Raouani, NEH., Claverie, E., Randoux, B., Chaveriat, L., Yaseen, Y., Yada, B., Martin, P., Cabrera, JC., Jacques, P., Reignault, P., Magnin-Robert, M., Lounès-Hadj, & Sahraoui A. Bio-inspired rhamnolipids, cyclic lipopeptides and a chito-oligosaccharide confer protection against wheat powdery mildew and inhibit conidia germination. (2022). *Molecules*. *27*(19), 6672. https://doi.org/10.3390/molecules27196672

Razafindralambo, H., Dufour, S., Paquot, M., & Deleu, M. (2009). Thermodynamic studies of the binding interactions of surfactin analogues to lipid vesicles. *J Therm Anal Calorim*, *95*, 817–821. https://doi.org/10.1007/s10973-008-9403-6

Reina-Pinto, JJ., & Yephremov, A. (2009). Surface lipids and plant defenses. *Plant Physiol. Biochem*, *47*(6), 540–549. https://doi.org/10.1016/j.plaphy.2009.01.004

Rigolet, A., Argüelles Arias, A., Anckaert, A., Quinton, L., Rigal, S., Tellatin, D., Burguet, P., & Ongena, M. (2024). Lipopeptides as rhizosphere public goods for microbial cooperation. *Microbiol Spectr*, *12*(1), e0310623. https://doi.org/10.1128/spectrum.03106-23

Robe, K., Conejero, G., Gao, F., Lefebvre-Legendre, L., Sylvestre-Gonon, E., Rofidal, V., Hem, S., Rouhier, N., Barberon, M., Hecker, A., Gaymard, F., Izquierdo, E., & Dubos, C. (2021). Coumarin accumulation and trafficking in *Arabidopsis thaliana*: a complex and dynamic process. *New Phytol*, *229*(4), 2062–2079. https://doi.org/10.1111/nph.17090

Robe, K., Izquierdo, E., Vignols, F., Rouached, H., & Dubos, C. (2021). The coumarins: secondary metabolites playing a primary role in plant nutrition and health. *Trends Plant Sci*, *26*(3), 248–259. https://doi.org/10.1016/j.tplants.2020.10.008

Rodríguez, J., Tonelli, ML., Figueredo, MS., Ibáñez, F., & Fabra, A. (2018). The lipopeptide surfactin triggers induced systemic resistance and priming state responses in *Arachis hypogaea* L. *Eur. J. Plant Pathol*, *152*(3), 845–851. https://doi.org/10.1007/s10658-018-1524-6

Romanowski, SB., Lee, S., Kunakom, S., Paulo, BS., Recchia, MJJ., Liu, DY., Cavanagh, H., Linington, RG., & Eustáquio, AS. (2023). Identification of the lipodepsipeptide selethramide encoded in a giant nonribosomal peptide synthetase from a *Burkholderia* bacterium. *PNAS*, *120*(42), e2304668120. https://doi.org/10.1073/pnas.2304668120

Roongsawang, N., Washio, K., & Morikawa, M. (2011). Diversity of nonribosomal peptide synthetases involved in the biosynthesis of lipopeptide biosurfactants. *Int. J. Mol. Sci*, *12*(1), 141–172. https://doi.org/10.3390/ijms12010141

Rutledge, PJ., & Challis, GL. (2015). Discovery of microbial natural products by activation of silent biosynthetic gene clusters. *Nat. Rev. Microbiol*, *13*(8), 509–523. https://doi.org/10.1038/nrmicro3496

Salwan, R., Sharma, A., Kaur, R., Sharma, R., & Sharma, V. (2022). The riddles of *Trichoderma* induced plant immunity. *Biol. Control*, *174*, 105037. https://doi.org/10.1016/j.biocontrol.2022.105037

Salwan, R., Sharma, M., Sharma, A., & Sharma, V. (2023). Insights into plant beneficial microorganism-triggered induced systemic resistance. *Plant Stress*, *7*, 100140. https://doi.org/10.1016/j.stress.2023.100140

Sani, A., Qin, WQ., Li, JY., Liu, YF., Zhou, L., Yang, SZ., & Mu, BZ. (2024). Structural diversity and applications of lipopeptide biosurfactants as biocontrol agents against phytopathogens: a review. *Microbiol. Res*, *278*, 127518. https://doi.org/10.1016/j.micres.2023.127518

Saxena, AK., Kumar, M., Chakdar, H., Anuroopa, N., & Bagyaraj, DJ. (2020). *Bacillus* species in soil as a natural resource for plant health and nutrition. *J. Appl. Microbiol*, *128*(6), 1583–1594. https://doi.org/10.1111/jam.14506

Schneider, A., Stachelhaus, T., & Marahiel, MA. (1983). Targeted alteration of the substrate specificity of peptide synthetases by rational module swapping. *Mol Gen Genet*, *257*, 308–318. https://doi.org/10.1007/s004380050652

Shafi, J., Tian, H., & Ji, M. (2017). *Bacillus* species as versatile weapons for plant pathogens: a review. *Biotechnol. Biotechnol. Equip*, *31*(3), 446–459. https://doi.org/10.1080/13102818.2017.1286950

Shah, S., Chen, C., Sun, Y., Wang, D., Nawaz, T., El-Kahtany, K., & Fahad, S. (2023). Mechanisms of nitric oxide involvement in plant-microbe interaction and its enhancement of stress resistance. *Plant Stress*, *10*, 100191. https://doi.org/10.1016/j.stress.2023.100191

Spoel, SH., & Dong, X. (2012). How do plants achieve immunity? Defence without specialized immune cells. *Nat. Rev. Immunol*, *12*(2), 89–100. https://doi.org/10.1038/nri3141

Stassen, MJJ., Hsu, SH., Pieterse, CMJ., & Stringlis, IA. (2021). Coumarin communication along the microbiome–root–shoot axis. *Trends Plant Sci*, *26*(2), 169–183. https://doi.org/10.1016/j.tplants.2020.09.008

Stenberg, JA., Sundh, I., Becher, PG., Björkman, C., Dubey, M., Egan, PA., Friberg, H., Gil, JF., Jensen, DF., Jonsson, M., Karlsson, M., Khalil, S., Ninkovic, V., Rehermann, G., Vetukuri, RR., & Viketoft, M. (2021). When is it biological control? A framework of definitions, mechanisms, and classifications. *J. Pest Sci*, *94*(3), 665–676. https://doi.org/10.1007/s10340-021-01354-7

Stoll, A., Salvatierra-Martínez, R., González, M., & Araya, M. (2021). The role of surfactin production by *Bacillus velezensis* on colonization, biofilm formation on tomato root

and leaf surfaces and subsequent protection (ISR) against *Botrytis cinerea*. *Microorganisms*, *9*(11), 2251. https://doi.org/10.3390/microorganisms9112251

Strieker, M., Tanović, A., & Marahiel, MA. (2010). Nonribosomal peptide synthetases: structures and dynamics. *Curr. Opin. Struct. Biol*, *20*(2), 234–240. https://doi.org/10.1016/j.sbi.2010.01.009

Stringlis, IA., De Jonge, R., & Pieterse, CMJ. (2019). The age of coumarins in plant-microbe interactions. *Plant Cell Physiol*, *60*(7), 1405–1419. https://doi.org/10.1093/pcp/pcz076

Stringlis, IA., Yu, K., Feussner, K., De Jonge, R., Van Bentum, S., Van Verk, MC., Berendsen, RL., Bakker, PAHM., Feussner, I., & Pieterse, CMJ. (2018). MYB72-dependent coumarin exudation shapes root microbiome assembly to promote plant health. *PNAS*, *115*(22), E5213–E5222. https://doi.org/10.1073/pnas.1722335115

Tabassum, B., Khan, A., Tariq, M., Ramzan, M., Iqbal Khan, MS., Shahid, N., & Aaliya, K. (2017). Bottlenecks in commercialisation and future prospects of PGPR. *Appl. Soil Ecol*, *121*, 102–117. https://doi.org/10.1016/j.apsoil.2017.09.030

Teixeira, PJP., Colaianni, NR., Fitzpatrick, CR., & Dangl, JL. (2019). Beyond pathogens: microbiota interactions with the plant immune system. *Curr. Opin. Microbiol*, *49*, 7–17. https://doi.org/10.1016/j.mib.2019.08.003

Théatre, A., Cano-Prieto, C., Bartolini, M., Laurin, Y., Deleu, M., Niehren, J., Fida, T., Gerbinet, S., Alanjary, M., Medema, MH., Léonard, A., Lins, L., Arabolaza, A., Gramajo, H., Gross, H., & Jacques, P. (2021). The surfactin-like lipopeptides from *Bacillus* spp.: natural biodiversity and synthetic biology for a broader application range. *Front. Bioeng. Biotechnol*, *9*, 623701. https://doi.org/10.3389/fbioe.2021.623701

Théatre, A., Hoste, ACR., Rigolet, A., Benneceur, I., Bechet, M., Ongena, M., Deleu, M., & Jacques, P. (2022). *Bacillus* sp.: a remarkable source of bioactive lipopeptides. *Adv. Biochem. Eng. Biotechnol*, *181*, 123–179. https://doi.org/10.1007/10_2021_182

Thérien, M., Kiesewalter, HT., Auria, E., Charron-Lamoureux, V., Wibowo, M., Maróti, G., Kovács, ÁT., & Beauregard, PB. (2020). Surfactin production is not essential for pellicle and root-associated biofilm development of *Bacillus subtilis*. *Biofilm*, *2*, 100021. https://doi.org/10.1016/j.bioflm.2020.100021

Thies, S., Santiago-Schübel, B., Kovačić, F., Rosenau, F., Hausmann, R., & Jaeger, KE. (2014). Heterologous production of the lipopeptide biosurfactant serrawettin W1 in *Escherichia coli*. *J. Biotechnol*, *181*, 27–30. https://doi.org/10.1016/j.jbiotec.2014.03.037

Tran, H., Ficke, A., Asiimwe, T., Höfte, M., & Raaijmakers, JM. (2007). Role of the cyclic lipopeptide massetolide A in biological control of *Phytophthora infestans* and in colonization of tomato plants by *Pseudomonas fluorescens*. *New Phytol*, *175*(4), 731–742. https://doi.org/10.1111/j.1469-8137.2007.02138.x

Tripathi, A., Pandey, VK., Jha, AK., Srivastava, S., Jakhar, S., Vijay, Singh, G., Rustagi, S., Malik, S., & Choudhary, P. (2024). Intricacies of plants' innate immune responses and their dynamic relationship with fungi: a review. *Microbiol. Res*, *285*, 127758. https://doi.org/10.1016/j.micres.2024.127758

Uttlová, P., Pinkas, D., Bechyňková, O., Fišer, R., Svobodová, J., & Seydlová, G. (2016). *Bacillus subtilis* alters the proportion of major membrane phospholipids in response to surfactin exposure. *Biochim. Biophys. Acta Biomembr*, *1858*(12), 2965–2971. https://doi.org/10.1016/j.bbamem.2016.09.006

Van der Ent, S., Verhagen, BWM., Van Doorn, R., Bakker, D., Verlaan, MG., Pel, MJC., Joosten, RG., Proveniers, MCG., Van Loon, LC., Ton, J., & Pieterse, CMJ. (2008). *MYB72* is required in early signaling steps of rhizobacteria-induced systemic resistance in *Arabidopsis*. *Plant Physiol*, *146*(3), 1293–1304. https://doi.org/10.1104/pp.107.113829

van Gestel, J., Vlamakis, H., & Kolter, R. (2015). From cell differentiation to cell collectives: *Bacillus subtilis* uses division of labor to migrate. *PLoS Biol*, *13*(4), e1002141. https://doi.org/10.1371/journal.pbio.1002141

Van Wees, SC., Van der Ent, S., & Pieterse, CMJ. (2008). Plant immune responses triggered by beneficial microbes. *Curr. Opin. Plant Biol*, *11*(4), 443–448. https://doi.org/10.1016/j.pbi.2008.05.005

Vessey, JK. (2003). Plant growth promoting rhizobacteria as biofertilizers. *Plant Soil*, *255*(2), 571–586. https://doi.org/10.1023/A:1026037216893

Verbon, EH., Trapet, PL., Stringlis, IA., Kruijs, S., Bakker, PAHM., & Pieterse, CMJ. (2017). Iron and immunity. *Annu. Rev. Phytopathol*, *55*, 355-375. https://doi.org/10.1146/annurev-phyto-080516-035537

Vieira, MEO., Nunes, VV., Calazans, CC., & Silva-Mann, R. (2024). Unlocking plant defenses: harnessing the power of beneficial microorganisms for induced systemic resistance in vegetables – a systematic review. *Biol. Control*, *188*, 105428. https://doi.org/10.1016/j.biocontrol.2023.105428

Villavicencio-Vásquez, M., Espinoza-Lozano, F., Espinoza-Lozano, L., & Coronel-León, J. (2025). Biological control agents: mechanisms of action, selection, formulation and challenges in agriculture. *Front. Agron*, *7*, 1578915. https://doi.org/10.3389/fagro.2025.1578915

Vlot, AC., Sales, JH., Lenk, M., Bauer, K., Brambilla, A., Sommer, A., Chen, Y., Wenig, M., & Nayem, S. (2021). Systemic propagation of immunity in plants. *New Phytol*, *229* (3), 1234–1250. https://doi.org/10.1111/nph.16953

Wang, Y., Pei, Y., Wang, X., Dai, X., & Zhu, M. (2024). Antimicrobial metabolites produced by the plant growth-promoting rhizobacteria (PGPR): *Bacillus* and *Pseudomonas*. *Adv. Agrochem*, *3*(3), 206–221. https://doi.org/10.1016/j.aac.2024.07.007

Wang, Z., Liu, C., Shi, Y., Huang, M., Song, Z., Simal-Gandara, J., Li, N., & Shi, J. (2024). Classification, application, multifarious activities and production improvement of lipopeptides produced by *Bacillus*. *Crit. Rev. Food Sci. Nutr*, *64*(21), 7451–7464. https://doi.org/10.1080/10408398.2023.2185588

Waszczak, C., Carmody, M., & Kangasjärvi, J. (2018). Reactive oxygen species in plant signaling. *Annu. Rev. Plant Biol*, *69*(1), 209–236. https://doi.org/10.1146/annurev-arplant-042817-040322

Westman, SM., Kloth, KJ., Hanson, J., Ohlsson, AB., & Albrectsen, BR. (2019). Defence priming in *Arabidopsis* – a meta-analysis. *Sci. Rep*, *9*(1), 13309. https://doi.org/10.1038/s41598-019-49811-9

Wilson, J., Cui, J., Nakao, T., Kwok, H., Zhang, Y., Kayrouz, CM., Pham, TM., Roodhouse, H., & Ju, KS. (2023). Discovery of antimicrobial phosphonopeptide natural products from *Bacillus velezensis* by genome mining. *Appl Environ Microbiol*, *89*(6), e00338-23. https://doi.org/10.1128/aem.00338-23

Wolf, S. (2022). Cell wall signaling in plant development and defense. *Annu. Rev. Plant Biol*, *73*(1), 323–353. https://doi.org/10.1146/annurev-arplant-102820-095312

Wu, G., Liu, Y., Xu, Y., Zhang, G., Shen, Q., & Zhang, R. (2018). Exploring elicitors of the beneficial rhizobacterium *Bacillus amyloliquefaciens* SQR9 to induce plant systemic resistance and their interactions with plant signaling pathways. *MPMI*, *31*(5), 560–567. https://doi.org/10.1094/MPMI-11-17-0273-R

Wu, JJ., Chou, HP., Huang, JW., & Deng, WL. (2021). Genomic and biochemical characterization of antifungal compounds produced by *Bacillus subtilis* PMB102 against *Alternaria brassicicola*. *Microbiol. Res*, *251*, 126815. https://doi.org/10.1016/j.micres.2021.126815

Wu, Q., Zhi, Y., & Xu, Y. (2019). Systematically engineering the biosynthesis of a green biosurfactant surfactin by *Bacillus subtilis* 168. *Metab. Eng*, *52*, 87–97. https://doi.org/10.1016/j.ymben.2018.11.004

Xia, L., & Wen, J. (2023). Available strategies for improving the biosynthesis of surfactin: a review. *Crit. Rev. Biotechnol*, *43*(7), 1111–1128. https://doi.org/10.1080/07388551.2022.2095252

Xie, S., Jiang, H., Ding, T., Xu, Q., Chai, W., & Cheng, B. (2018). *Bacillus amyloliquefaciens* FZB42 represses plant miR846 to induce systemic resistance via a jasmonic acid-dependent signalling pathway. *Mol. Plant Pathol*, *19*(7), 1612–1623. https://doi.org/10.1111/mpp.12634

Xu, D., & Yang, L. (2025). Regeneration and defense: unveiling the molecular interplay in plants. *New Phytol*, *246*(6), 2484–2494. https://doi.org/10.1111/nph.70171

Yakimov, MM., Timmis, KN., Wray, V., & Fredrickson, HL. (1995). Characterization of a new lipopeptide surfactant produced by thermotolerant and halotolerant subsurface *Bacillus licheniformis* BAS50. *Appl. Environ. Microbiol*, *61*(5), 1706-1713. https://doi.org/10.1128/aem.61.5.1706-1713.1995

Yamamoto, S., Shiraishi, S., & Suzuki, S. (2015). Are cyclic lipopeptides produced by *Bacillus amyloliquefaciens* S13-3 responsible for the plant defence response in strawberry against *Colletotrichum gloeosporioides*? *Lett. Appl. Microbiol*, *60*(4), 379–386. https://doi.org/10.1111/lam.12382

Yang, C., Lai, YM., & Yao, N. (2025). Plant sphingolipids: subcellular distributions and functions. *Curr. Opin. Plant Biol*, *85*, 102704. https://doi.org/10.1016/j.pbi.2025.102704

Yang, R., Lei, S., Xu, X., Jin, H., Sun, H., Zhao, X., Pang, B., & Shi, J. (2020). Key elements and regulation strategies of NRPSs for biosynthesis of lipopeptides by

Bacillus. *Appl Microbiol Biotechnol*, *104*, 8077–8087. https://doi.org/https://doi.org/10.1007/s00253-020-10801-x

Yasmin, A., Aslam, F., & Fariq, A. (2022). Genetic evidences of biosurfactant production in two *Bacillus subtilis* strains MB415 and MB418 isolated from oil contaminated soil. *Front. Bioeng. Biotechnol*, *10*, 855762. https://doi.org/10.3389/fbioe.2022.855762

Youssef, NH., Duncan, KE., & McInerney, MJ. (2005). Importance of 3-hydroxy fatty acid composition of lipopeptides for biosurfactant activity. *Appl. Environ. Microbiol*, *71*(12), 7690–7695. https://doi.org/10.1128/AEM.71.12.7690-7695.2005

Youssef, NH., Wofford, N., & McInerney, MJ. (2011). Importance of the long-chain fatty acid beta-hydroxylating cytochrome P450 enzyme YbdT for lipopeptide biosynthesis in *Bacillus subtilis* strain OKB105. *Int. J. Mol. Sci 12*(3), 1767–1786. https://doi.org/10.3390/ijms12031767

Yu, F., Shen, Y., Pang, Y., Fan, H., Liu, M., & Liu, X. (2024). Effects of branched-chain amino acids on surfactin structure and antibacterial activity in *Bacillus velezensis* YA215. *Plant Cell Environ*, *40*(9), 281. https://doi.org/10.1007/s11274-024-04088-7

Yu, K., Pieterse, CMJ., Bakker, PAHM., & Berendsen, RL. (2019). Beneficial microbes going underground of root immunity. *Plant Cell Environt*, *42*(10), 2860–2870. https://doi.org/10.1111/pce.13632

Yu, X., Feng, B., He, P., & Shan, L. (2017). From chaos to harmony: responses and signaling upon microbial pattern recognition. *Annu Rev Phytopathol*, *55*, 109–146. https://doi.org/10.1146/annurev-phyto-080516-035649

Yu, Y., Gui, Y., Li, Z., Jiang, C., Guo, J., & Niu, D. (2022). Induced systemic resistance for improving plant immunity by beneficial microbes. *Plants*, *11*(3), 386. https://doi.org/10.3390/plants11030386

Yuan, M., Jiang, Z., Bi, G., Nomura, K., Liu, M., Wang, Y., Cai, B., Zhou, JM., He, SY., & Xin, XF. (2021). Pattern-recognition receptors are required for NLR-mediated plant immunity. *Nature*, *592*(7852), 105–109. https://doi.org/10.1038/s41586-021-03316-6

Yuan, M., Ngou, BPM., Ding, P., & Xin, XF. (2021). PTI-ETI crosstalk: an integrative view of plant immunity. *Curr. Opin. Plant Biol*, *62*, 102030. https://doi.org/10.1016/j.pbi.2021.102030

Yuan, X., Yang, F., Wang, Y., Li, S., Zhang, D., Liang, W., & Yang, Q. (2024). Scopoletin negatively regulates the HOG pathway and exerts antifungal activity against *Botrytis cinerea* by interfering with infection structures, cell wall, and cell membrane formation. *Phytopathol. Res*, *6*(1), 1. https://doi.org/10.1186/s42483-023-00219-4

Zafar, MM., Razzaq, A., Farooq, MA., Rehman, A., Firdous, H., Shakeel, A., Mo, H., & Ren, M. (2020). Insect resistance management in *Bacillus thuringiensis* cotton by MGPS (multiple genes pyramiding and silencing). *J. Cotton Res*, *3*(1), 33. https://doi.org/10.1186/s42397-020-00074-0

Zamioudis, C., Korteland, J., Van Pelt, JA., Van Hamersveld, M., Dombrowski, N., Bai, Y., Hanson, J., Van Verk, MC., Ling, HQ., Schulze-Lefert, P., & Pieterse, CMJ. (2015). Rhizobacterial volatiles and photosynthesis-related signals coordinate *MYB72*

expression in *Arabidopsis* roots during onset of induced systemic resistance and iron-deficiency responses. *Plant J*, *84*(2), 309–322. https://doi.org/10.1111/tpj.12995

Zeidler, D., Zä Hringer, U., Gerber, I., Dubery, I., Hartung, T., Bors, W., Hutzler, P., & Rg Durner, J. (2004). Innate immunity in *Arabidopsis thaliana*: lipopolysaccharides activate nitric oxide synthase (NOS) and induce defense genes. *PNAS*, *101*(44), 15811-15816. https://doi.org/10.1073/pnas.0404536101

Zhan, C., Wu, M., Fang, H., Liu, X., Pan, J., Fan, X., Wang, M., & Matsumoto, H. (2023). Characterization of the chemical fungicides-responsive and bacterial pathogen-preventing *Bacillus licheniformis* in rice spikelet. *Food qual*. *saf*, *7*, fyad005. https://doi.org/10.1093/fqsafe/fyad005

Zhang, S., Chen, Y., Zhu, J., Lu, Q., Cryle, MJ., Zhang, Y., & Yan, F. (2023). Structural diversity, biosynthesis, and biological functions of lipopeptides from *Streptomyces*. *Nat. Prod. Rep*, *40*(3), 557–594. https://doi.org/10.1039/D2NP00044J

Zhang, Z., Wang, Q., Yan, H., Cang, X., Li, W., He, J., Zhang, M., Lou, L., Wang, R., & Chang, M. (2024). Lighting-up wars: stories of Ca^{2+} signaling in plant immunity. *New Crops*, *1*, 100027. https://doi.org/10.1016/j.ncrops.2024.100027

Zheng, D., Wang, H., Zhong, H., Ke, W., Hu, H., Sun, M., & Ruan, L. (2021). Elucidation of the pathogenicity-associated regulatory network in *Xanthomonas oryzae* pv. oryzae. *mSystems*, *6*(10), 1128. https://doi.org/10.1128/msystems.00789-20

Zhou, L., Höfte, M., & Hennessy, RC. (2024). Does regulation hold the key to optimizing lipopeptide production in *Pseudomonas* for biotechnology? *Front. Bioeng. Biotechnol*, *12*, 1363183. https://doi.org/10.3389/fbioe.2024.1363183

Zhou, L., Song, C., Muñoz, CY., & Kuipers, OP. (2021). *Bacillus cabrialesii* BH5 protects tomato plants against *Botrytis cinerea* by production of specific antifungal compounds. *Front. Microbiol*, *12*, *707609*. https://doi.org/10.3389/fmicb.2021.707609

Appendix

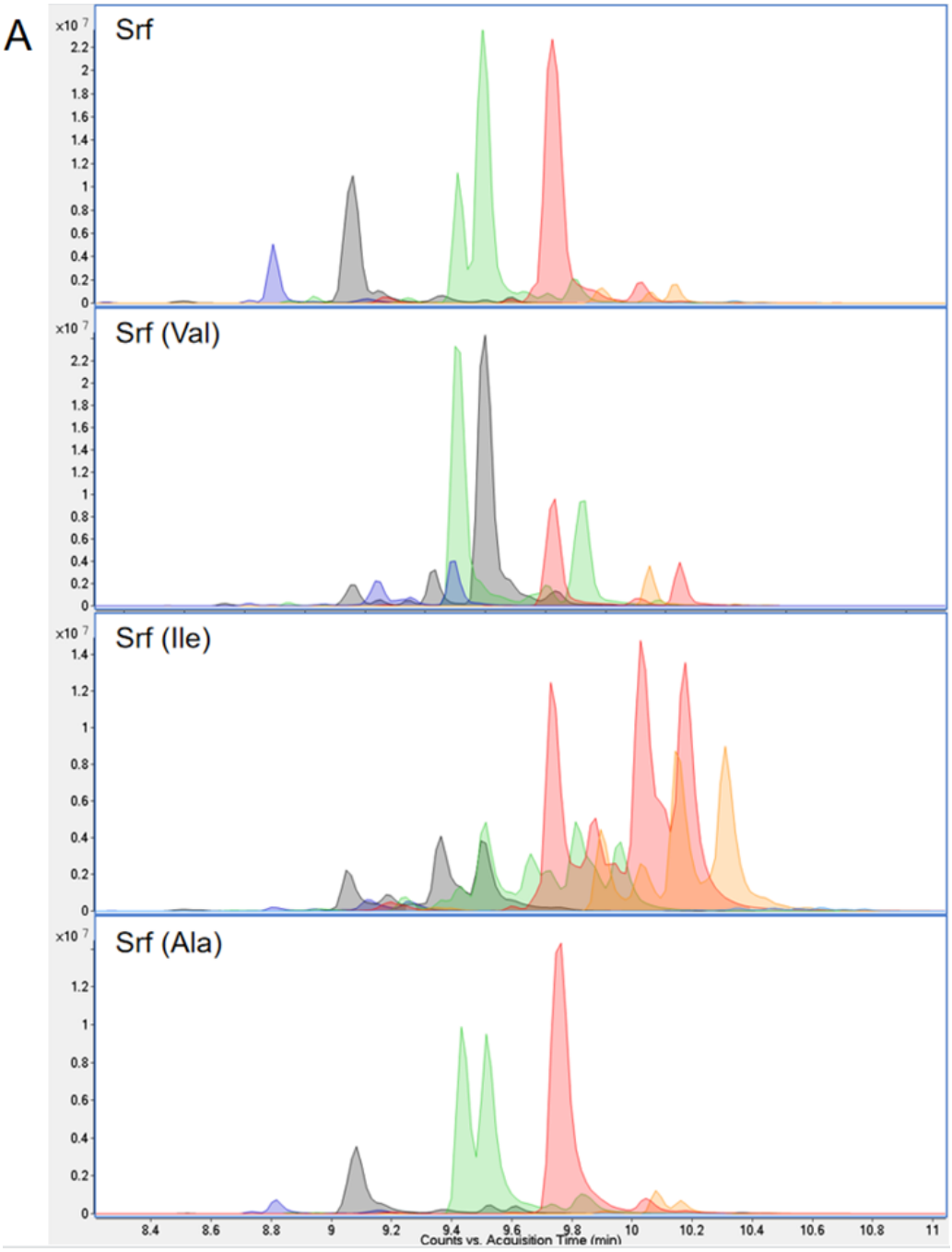

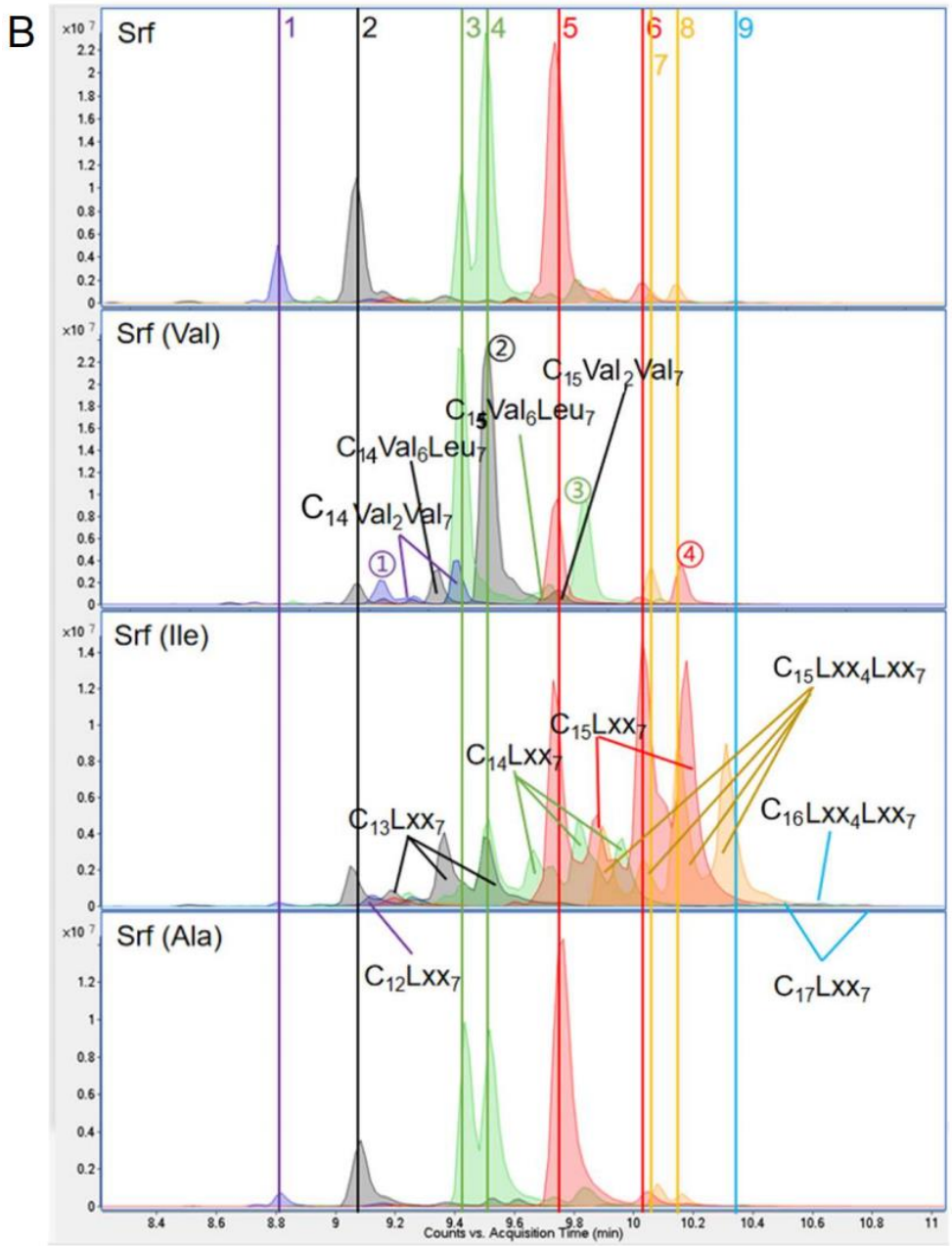

Figure A1-1 Structures of Srf variants

A. and **B.** repsent chromatograms of Srf homologs, different colors present different masses (see in the below Table A1-1). Each of the purified CLP component was collected and mixed as a purified CLP mixture used in this study. The blue, black, green, red, orange, blue color represtents CLP mass: 994, 1008, 1022, 1036, 1050, 1064 respectively.

Table A1-1 Information of Srf variants.

Mass	994	1008	1022	1036	1050	1064	994	1008	1022	1036
Line	1	2	3,4	5,6	7,8	9	①	②	③	④
Retension time	8.8 s	9.17 s	9.42-9.52 s	9.75 s	10.13-10.17 s	10.37 s	9.2 s	9.55 s	9.85 s	10.2 s
Srf homologue	$C_{12}Leu_7$	$C_{13}Leu_7$	$C_{14}Leu_7$	$C_{15}Leu_7$	$C_{16}Leu_7$	$C_{17}Leu_7$	$C_{12}Val_7$	$C_{14}Val_7$	$C_{15}Val_7$	$C_{16}Val_7$

A

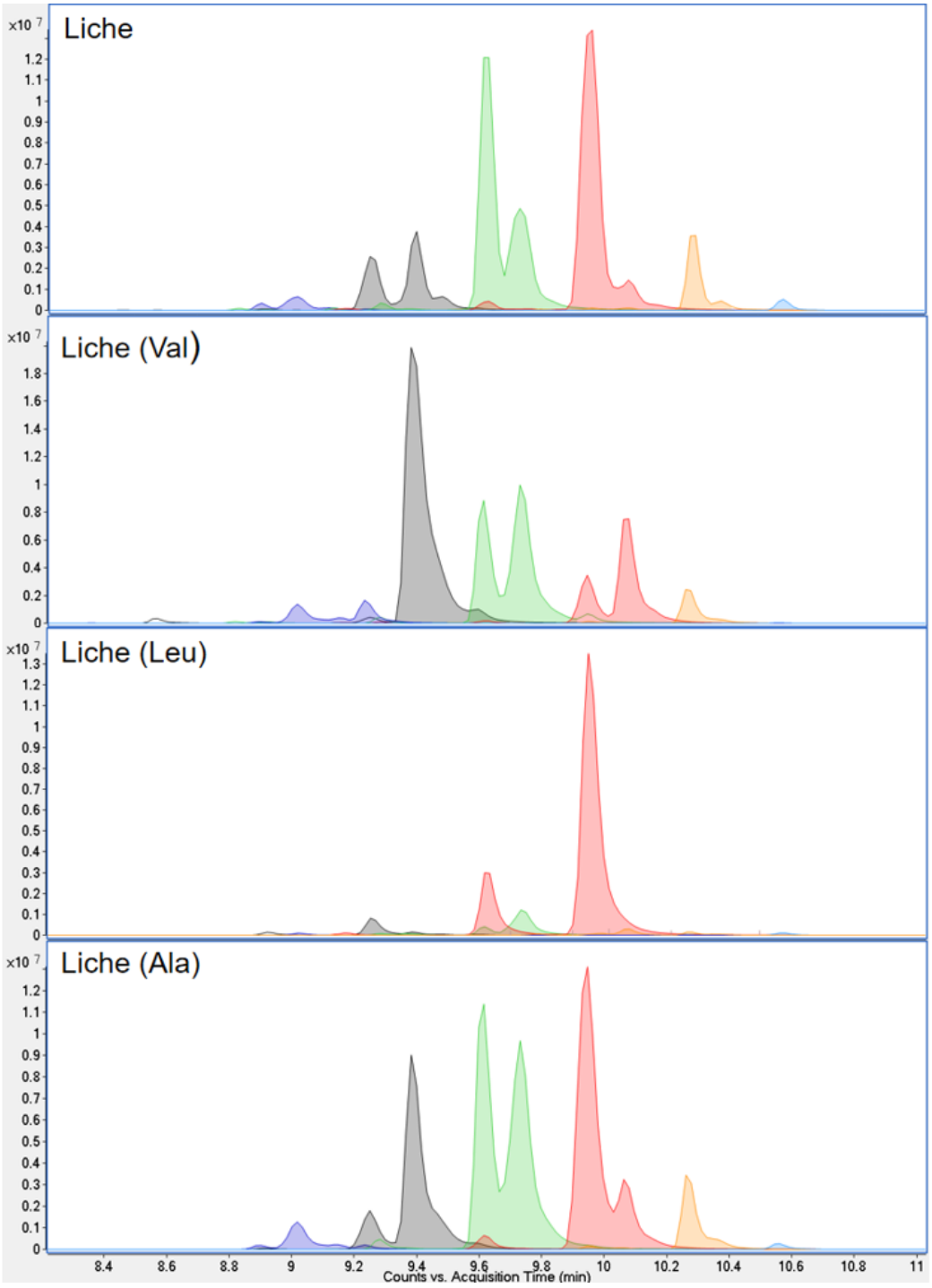
Liche
Liche (Val)
Liche (Leu)
Liche (Ala)
x10 7
Counts vs. Acquisition Time (min)

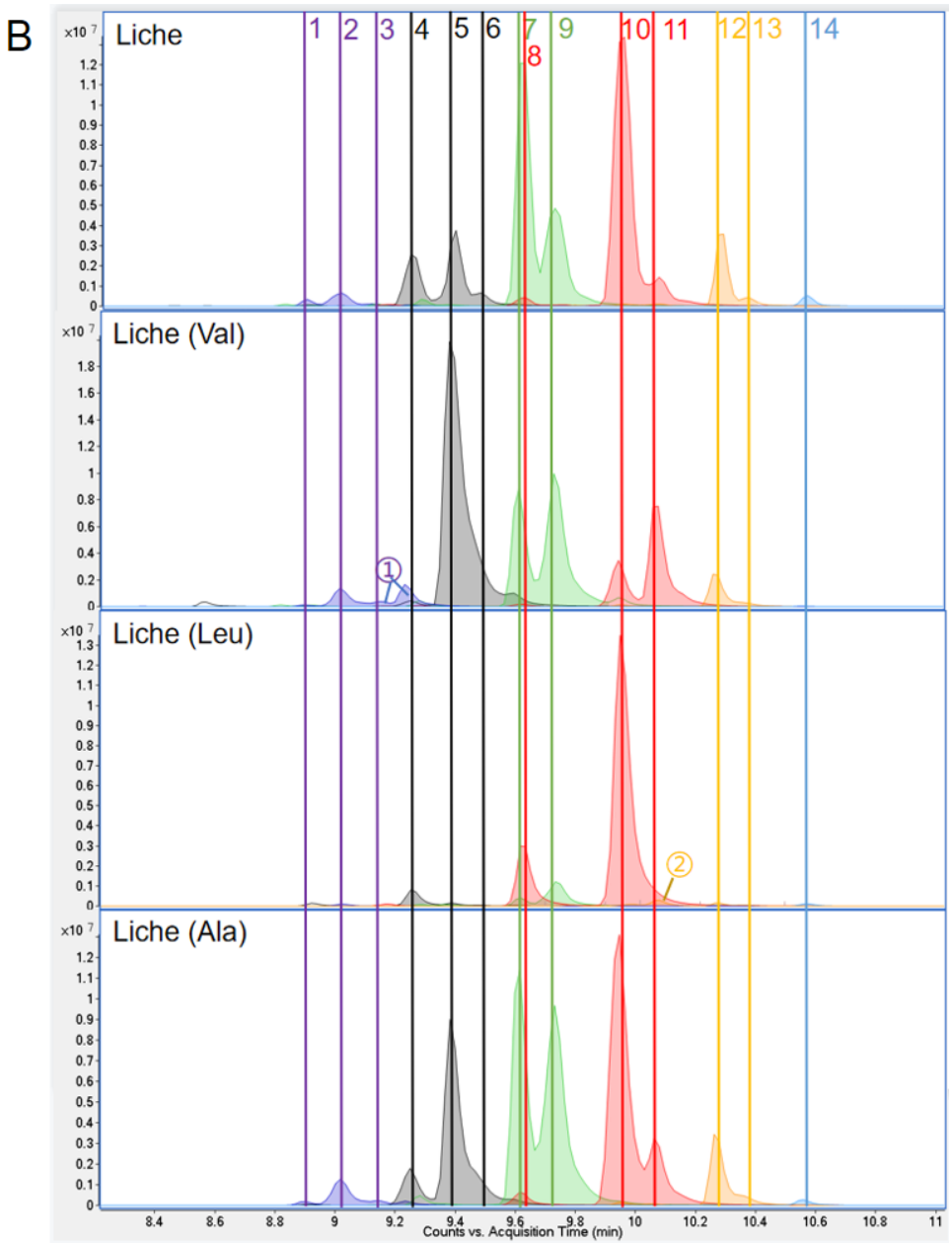

Figure A1-2 Structures of Liche variants.

A. and **B.** repsent chromatograms of Liche homologs, different colors present different masses (see in the below Table A1-2). Each of the purified CLP component was collected and mixed as a purified CLP mixture used in this study. The blue, black, green, red, orange, blue color represtents CLP mass: 9943, 1007, 1021, 1035, 1049, 1063, respectively.

Table A1-2 Information of Liche variants.

Mass	993		1007		1021		1035		1049		1063	993	1049
Line	1,2	3	4,5	6	7	9	8,10	11	12	13	14	①	②
Retension time	8.9-9.02 s	9.15 s	9.25-9.4 s	9.5 s	9.6 s	9.7s	9.65 s, 9.95 s	10.1 s	10.3 s	10.4 s	10.57 s	9.18-9.24 s	10.1 s
Liche homologue	$C_{12}Ile_7$	$C_{13}Val_7$	$C_{13}Ile_7$	$C_{14}Val_7$	$C_{14}Ile_7$	$C_{15}Val_7$	$C_{15}Ile_7$	$C_{16}Val_7$	$C_{16}Ile_7$	$C_{17}Val_7$	$C_{17}Ile_7$	$C_{14}Val_2Val_7$	$C_{15}Lxx_4Lxx_7$

A

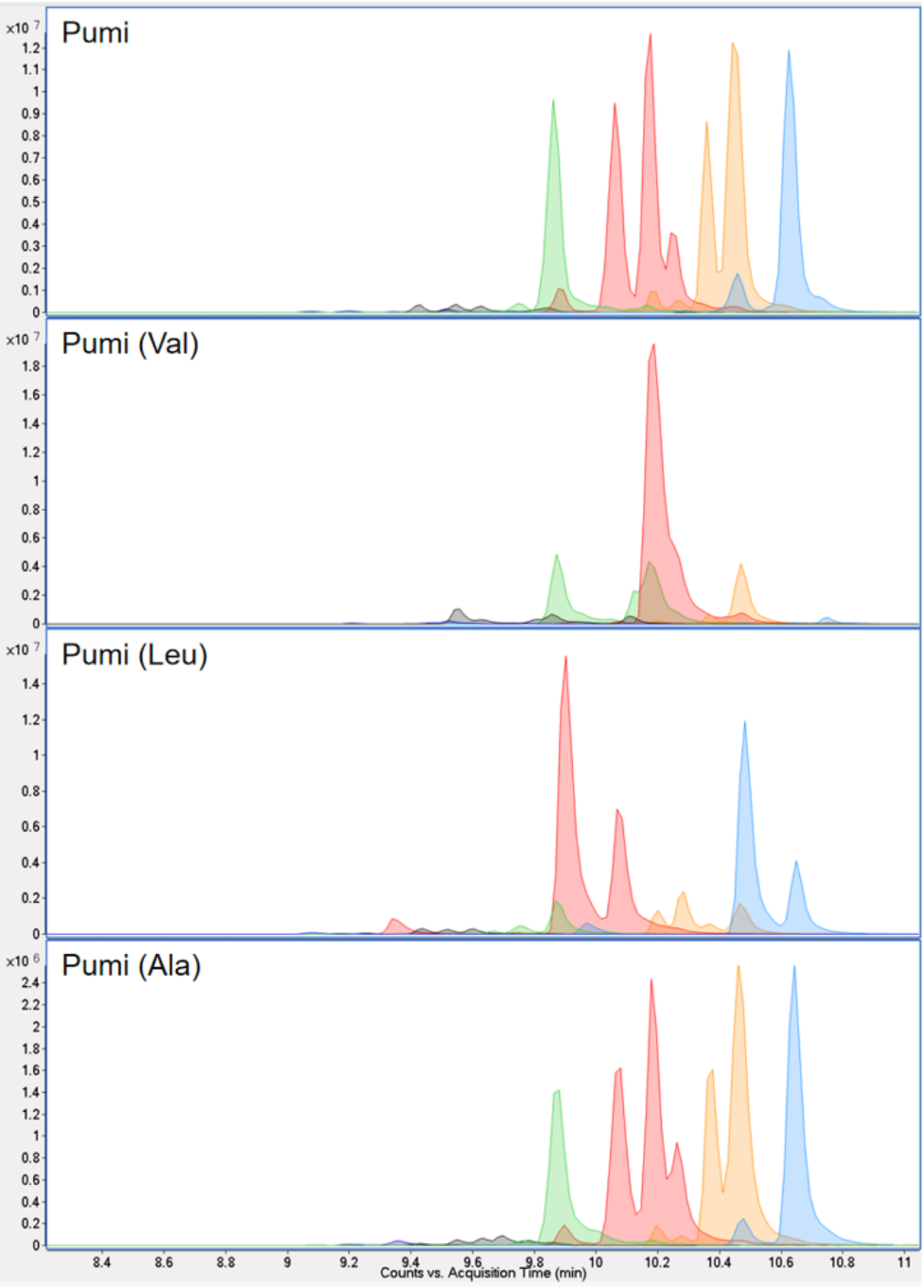
Pumi
Pumi (Val)
Pumi (Leu)
Pumi (Ala)
Counts vs. Acquisition Time (min)

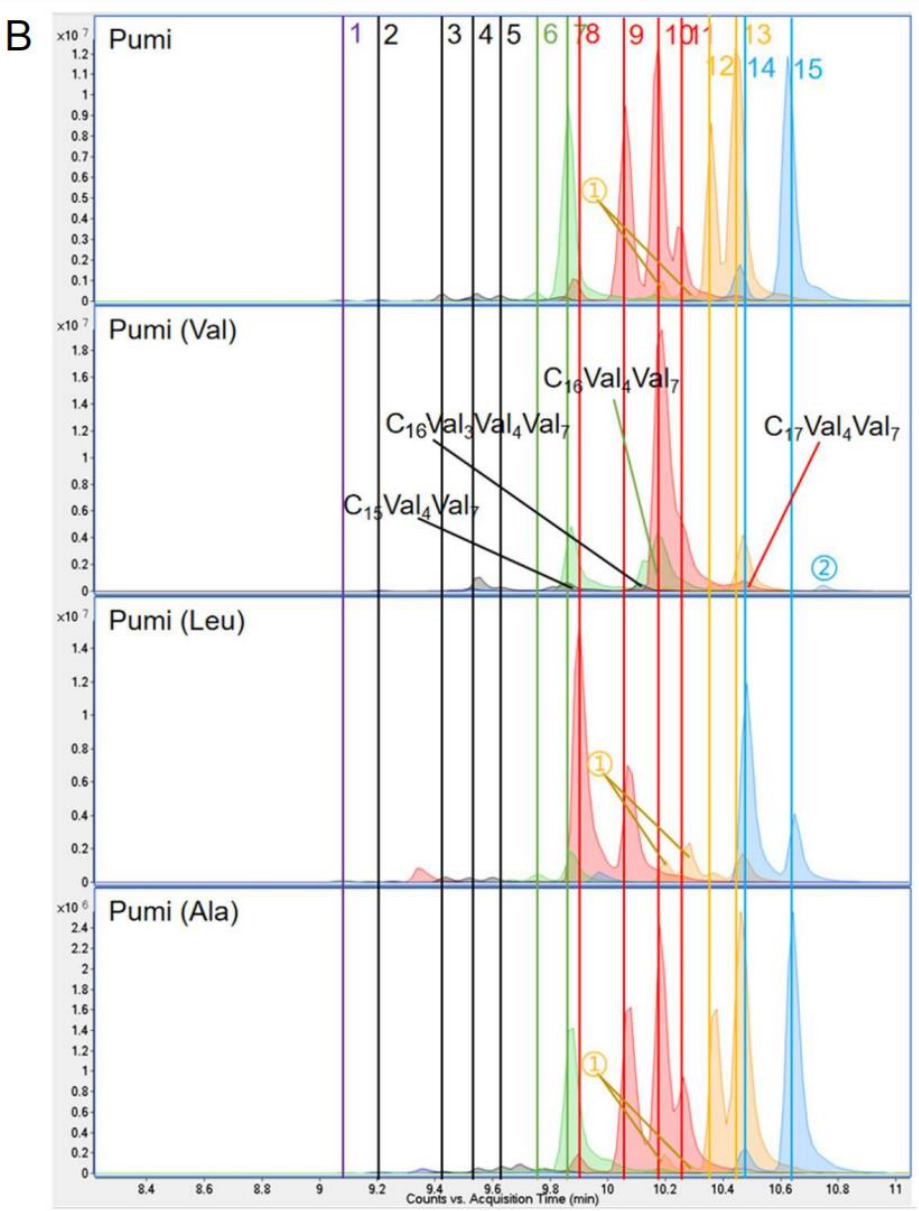

Figure A1-3 Structures of Pumi variants.

A. and **B.** repsent chromatograms of Pumi homologs, different colors present different masses (see in the below Table A1-3). Each of the purified CLP component was collected and mixed as a purified CLP mixture used in this study. The blue, black, green, red, orange, blue color represtents CLP mass: 1008, 1022, 1036, 1050, 1064, 1078, respectively.

Table A1-3 Information of Pumi variants.

Mass	1008	1022		1036	1050		1064		1078	
Line	1	2	3,4,5	6,7	8,9	10,11	①,12	13	14,15	②
Retension time	9.1 s	9.2 s	9.4-9.65s	9.75-9.85 s	9.9 s,10.05 s	10.2-10.25 s	10.2-10.4 s	10.47 s	10.47 s,10.63 s	10.8 s
Pumi homologue	$C_{13}Val_7$	$C_{13}Ile_7$	$C_{14}Val_7$	$C_{15}Val_7$	$C_{15}Ile_7$	$C_{16}Val_7$	$C_{16}Ile_7$	$C_{17}Val_7$	$C_{17}Ile_7$	$C_{18}Val_7$